INSIGHTS INTO THE ROLE OF NUCLEIC ACID STRUCTURE AND TOPOLOGY IN CONTROLLING CONDENSATION

A Thesis

Presented to

The Academic Faculty

by

Tumpa Sarkar

In Partial Fulfillment

of the Requirements for the Degree

Doctor of Philosophy in Chemistry and Biochemistry

Georgia Institute of Technology

August 2007

INSIGHTS INTO THE ROLE OF NUCLEIC ACID STRUCTURE AND TOPOLOGY IN CONTROLLING CONDENSATION

Approved By:

Dr. Nicholas V. Hud, Advisor
School of Chemistry and Biochemistry
Georgia Institute of Technology

Dr. Donald F. Doyle
School of Chemistry and Biochemistry
Georgia Institute of Technology

Dr. Andrew Lyon
School of Chemistry and Biochemistry
Georgia Institute of Technology

Dr. Stephen Harvey
School of Biology
Georgia Institute of Technology

Dr. Roger M. Wartell
School of Biology
Georgia Institute of Technology

Date Approved: July 05, 2007

To my parents and my grandma

ACKNOWLEDGEMENTS

This dissertation could not have been completed without the guidance, collaboration, and support of many people. Here, I express my deepest appreciation to all of them. First, I would like to express my sincere gratitude to my advisor, Dr. Nicholas Hud, for giving me an opportunity to work in his lab. Without his patient guidance, I wouldn't have completed this journey. Thank you for being so supportive; your dedication and enthusiasm for science are unparalleled.

I would also like to acknowledge my committee members for their valuable advice during this research study and it is my privilege to have them on my thesis committee. I am especially grateful to Professor Ishita Mukerji, Wesleyan University for helping me with the proteins, without which this work would not have taken the shape and also for her invaluable advice. I would like to thank Yolande Berta for teaching me how to use the TEM, and always be there whenever I need any help.

I was fortunate to have many exceptional colleagues in my research group. I wish to thank all of them for their help, invaluable input and for their amazing friendships. I wish to thank Dr. Pat Bishop, for her valuable advice and relentless encouragement.

I would like to thank my family, for always believing in me; my father for encouraging me to pursue my dreams, my mother for her sacrifices, my sister for being my best friend. I would not be here without their love and constant support. I am also grateful to my in-laws, Asit Mama, my uncle and aunt. Their support and encouragement have been invaluable. Finally, I would like to thank my husband and my dearest friend, Susnata for his love and support especially when I felt overwhelmed in my studies. Thank you for being there always for me.

TABLE OF CONTENTS

Page

LIST OF TABLES

Page

LIST OF FIGURES

Page

LIST OF SYMBOLS AND ABBREVIATIONS

A	Adenine
T	Thymine
G	Guanine
C	Cytosine
U	Uracil
bp	Base pair
kb	kilo base pair
UV	Ultraviolet
ΔG	Change in Gibbs Free Energy
ΔH	Change in Enthalpy
ΔS	Change in Entropy
K_d	Equilibrium dissociation constant
R	Universal gas constant
R_h	Radii of hydration
σ	Standard deviation
DNA	Deoxyribonucleic acid
RNA	Ribonucleic acid
PAGE	Polyacrylamide Gel Eletrophoresis
HPLC	High Performance Liquid Chromatography
AFM	Atomic Force Microscopy

DLS	Dynamic Light Scattering
TEM	Transmission Electron Microscopy
Cryo-TEM	Cryo-Transmission Electron Microscopy

SUMMARY

DNA condensation is a process in which DNA undergoes a polymer phase transition from an extended state in solution to a much more compacted and ordered state. This process is most often driven by the association of multivalent cations with DNA or by molecular crowding effects. DNA condensation is widely appreciated as a fundamental process in all living organisms. Understanding the organization of DNA within condensates and the dynamics of their formation has been of interest for many years as a model of DNA condensation within biological organisms.

More recently, DNA condensation has attracted much attention for its relevance in optimizing artificial DNA delivery systems for gene therapy, where packaging of the nucleic acid into particles of the smallest possible size is believed to be important for efficient cellular uptake. Presently, most efforts to improve the condensation and delivery of nucleic acids have focused on the synthesis of novel condensing agents. In contrast, the potential for DNA structure and topology to control condensation for packaging nucleic acids for cellular delivery has received far less attention. The research presented in this dissertation provides in depth biophysical studies that demonstrate how local modulations in the nucleic acid structure can be used to control both the size and the morphology DNA condensates.

During the past decade major advances have been made in the development of oligonucleotides as therapeutic agents. However, short oligonucleotides are not as easy to condense into well-defined particles as compared to gene-length DNA polymers. We describe a novel strategy for improving the condensation and packaging of

oligonucleotides that is based on the self-organization of half-sliding complementary oligonucleotides into long duplexes (ca. kb) with flexible sites at regular intervals along the duplex backbones, in the form of single-stranded nicks or single-stranded gaps. The results presented in this dissertation also provide new insights into the role of DNA flexibility in condensate formation and suggest the potential for the use of this DNA structure in the design of vectors for oligonucleotide and gene delivery.

In both bacteria and eukaryote the active regulation of DNA condensation is known to be an essential part of the cell cycle. Chromosome packaging in the bacterial nucleoid involves DNA organization and compaction at multiple levels. The protein HU, one of the most abundant nucleoid-associated proteins in bacteria, has been shown by mutant studies to play an important role in shaping the bacterial nucleoid. However, the mechanism by which HU regulates or promotes DNA condensation is not well understood. IHF is another high-expression nucleoid-associated protein in bacteria that is a homolog of HU and is also believed to contribute in compaction of chromosomal DNA. HU binds DNA without any apparent sequence preference, whereas IHF binds DNA in both non-sequence specific as well as sequence-specific modes. The similarity of these two proteins in functionality is illustrated by the fact that IHF can be substituted by HU in numerous cellular functions. The results presented in this dissertation demonstrate that both HU and IHF guide DNA to condense into linear bundle-like structures in presence of cellular condensing components, but the proteins alone do not condense DNA into densely packed structures. These results suggest a mechanism by which HU and IHF could act as architectural proteins during DNA condensation. The similar effects on DNA condensation of IHF and HU suggest that both proteins have related general functions in

the modulation of chromosome structure in bacteria. IHF and HU, as architectural factors, are proposed to locally organize bacterial chromosomal DNA in the presence of cellular condensing environment to facilitate its condensation into a more ordered, bundle-like state *in vivo*. The results presented for IHF and HU also suggest that these proteins could be used in artificial gene packaging and delivery protocols where rod-like condensates would be advantageous.

CHAPTER 1

INTRODUCTION

DNA condensation is generally described as the collapse of a DNA molecule from an extended state in solution into a more compact and ordered state. The condensed particle may contain a single DNA molecule or multiple DNA molecules. The term DNA condensation is generally restricted to a process in which the resulting DNA particle is of finite size with a well-defined morphology and containing ordered DNA packing, which is distinguished from DNA aggregation or precipitation [1].

1.1. DNA CONDENSATION IN NATURE

Nucleic acid condensation is of fundamental importance to biological organisms [2]. DNA molecule is the carrier of genetic information in all living cells and therefore genomic DNA molecules are extremely long (on the order of millimeters in length). However, genomic DNA molecules must package into a very small space inside a cell or a virus particle (e.g. with dimensions measured in nanometers). Several DNA packing systems have evolved to condense genomic DNA from relatively simple particles in viruses to the complex chromatin of eukaryotic cells.

A classic example of DNA packing in nature comes from the bacteriophage. In solution, the 40 kb T7 genome with its contour length of 13.6 μm, which can span a space of several μm, is packaged into a 55 nm wide virus capsid, a compaction that represents ~10^4 fold increased density [3]. During packaging, genomic DNA is

translocated into an empty prohead in an ATP-driven process and condensed as a highly ordered structure at a density near that of a crystalline state [3-6]. This process results in a highly compressed and strongly bent viral DNA, forming a spool-like condensate, and storing enormous elastic energy that has been proposed to help eject the bacteriophage DNA into a bacterial cell [7-9].

The 4.6 Mb circular chromosome of *Escherichia coli* with an unfolded circumference of approximately 1.6 mm in solution is packed into a nucloid region about 1 μm in diameter, with over a thousand fold linear compaction. Although the detailed organization of the chromosome in the bacterial nucleoid is not well understood yet, it is clear that condensation is achieved by the combined effects of supercoiled chromosomal domains, nucleoid-associated proteins, polyamines and crowding effects exerted by RNA and proteins [10-12]. Condensation of the eukaryotic genome in the cell nucleus is a complex phenomenon as the eukaryotic genome is several orders of magnitude larger than in viruses or prokaryotes.

The average human chromosomal DNA of 1.7×10^8 bp with a contour length of 5.8 cm is condensed by a linear factor of 10^4 to 10^5 to fit inside the cell nucleus. The chromosome compaction is achieved primarily by histone proteins, although other chromosomal proteins also have important roles. DNA is wrapped around nucleosomes that further compact DNA into the 30 nm chromatin fiber [13]. Long loops of chromatin fiber then attach to the chromosome scaffold composed of nonhistone proteins to form the chromosomes [13,14]. These structures do not occur in all eukaryotic sperm cells. Rather, the transcriptionally inactive DNA is packaged within the sperm cell nuclei of

many vertebrates and all mammals by arginine-rich protamines into a highly condensed structure with near crystalline density [15-17].

1.2. STUDIES OF DNA CONDENSATION *IN VIVO*

DNA packaging in viruses and sperm cells has long attracted the attention of biophysicists because of the above mentioned remarkable packing density inside phage capsids and sperm cell nuclei. Early studies of DNA condensation focused primarily on unraveling the structural organization of phage DNA and the morphology of DNA compacted in virus capsids and sperm heads [3,18-22]. X-ray diffraction patterns from phage heads showed that DNA is packed tightly into locally parallel bundles [23,24]. Further information emerged from electron microscopic studies of phage DNA released from disrupted bacteriophage capsids that revealed that DNA is packed in an orderly toroid like structure inside the phage head [18,25]. Early X-ray diffraction and electron microscopy studies provided information on the spacing between the DNA strands and about the overall low-resolution structure. Based on these different sources of information diverse models have been proposed. These models include the ball of string [18], coaxial spool model [18,19], nontoroidal kink model [26], nematic liquid crystal model [27] and the folded toroid [28]. The development of cryo-electron microscopy (cryo-EM) provided the advantages of visualizing bacteriophage DNA in its native conformation, without possible artifacts from negative staining and/or fixing. Cerritelli *et al.* have examined the conformation bacteriophage T7 DNA inside the capside by cryo-EM and computer-aided image processing techniques [3]. Their data strongly suggests DNA is densely packed within the phage capsid with 2.5 nm spacing and is wrapped

axially in concentric shells, as proposed by the coaxial spool models. However, a recent simulation study showed that DNA within the slightly elongated capsid of bacteriophage φ29 is not coaxially spooled, instead, DNA resembles a folded-toroidal conformation [6]. This suggests that the conformation of DNA inside the bacteriophage is determined by the shape of the virus capsid [6].

1.3. CONDENSING AGENTS FOR *IN VITRO* DNA CONDENSATION

Over thirty years ago it was discovered that the polyamine spermidine can cause the *in vitro* condensation of DNA into toroidal structures with dimensions similar to the structure observed when encapsidated phage genome is released by the gentle lysis of a bacteriophage capsid [18,25,29]. The genome packaged in the vertebrate sperm cells was found to be condensed into a toroidal morphology [16,22,30]. Thus, DNA toroids represent a fundamental morphology selected by the nature for the high-density packaging of genomes. Furthermore, the elemental packing unit of DNA in some bacteriophages and in mammalian sperm cells is in excellent agreement with the DNA packing in DNA condensates produced *in vitro* [3,22,31,32]. Thus, *in vitro* DNA condensation has long been considered a potential model for DNA condensation in biological organisms.

Numerous studies have demonstrated that in aqueous solution DNA can be condensed at room temperature by a wide range of multivalent cations of charge 3+ or greater (e.g., natural polyamines spermidine^{3+} and spermine^{4+}, inorganic cation $Co(NH_3)_6^{3+}$, cationic polypeptide polylysine, basic proteins histones H1) [29,33-37]. Divalent cations, however, do not generally induce DNA condensation in aqueous

solution at room temperature, but can in water-alcohol mixtures [38,39]. However, the divalent cation, Mn^{2+}, was shown to condense supercoiled plasmid DNA into toroidal condensates, but not linear plasmid DNA [40]. Multivalent cations reduce the repulsion between DNA segments by neutralizing DNA backbone charge and thereby promote condensation of DNA. Alcohols can also induce DNA condensation. Alcohols facilitate condensation by multivalent cations by reducing the dielectric constant of the solution, which increases the interaction between DNA and counterions. It was demonstrated that even divalent cations, such as Mg^{2+} initiate condensation of DNA in presence of 50% methanol solution [39]. Arscott *et al*. observed well-defined condensate morphology when ethanol is used in low concentration in the presence of $Co(NH_3)_6^{3+}$ at low ionic strength and verified that alcohol reduces the critical concentration of condensing agent required for condensation [41]. DNA can even be condensed into an ordered morphology by crowding agents such as polyethylene glycol, albumin in presence the monovalent cations [42-44]. These crowding agents promote ψ-DNA (Polymer-and-Salt-Induced) condensation primarily by the excluded volume effect of crowding agents, as these polymers do not strongly interact with DNA [44-46].

1.4. INTRAMOLECULAR FORCES IN DNA CONDENSATION

Ever since *in vitro* DNA condensation was first reported there has been a constant stream of theoretical and experimental investigations focused on unraveling the forces and the factors that govern DNA condensation. DNA condensation was found to be the result of a combination of attractive and repulsive forces, where the attractive interactions must overcome repulsive ones at the onset of DNA compaction. The repulsive

contributions include DNA bending energy, entropy loss and electrostatic repulsion. The proposed attractive interactions include primarily correlated counterion electrostatics and hydration forces. Others attractive contributions come from cross-linking or bending by bound ligands.

1.4.1. DNA Bending Energy

The free energy required to bend or distort the DNA double helix for its compaction into orderly condensates is referred to as bending energy, which can be defined in terms of the length of the DNA segment being bent (*L*), persistence length of DNA (L_p), the radius of curvature of the bent segment (R_c) and temperature (T) [47].

$$\Delta G_{bend} = (RTL_pL) / (2 R_c^2) \quad (1.1)$$

The persistence length of DNA is a measure of DNA bending rigidity or stiffness. This parameter is defined as the length over which for a free DNA molecule in solution, the root-mean-square bend angle in any particular direction is one radian [48,49]. In other words, the persistence length is the distance over which correlations in the direction of the tangent to the helical axis are lost. The persistence length of a random DNA sequence in a salt buffer of physiological strength has been measured to be ~50 nm (~150 bp) [48]. However, the measured persistence length of DNA polymer depends on the intrinsic curvature of DNA molecules and also on solution conditions [48,50-53]. Below the persistence length, the molecular behavior of DNA approaches that of a rigid rod [48]. The energy required to bend the DNA shorter than the persistence length is energetically unfavorable. However, the DNA bending energy can be reduced or may even be

favorable by introducing sequence-directed curvature in the DNA [31,54], by altering the inherent stiffness of the DNA, by bending due to localized binding of the multivalent cations or by distorting the DNA helix by DNA binding proteins [46,47,55].

1.4.2. Mixing Free Energy

When a DNA polymer is condensed, it undergoes what has been termed as coil-globule transition. In the uncondensed state, the interaction between DNA and its solvent milieu is favorable and DNA remains in the extended state. Upon condensation, a coil-globule phase transition occurs in which solvent-DNA interaction become less favorable [47]. The demixing of DNA polymer and solvent upon condensation causes entropy loss which disfavors DNA condensation. The entropy loss due to this demixing was estimated by Reimer and Bloomfield [56] as

$$\Delta G_{mix} = - T \Delta S_{mix} = RT (L/L_p) \qquad (1.2)$$

where L is the contour length and L_p is the persistence length of DNA.

1.4.3. Electrostatic Energy

Electrostatic interactions are the most significant forces in DNA condensation. In the absence of positive counterions, strong electrostatic repulsive forces would develop as the polyanionic backbones of DNA approach during condensation. Ionic effects on DNA condensation were investigated by Wilson and Bloomfield, who studied condensation of DNA by different condensing agents including spermidine, spermine under a wide range of ionic conditions using light scattering and calculated the fraction of DNA phosphate

charge neutralized by counterions using Manning's counterion condensation theory [39]. Manning modeled DNA as a stiff anionic polymer and predicted that in aqueous solution at 25°C the quantity of phosphate charge neutralized by solutions of mono-, di- and trivalent cations would be 76%, 88% and 92%, respectively [38]. Wilson and Bloomfield estimated that a minimum of about 89-90% of the DNA charge must be neutralized for condensation to occur [39].

As it was predicted that optimal charge neutralization required for DNA condensation could not be accomplished by monovalent and divalent cations in aqueous solutions, monovalent and divalent cations cannot induce condensation under most circumstances [34,38,39,57]. Multivalent cations with charge 3^+ or greater are generally required to condense DNA [29,34,38,39,57]. However, in solutions of lower dielectric constant, divalent cations cause condensation, which is indicative of a greater percentage of phosphate charge neutralization in solvents of lower dielectric constant than water [39-41]. Alcohol facilitates DNA condensation by lowering the dielectric constant of the solution, but zwitterionic osmolytes inhibits condensation by increasing the dielectric constant [39,41,58-60]. Although the monovalent and divalent cations cannot initiate DNA condensation, they directly affect the critical concentration of the condensing agent. Increasing the concentrations of monovalent and divalent cations in the solution has been shown to increase the amount of condensing agent required to condense DNA, which confirms the competition between the condensing agent and other (mono-, di-valent) ions for binding to DNA [34,35,39,61-65]. Condensation is relatively insensitive to the chemical nature of the condensing agent but strongly depends on the valency of the counterion [34,39].

During condensation, counterions neutralize ~90% of the charge of the DNA and hence screen the repulsive electrostatic interaction between DNA helices. However, advancements in the polyelectrolyte theory over the past several years revealed that counterions also increase the attractive electrostatic interaction between helices in the condensed form through the correlated fluctuations of counterions shared between DNA molecules at close range [47,66-74]. The importance of correlations in macroion attraction was first suggested by Oosawa [66,67]. The theory of correlated fluctuations by Rouzina and Bloomfield proposed that the significant correlation occur when the counterion distribution has a pseudo-two-dimensional character very close to the highly charged macroion DNA surface [68]. According to this theory, although each of these surfaces are neutral on average, due to the coulombic repulsion between these surface adsorbed mobile counterions, an alternating pattern of positive and negative charges are formed. When two such DNA molecules with apposing but mobile ionic patterns approach each other, the mobile patterns or surface lattices adjust in a complementary way in order to minimize the total energy and ultimately a net attractive electrostatic potential between the DNA helices. This theory has been provided support by Brownian dynamics simulations but remain to be proved experimentally [75,76].

1.4.4. Hydration Forces

Hydration forces have been proposed to arise due to the reconfiguration of bound water molecules located between macromolecular surfaces [58,77]. X-ray diffraction has been used to measure forces between DNA double helices by analyzing the spacing of condensed DNA molecules as a function of osmotic stress [78]. Forces were observed to

decay exponentially and were independent of counterion nature or concentration. The results suggested that forces are not electrostatic in nature and are not due to ligand bridging [77]. Rau and Parsegian proposed that multivalent cations bound to DNA helices cause reconfiguration of the water between DNA surfaces to create attractive hydration forces [47,58,77].

A thermodynamic analysis of the hydration force during DNA condensation was accomplished by measuring the enthalpy and entropy at different temperatures [58,77,79]. It was observed that the entropy ΔS of the multivalent cation-induced DNA-assembly is positive, and ΔS is increased by increasing the bulk water entropy with chaotropic perchlorate anion. The increase in the entropy upon the rearrangement of water on DNA surfaces or the release of water from the surface is believed to be part of the attractive hydration forces that are associated with DNA condensation which in turn depends on counterion binding [58,77,79]. It has also been suggested that multivalent counterion adsorption reorganizes the water at discrete sites complementary to unadsorbed sites on the apposing surface [58,80].

1.5. MORPHOLOGY OF CONDENSED DNA

Multivalent cations cause free DNA in solution to condense into nanoscale particles with various morphologies such as toroids, rods, and spheres [1,47,81,82]. The morphology of DNA condensates depends on solution conditions (e.g. solvent polarity) and on properties of the DNA polymer (e.g. DNA length and DNA topology) [41,83-85]. The nature of the condensing agent (e.g. polarity, charge density) has also been shown to affect DNA condensate morphology [86,87]. The variation in particle morphology and

size have been used to study the mechanism of DNA condensation. Toroids represent the most commonly observed morphology, and have been studied the most.

1.5.1. Toroidal DNA Condensates

1.5.1.1. Mechanisms of Toroid Formation

Thirty years ago it was discovered that the polyamine spermidine can cause the condensation of DNA into toroidal structures that are approximately 100 nm in outside diameter [29]. This transition of DNA in solution from a wormlike polymer to tightly packed toroids represents a decrease in the DNA occupied volume by approximately four orders of magnitude. Toroidal DNA condensates have been reported to be the morphology of the highly-packed genome within some bacterial phages and sperm cells [3,18-22]. Thus, understanding the organization of the DNA within the toroidal condensates and the mechanism of their formation is of interest as a model of DNA condensation within biological organisms.

It is now known that a wide range of multivalent cations can condense DNA into toroids [22,33,34,37,86,88,89]. Furthermore, DNA lengths from 1 kb to 50 kb have been shown to produce toroids that measure around 100 nm in outside diameter [1], toroids from DNA around 50 kb can be unimolecular, whereas toroids formed from significantly shorter lengths are multimolecular. Toroids with outside diameters up to 200 nm have also been reported [90-93]. These larger toroids can result from the condensation of DNA with lengths greater than 50 kb [91], higher DNA concentrations [92], high concentrations of condensing agent [93] or by slowing condensation nucleation [94,95]. The wide range of solution conditions and different DNA lengths have been reported to

produce toroids of similar dimensions has been cited as evidence that 100 nm diameter toroid represents a minimum energy state for condensed DNA [1]. A significant number of theoretical models of toroid formation have attempted to explain why DNA toroids favor particular dimensions [1,96,97]. These theoretical studies have generally assumed that toroid size is thermodynamically controlled. However, the distribution of toroid sizes within a single condensation reaction had suggested that toroid formation may not be under equilibrium control but instead that toroid growth is kinetically limited [1,31]. Furthermore, single-molecule experiments and theoretical studies of DNA condensation have supported the nucleation-growth process of toroid formation [98-103].

The formation of a stable toroid begins with the nucleation event which is also the rate-limiting step of this process, as both DNA bending energy and persistence length constraints are required to be overcome in this step. The size of particles formed by such a process can depend on the kinetics of particle nucleation and subsequent growth. Recent studies by the Hud laboratory have sought to determine the respective influence of kinetic and thermodynamic factors that govern toroid dimension [54,85,94,95]. DNA toroids formation was systematically studied using a plasmid DNA containing sixty phased A-tracts, which was designed to produce two static loops in the plasmid DNA. An A-tract is a DNA sequence containing four to eight consecutive adenine residues and a single A-tract induce a bend of 12-21º into the helix of DNA [50,104,105]. Under low salt condition, toroids formed by the condensation of DNA molecules containing the static loops were significantly smaller than toroids produced by the DNA without static loops [54,95]. The mean diameter of DNA toroids (i.e. average of inside and outside diameters) with static A-tract loops was determined to be essentially the same as the A-

tract loops, which provided support for the proposal that static loops in the DNA act as built-in sites for toroid nucleation. In contrast, DNA without static loops formed larger toroids, because DNA loops formed by random DNA fluctuations are on average larger than those of the static A-tract loops. However, the toroid thickness of DNA with and without static loops was found to be virtually identical, which demonstrated that under low salt condition toroid thickness is independent of nucleation size [95]. A quantitative comparison of toroid dimensions formed at the low ionic strength with those formed in the presence of additional salts (NaCl or $MgCl_2$) demonstrated that toroid thickness is a salt-dependent phenomenon [94,95]. Based on these results a nucleation-growth model of DNA toroid formation has been developed in which toroid diameter is determined by the size distribution of the nucleation loops along the DNA at the onset of condensation and toroid thickness is governed by the solution-dependent growth rate [54,81,95].

Condensation studies by Conwell & Hud that focused on the effects of $MgCl_2$ on toroid size have also provided substantial insights into toroid growth limits. When $MgCl_2$ is present during DNA condensation the toroids formed are much larger than those observed when $MgCl_2$ is present prior to condensation or when added after condensation has occurred [94]. These results provided further evidence that the vast majority of toroidal DNA condensates reported in the literature were formed under conditions where toroid growth was limited by the kinetics of condensation, rather than thermodynamic limits. Thus, to explain the final toroid dimensions theoretical calculations are required which consider toroid nucleation along with polyelectrolyte bundle growth [81,106].

1.5.1.2. DNA Packing within Toroids

The organization of DNA within toroidal condensates was a matter of debate for more than twenty five years. It was generally been assumed that DNA within toroids is wound in a circumferential manner and, for optimal packing density, with DNA strands packed in a hexagonal lattice. Early X-ray diffraction studies by Schellman *et al.* demonstrated that the spacing between the DNA helices within a toroid was consistent with hexagonal packing [107]. The first experimental evidence of circumferential DNA wrapping in the toroidal condensate came from the studies done by Marx and Ruben using freeze-fracture electron microscopy technique [108,109]. However, the degree of DNA organization was not clear, and some experimental observations and simple theoretical arguments regarding the packing of a semi-rigid polymer into a toroidal particle suggested that DNA might not be packed throughout the toroid in a perfect hexagonal lattice [28,110].

The emergence of cryo-transmission electron microscopy as a powerful method to visualize macromolecules in its native conformation, made it possible to directly image DNA in condensates without artifacts from negative staining and/or fixing. Böttcher and coworkers were the first to study DNA toroids by cryo-TEM. For condensates produced by 7.7 kb DNA and spermine, they reported an interhelix spacing for DNA within toroids as 1.8 nm [111]. Based upon the unusual close packing of DNA helices obtained from electron micrographs, as well as circular dichroism spectra, the authors suggested that the DNA present in the air dried toroidal condensate is in the C-form DNA. However, the spacing reported by Böttcher *et al.* appears to be in error based upon subsequent studies [32].

The fine structure of DNA organization within DNA toroids was investigated in detail by Hud and Downing using cryo-TEM [32]. In this study, DNA toroids were prepared by the condensation of λ phage DNA with hexammine cobalt chloride and condensates were rapidly frozen before imaging. Top-view images of toroids, in which the principle axis of a toroid was approximately normal to the image plane of the microscope, revealed that some toroids have regular organization of DNA throughout most of the particle (Figure 1.1A). However, no single toroid was observed to have perfect DNA organization throughout. Edge-view images of toroids provided the first direct observation of the hexagonal packing lattice of DNA within toroidal condensates (Figure 1.1B). A Fourier transform of a region of an edge-view toroid micrograph that contained a highly ordered DNA lattice produced diffraction-like patterns typical of a hexagonal array with a Bragg spacing of 2.4 nm. This spacing corresponds to a radial spacing of 2.8 nm between the helices, as the Bragg spacing is related to the inverse of the lattice spacing by a factor of $2/\sqrt{3}$ for a hexagonal lattice. A DNA interhelical spacing of 2.8 nm in DNA toroidal condensate is in excellent agreement with the previous reports regarding the interhelical spacing of DNA condensed with hexammine cobalt chloride determined by X-ray scattering studies [107]. Edge-view images also revealed regions in which DNA was packed in a non-hexagonal lattice (Figure 1.1C). These nonhexagonal regions were attributed to crossovers of DNA strands within the toroid.

A three-dimensional computer model of a DNA toroid was reconstructed by a program that simulated the wrapping a semi-flexible polymer using a hard-cylinder potential for DNA-DNA interaction and several topological constraints [107]. Simulated electron microscopy images of these model-toroids in different orientations were able to

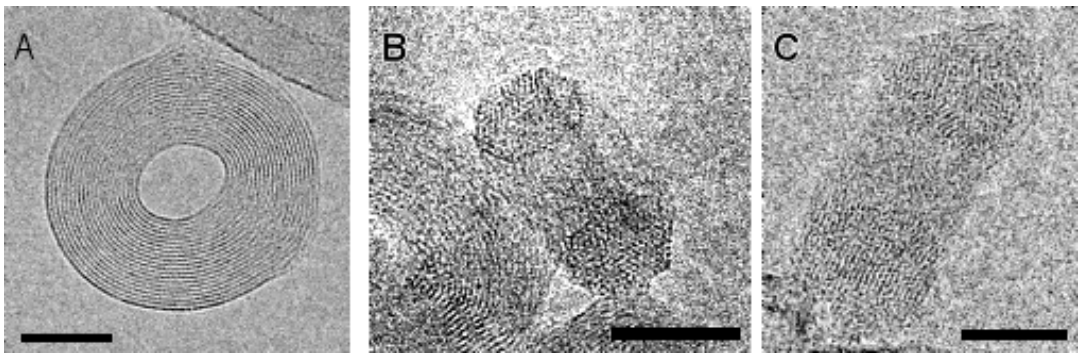

Figure 1.1. Cryo-EM images of DNA toroids formed by condensation of λ phage DNA with hexammine cobalt chloride. A) Top-view image of a toroid with DNA fringes visible around almost the entire circumference of the toroid. B) Edge-view image of a toroid where hexagonal packing of DNA helices is apparent in the outer regions. C) Edge-view image of a toroid in which the outer regions appear to have DNA packed in a nonhexagonal lattice. All scale bars are equivalent to 50 nm. Adapted from reference [32].

reproduce most of the structural features observed in micrographs of toroids. As was observed in DNA toroids imaged by cryo-EM, the simulated EM micrographs of 3D models revealed that a toroid will appear uniformly ordered for most of its circumference in a top-view image, but still contains substantial regions with both hexagonal and non-hexagonal DNA packing. It was found that the circumferential angle between the regions of apparent disorder was approximately one-half the circumferential angle over which DNA deviates from an ideal packing hexagonal lattice. Thus, the cryo-electron micrographs of toroids presented the first direct evidence that DNA within the toroid is organized in a perfect hexagonal packing with regions of non-hexagonal DNA packaging. Additionally, the model demonstrated a well-defined mechanism for DNA toroid packaging that simultaneously explains the regions of local disorder and the possibility for crossovers in DNA packaging [32,81].

1.5.2. Rod-Like DNA Condensates

Rod-like condensates are often observed along with toroids when DNA is condensed by multivalent cations. The population of rod-like condensates is typically 10% or less with respect to toroids for DNA greater than 3 kb in length [1,47]. Bloomfield and co-workers have demonstrated that the population of rod-like condensates can be substantially increased when DNA is condensed by certain condensing agents, such as me_8spermidine [86], or with other condensing agents in water-alcohol mixtures [41]. DNA that is shorter than 1 kb has been shown to produce a greater percentage of rods than longer DNA [83,84]. However, the actual mechanism of rod-like condensate formation, and the relationship between rods and toroids, remains largely unsolved.

DNA condensate formation has been shown to be the result of a nucleation-growth process [1,54,94,95,98,103]. It has also been known for decades that both toroidal and rod-like DNA condensates can be formed in the same condensation reaction. Thus, the rod-like condensates formation could result either from the nucleation of rods at the onset of condensation (i.e. kinetic origin), or rod-like structures could co-existed with toroids in thermodynamic equilibrium (i.e. under equilibrium control) [31,54,95,98]. Interestingly, the length and diameter of the rods are found to be similar to the circumference and thickness of the toroids respectively [83]. This similarity led to the speculation that rod is a structural intermediate in toroid formation and rod spontaneously convert into toroids by bending and end fusion, but this theory has never been proven [112,113]. However, experimental studies using AFM (atomic force microscopy) have presented evidence that unimolecular DNA condensates can convert from a toroid to a

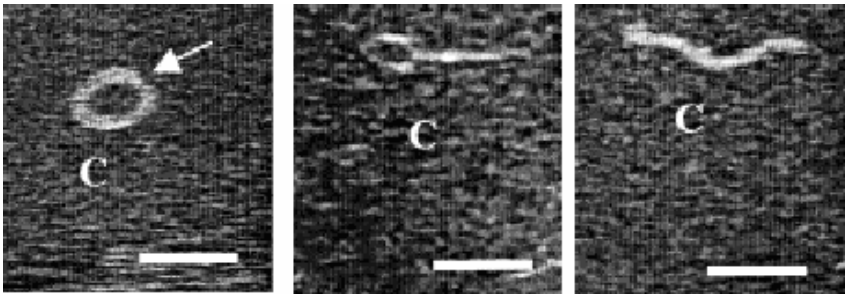

Figure 1.2. Aqueous AFM images displaying dynamic equilibrium between toroidal and rod-like condensates. All scale bars are equivalent to 200 nm. Adapted from reference [114].

rod by the collapse of toroidal loop (Figure 1.2), not by the bending of a rod into a toroid [114]. Molecular and Brownian dynamics simulations have predicted the toroid to be a minimum energy structure for condensed DNA, and monomolecular rod–like condensate to be one of several metastable structures. A rod can be converted into the more thermodynamically stable toroid by internal conversion or by complete decondensation followed by recondensation into a toroid [100,101,115-117]. However, most theoretical studies of DNA condensation mechanism have been limited to the studies of monomolecular DNA condensate formation and have not provided any insight into the intermolecular growth of DNA condensate. It has also been proposed that the packing of DNA in rods and toroids is nearly isoenergetic including the energy required for the smooth bending of DNA within toroids versus that required to produce sharp bends at the ends of the rods, suggesting that these two morphologies could coexist in a Boltzmann distribution at equilibrium [1]. It is, therefore, possible that the observed distribution of toroids and rods actually depends on both the thermodynamics and kinetics of DNA condensate formation.

Recent experiments by Vilfan *et al*. involving the analyses of DNA condensate morphology statistics, as a function of time and DNA structure, have demonstrated that both kinetic and thermodynamic factors can influence experimentally observed relative populations of DNA rods and toroids [85]. It has been shown that rod populations are overrepresented, with respect to their equilibrium populations, at earlier times following the initiation of condensation. This higher population of rods at earlier time points provided the experimental evidence that rod formation is kinetically favored during the nucleation phase of condensation and is consistent with the theoretical studies that have suggested a favorable kinetic pathway for rod nucleation [100,101,115-117]. These results revealed that both rods and toroids represent equilibrium morphologies with their populations being determined by their relative thermodynamic stabilities.

It has long been appreciated that greater relative rod populations are observed as DNA fragment length is decreased [83,84]. Vilfan *et al*. have documented that the shift in condensate morphology is primarily due to a change in the relative thermodynamic stability of rods with respect to toroids, rather than a change in the kinetics of condensate nucleation. The results of these rod formation studies further revealed that the interconversion of multimolecular DNA rods to toroids over time occurs as a result of DNA strands exchange with solution, which allows a redistribution of DNA into a relative population of rods and toroids that is largely determined by relative thermodynamic stability [85].

1.6. DNA LENGTH AND STRUCTURAL EFFECTS

The size of DNA toroids formed within single condensate preparation have been shown to vary appreciably, however, a wide range of DNA lengths (1-50 kb) have been known to produce similar sized toroids [1,31]. Thus, as mentioned above, toroids can be formed either by the monomolecular collapse of longer DNA molecule or by multimolecular condensation of shorter DNA molecules [31]. This observation suggests that the size of the toroid is determined by the quantity of DNA packaged as opposed to the length of any one DNA molecule that is incorporated into the structure. Widom and Baldwin observe that DNA shorter than 400 bp will not condense into orderly, discrete particles [34]. The requirement for minimum DNA length to condense into orderly particles is explained by the stability of the nucleation structure during the condensation process [1,46]. For DNA condensates to form, there must be a minimal attractive potential between the packed strands, which must be greater than competing energetic terms that favor DNA remaining as an extended polymer in solution. Bloomfield calculated the free energy of a nucleating condensed particle as a function of DNA length, and concluded that the net attractive interactions per base pair are very small, therefore, at least several hundred base pairs must interact intra- or inter-molecularly to form a stably condensed nucleation structure [1].

The topology of the DNA molecule has been shown to influence the size and shape of the condensates particles [40,83,111,118]. Negative supercoiling may facilitate condensation by bringing stretches of a DNA molecule into close proximity and by stabilizing distortions that unwind the helix [40,119]. Böttcher *et al*. condensed three forms of the same plasmid DNA; supercoiled, linear and relaxed circle with spermine,

and compared the morphology of the resulting condensates using electron microscopy [111]. The linearized DNA produced toroids that tended to cluster; supercoiled DNA produced toroids, linear or loop like assemblies. The nicked circular DNA (i.e. relaxed circle) produced quantitative yields of individual toroid. The observed variation in condensate structure and aggregation was attributed to the difference in the flexibility between the three types of DNA, with supercoiled DNA being most rigid, relaxed circles of intermediate flexibility and linear DNA being most flexible [111]. It has been suggested that the supercoiled DNA allows smaller condensates than linear or relaxed circular DNA due to its increased propensity for bending, not because supercoiled DNA is more flexible than linear DNA, This size dependence on DNA topology was experimentally demonstrated by Marx and Ruben and also by Arscott *et al*. [83,120,121]. The toroids formed by the condensation of closed circular pUC12 DNA molecules with hexammine cobalt(III) chloride were significantly smaller and contained less DNA molecules than the toroids formed from the linear DNA. An increased propensity for kinking of supercoiled DNA may also explain the increased formation of rod-like condensate formation in a preparation of supercoiled DNA condensation.

For the thirty years much work has been done to characterize the effects of solution conditions on DNA condensation including the development of new condensing agents. The potential for nucleic acid structure to govern DNA condensation has received far less attention, although DNA sequence and secondary structure has been found to play an important role in determining the morphology of DNA condensates [41,122,123] [54,124]. It has been shown that the introduction of a highly repetitive G-rich sequence into plasmid DNA can decrease the size of the toroidal condensate by 22% [124]. Studies

on the plasmid with longer $d(CG)_n$ inserts capable of undergoing the B- to Z-DNA transition showed that these DNAs have an increased DNA condensability [123]. DNA with longer $d(CG)_n$ inserts formed a higher proportion of the rods at lower concentrations of condensing agent and toroids at higher concentrations of condensing agent with smaller inner radii relative to DNA without inserts. This was attributed to the higher flexibility or kinking of the secondary structure near $d(CG)_n$ inserts forming B-Z junctions that allows the tight curvature required for the condensates [123]. Arscott *et al*. monitored condensation promoted by hexammine cobalt(III) chloride under conditions that favor the formation of A-DNA in random sequences, and observed an increased in rod-like condensates from toroid-like condensates and finally loss of ordered condensate morphology, and formation of a network of multistranded fibers [41].

The mechanical properties of double stranded DNA in solution are reflected by the measured persistence length of ~150 bp [48]. Thus a free DNA molecule in solution is generally considered to be a semi-rigid polymer. However, in genome packaging, transcription, recombination and other genomic events DNA *in vivo* is required to be tightly bend with enhanced local flexibility [55,125-127]. Bends can be induced in the DNA helix through the intrinsic curvature associated with certain sequence elements [50,128] or upon participation of protein machineries that remodel DNA structure [129,130]. Sequence-directed curvature can be generated by A-tract sequences. Long-range static curvature is produced by multiple A-tracts if the incremental bends are in phase with the helical twist of DNA. The condensation of DNA containing A-tract directed static loops has been shown to form smaller toroids than DNA polymers without static loops [54,95,122].

Another means of introducing bending in DNA is through protein-DNA interactions. The free energy release associate with protein binding to DNA is sufficient to overcome the energetic cost of deforming the relatively stiff DNA polymer over short lengths [49]. In both prokaryote and eukaryote, the genome is organized in a compacted form by the nucleoprotein complexes. The eukaryotic chromosome is organized into chromatin with fundamental nucleosome subunits in which the histone octamer wraps 146 bp of DNA in a 1.6 left-handed superhelical turn. This induces a 47º deflection of the DNA for each helical turn [55]. This remarkable tight folding of DNA in the histone-DNA complex is required for chromosome compaction in the nucleus [13]. Besides the ability of the histones to significantly modify the flexibility of the DNA helix, many DNA binding proteins of both prokaryote and eukaryote, act as DNA chaperones or architectural proteins and alter the local DNA structure for several cellular functions [55,125-127].

Bacterial proteins HU, integration host factor (IHF) and eukaryotic high mobility group proteins (HMG) are well-characterized DNA bending proteins. The HU dimer, which binds in the minor groove of DNA without sequence specificity, induces a substantial DNA bend, although the structural homolog of HU, integration host factor (IHF), binds to sequence specific sites with a higher affinity and induces a ~160º DNA bend over ~35 bp [131-133]. Due to their high cellular abundance and DNA bending ability, HU and IHF have been implicated in the compaction of the bacterial nucleoid *in vivo* [12,134]. HU has no structural similarity with eukaryotic HMG proteins but functionally, HU is analogous to high mobility group proteins. HMG proteins are abundant in eukaryotes and like HU, bind to DNA with only limited sequence selectivity,

but have a high affinity for bent or distorted DNA [135-137]. HMGB proteins are observed to be effective in substituting for HU (or IHF) proteins in promoting the nucleoprotein assembly for many cellular reactions, like invertasome formation in prokaryotes and chromosome segregation, confirming that these proteins function strictly as DNA architectural factors [138,139]. In eukaryotes, HMG proteins primarily act as DNA bending proteins in a wide variety of cellular functions, including DNA replication, transcription, and chromosome organization [55,138-145]. The ability of the above mentioned architectural proteins to induce a high degree of bending and their implicated role in genome packing suggest an enormous potential for the application of these proteins for *in vitro* DNA condensation. Further studies are required to understand in finer detail, the exact contribution of DNA architectural proteins like HU, IHF and HMG in DNA condensation.

DNA persistence length has shown by theoretical studies to be a major determinant of condensate morphology [97], and DNA persistence length is recognized as a principal factor governing the size of toroids [31,54,95]. Thus, by decreasing the persistence length of the DNA, it may be possible to form smaller condensate structures due to the reduced bending energy required during condensation. The intrinsic rigidity of the DNA double helix can be altered by the introduction of single-stranded nicks and gaps in the DNA helix [146-148]. Electron microscopic studies have suggested that nicks significantly reduce the persistence length of the DNA in low salt conditions [149]. However, nicked DNA molecules displayed small retardation with respect to unnicked molecules in native polyacrylamide gel electrophoresis [147,150] suggesting that nick-induced bends are in dynamic exchange between bent and linear structures (i.e. stacked

helices at nick sites). The significant increase in the flexibility of DNA structure by the incorporation of single-stranded gaps in the DNA helix has been specifically addressed experimentally in previous reports [146-148]. Detailed studies of DNA with single-stranded nicks and gaps were necessary to determine the influence of DNA persistence length on condensation, and are presented in Chapters 2 of this thesis.

1.7. DNA CONDENSATION FOR GENE THERAPY

DNA condensation has also attracted much interest for its direct relevance in the development of gene therapy [151-154]. Gene therapy shows great potential for treating diseases ranging from genetic disorders, acquired diseases, cancer, viral infections to neurodegenerative diseases [155-158]. However, significant progress must still be made as the clinical application of gene therapy still faces numerous challenges [154,159]. A key challenge is the development of a system that can selectively and efficiently deliver a gene to target cells, and in a way that permits the gene to express efficiently [154]. Two broad approaches have been used for DNA delivery to cells, namely viral and non-viral delivery systems. Viral delivery systems are highly efficient in DNA delivery and expression. However, nonviral delivery systems are attractive as alternatives to viral delivery system because their potential for reduced immunogenic response and lower toxicity [160]. Nevertheless, non-viral vectors also have significant limitations. Nonviral gene delivery methods generally exhibit low transfection efficiency. This low efficiency is due to a combination of extracellular and intracellular barriers including instability of the complex containing DNA and the delivery agent, poor uptake across the plasma membrane, inability to release DNA from the endosome into the cytoplasm, degradation

of the DNA, and inefficient targeting to the nucleus [154,161,162]. The condensation of DNA into compact particles is believed to be essential for the improvement of DNA uptake by the cell via diffusion and endocytosis and also for improvement in chemical and physical stability. Intercellular diffusion, which is necessary for gene delivery to many tissues *in vivo*, and the intracelluar uptake and transgene expression, have been observed to be greatly facilitated by the packing of DNA into particles with dimensions smaller than 50 nm [151,154,161,163-166]. Thus, being able to control DNA condensation *in vitro* could play a major role in the development of novel approaches to gene therapy. The possibilities for improving gene therapy have motivated much of the work presented in this thesis.

CHAPTER 2

CONDENSATION OF OLIGONUCLEOTIDES ASSEMBLED INTO NICKED AND GAPPED DUPLEXES: POTENTIAL STRUCTURES FOR OLIGONUCLEOTIDE DELIVERY

2.1. INTRODUCTION

During the past several years major advances have been made in the development of oligonucleotides as therapeutic agents. Triplex forming oligonucleotides (i.e. antigene), antisense oligonucleotides, aptamers and ribozymes (catalytic RNA) have shown promise in modulating gene expression [167-170]. More recently, the discovery of RNA interference (RNAi) has revealed how duplex RNA oligonucleotides can be used for gene-silencing, a mechanism that is both useful for basic research and very promising for the treatment of acquired and genetic diseases [171-176]. Effective implementation of oligonucleotide technology in biology and medicine depends on the efficient transfection of oligonucleotides. However, the cell membrane is a formidable barrier to the delivery of therapeutic nucleic acids [154,161,177]. Most chemical-based (i.e. non-viral and non-mechanical) artificial DNA delivery systems involve charge-neutralization and condensation of DNA into small particles that facilitate DNA entry into cells by endocytosis and in some cases, a mechanism for escape into the cytoplasm before endosomal degradation. Even the widely implemented method of cell transfection using

cationic lipids can be enhanced several fold when DNA is pre-condensed by cationic polymers into nanometer-scale condensates [166].

Efforts to improve oligonucleotide delivery have driven the development of novel reagents for DNA condensation that include cationic liposomes [178,179], polycationic dendrimers [180], polyethylenimine (PEI) [181-183] and various cationic peptides [184]. In contrast, relatively few studies have addressed the potential for alterations in nucleic acid structure to improve DNA packaging for delivery. Nevertheless, altering DNA structure appears to be a promising approach to controlling DNA condensation. For example, the introduction of a particular G-rich sequence into plasmid DNA can decrease condensate particle size by 22%, and supercoiled DNA has been shown to condensed into smaller particles than linear DNA [83,124]. Our laboratory has also demonstrated that the size of DNA condensates produced by plasmid DNA is substantially reduced if static DNA loops are incorporated into the plasmid to act as nucleation sites for condensation [54,95]. These studies suggest that the influence of DNA structure on condensation can be as great as the effects of condensing agent structure.

In this report, we describe the development of a new strategy for the compaction of short oligonucleotides into well-defined condensates. We have designed oligonucleotides with half-sliding complementary sequences [185] that self-assemble to produce duplexes with flexible sites at regular points along the double helix, in the form of single-stranded nicks and singled-stranded gaps. These nicked- and gapped-DNA duplexes were prepared by mixing equal amounts of two oligonucleotides that self-assemble into duplexes and reach lengths longer than 2 kb. The condensation behavior of nicked- and gapped-DNA are compared with the condensation of a 21-mer duplex and a

3 kb plasmid DNA by transmission electron microscopy and light scattering. Condensation studies were carried out using the trivalent cation hexammine cobalt(III), an arginine-rich peptide and two polymeric condensing agents. The peptide and polymeric condensing agents chosen for this study are each known for their ability to enhance artificial DNA delivery. The results presented here demonstrate that long nicked- and gapped-DNA duplexes generally condensed into smaller and more homogenous particles than short oligonucleotides duplexes. We also demonstrate that nicked- and gapped-DNA condenses more easily than continuous duplex DNA of comparable length. The substantial difference in the average size of nicked- and gapped-DNA condensates and those of continuous DNA duplexes demonstrate that the increased local flexibility of nicks and gaps provide both a kinetic and a thermodynamic advantage to DNA condensation. Because controlling the size of condensed DNA particles is a critical parameter for *in vivo* delivery [186], we propose that DNA with regular nicks or gaps represents a new class of nucleic acid structure that should prove useful in conjunction with a variety of non-viral mediated nucleic acid delivery systems.

2.2. EXPERIMENTAL PROCEDURES

2.2.1. Plasmid DNA Preparation

Bluescript II SK- (Stratagene, La Jolla, CA) (2961 bp), referred to as *3kbDNA* in the text, was grown in the *E. coli* cell line DH5α (Life Technologies, Carlsbad, CA) and isolated using the Qiagen Maxi-Prep kit (Valencia, CA). The circular plasmid DNA was linearized by incubation with the restriction enzyme *Hin*dIII (New England Biolabs, Beverly, MA). The linearized plasmid DNA was rinsed using a Microcon YM-30 spin

column (Millipore, Bedford, MA) five times with 5 mM Bis-Tris, 50 μM EDTA (pH 7.0) to remove excess salt introduced during restriction digestion. The DNA was then eluted from the spin column membrane with 5 mM Bis-Tris, 50 μM EDTA (pH 7.0). DNA concentration was verified spectrophotometrically.

2.2.2. Nicked-DNA, Gapped-DNA and Short DNA Duplex Preparation

To produce nicked-DNA, two 42-mer oligonucleotides were designed such that the 3' half-sequence (i.e. 21 bases at the 3' end) of one strand (N1) is complementary to the 3'-half sequence of another strand (N2), with the same being true for the 5' half-sequences of these two oligonucleotides.

```
5'-GCTGGTGAGACGACTATGAGTTCGAATGGCTTACTGACACCG-3' (N1)
                (N2) 3′-AGCTTACCGAATGACTGTGGCCGACCACTCTGCTGATACTCA-5′
```

DNA sequences were also designed to produce duplexes with short gaps at 21 bp intervals. These two 44-mer sequences, G1 and G2, were created by inserting two thymine nucleotides (TT) into the middle of the 42-mer oligonucleotide sequences.

```
5'-GCTGGTGAGACGACTATGAGTTTTCGAATGGCTTACTGACACCG-3' (G1)
                    (G2)3′-AGCTTACCGAATGACTGTGGCTTCGACCACTCTGCTGATACTCA-
5′
```

Oligonucleotides were purchased from Integrated DNA Technologies (Coralville, IA) and separated from truncation products by denaturing polyacrylamide gel electrophoresis. DNA was eluted from the gel matrix, precipitated with ethanol and then

further purified by passage over a Sephadex G-15 column (Sigma). Purified oligonucleotides were lyophilized and resuspended in dH_2O. Oligonucleotides concentrations were determined by UV-Vis spectroscopy using the following extinction coefficients: 42-mer (N1), ε_{260} = 406 700 M^{-1} cm^{-1}; 42-mer (N2), ε_{260} = 410 500 M^{-1} cm^{-1}; 44-mer (G1), ε_{260} = 422 900 M^{-1} cm^{-1}; 44-mer (G2), ε_{260} = 417 700 M^{-1} cm^{-1}.

To create nicked-DNA, oligonucletoides N1 and N2 were mixed in a buffer of 10 mM Bis-Tris, 100 μM EDTA (pH 7.0), annealed at 85°C for 5 min, and then slowly cooled to 4°C. The lengths of annealed products were determined by nondenaturing polyacrylamide gel electrophoresis.

Gapped-DNA duplexes were prepared and analyzed in the same manner as nicked-DNA, except using the oligonucleotides G1 and G2. Nicked-gapped-DNA, containing alternating nicks and gaps along the phosphate backbone, were produced by mixing and annealing equal amounts of oligonucleotides N1 and G2. The 21-mer oligonucleotide duplex used in the present study had the nucleotide sequence 5'-TCGAATGGCTTACTGACACCG-3' (complementary strand implied).

2.2.3. DNA Condensate Preparation

All solutions were filtered through Amicon Ultrafree-MC centrifugal filters with 0.22-μm pore diameter (Millipore) prior to use in condensation reactions. For light scattering and TEM experiments, condensates were prepared by mixing DNA (15 μM in bp) with an equal volume of the specified condensing agent in a buffer of 5 mM Bis-Tris, 50 μM EDTA (pH 7.0). Condensates were allowed to incubate for 5 min at room temperature before analysis by light scattering or TEM. The four condensing agents used

in this study were hexammine cobalt chloride (Sigma), poly-L-lysine (PLL) (Sigma; Mw (LALLS) 8.3 kDa), polyethylenimine (PEI) (Sigma; M_w 750 kDa) and TAT_{47-57} peptide (YGRKKRRQRRR) (Bachem). For all TEM studies with hexammine cobalt(III) as a condensing agent, 200 μM hexammine cobalt chloride was used. For condensate preparations involving the TAT peptide, PLL and PEI, the condensation reaction mixtures were prepared using appropriate concentrations of these condensing agents such that there were two positively charged nitrogens of the condensing agent for every phosphate group of DNA (at pH 7.0). Equivalents of condensing agents are defined as protonated nitrogen atoms of cationic groups of the condensing agents (For PEI, one out of the six of amino nitrogen atoms [187]).

2.2.4. Light Scattering

DNA condensation was monitored by measuring the average intensity of scattered light at a 90° scattering collection angle using a DynaPro MS/X dynamic light-scattering instrument (Proterion, Piscataway, NJ) with a laser of wavelength 824.8 nm. All light scattering measurements were performed at room temperature. Each measurement reported is the average of thirty 10s scattering intensity accumulations taken over the course of five minutes.

2.2.5. Transmission Electron Microscopy (TEM)

DNA condensate reaction mixtures were deposited on carbon-coated copper EM grids (Ted Pella, Redding, CA) and allowed to settle for 10 min. The solutions were negatively stained with aqueous (2% w/v) uranyl acetate (Ted Pella) for 1 min to enhance

contrast. The grids were rinsed with 95% ethanol and subsequently air-dried. The TEM images of DNA condensates were collected using a JEOL-100C transmission electron microscope. Images were recorded on film at 100,000× magnification. Negatives were scanned into electronic format at 300 pixels/inch, and a computer graphics program was used to measure the size of DNA condensates. The average size of the DNA condensates in each sample was calculated by measuring the diameter of a minimum of 100 particles.

2.3. RESULTS AND DISCUSSION

2.3.1. Assembly of Duplex DNA with Regularly Spaced Single-Stranded Nicks and/or Gaps

A pair of 42-mer oliogonucleotides was designed such that each was a half-sliding Watson-Crick complement of the other (sequences N1 and N2, Materials and Methods). The annealing of such oligonucleotides would be expected to produce long DNA duplexes (Figure 2.1). The backbones of these duplexes would not be continuous along either strand, but would possess nicks at every 21 bp in alternate strands. Because the synthetic oligonucleotides are not phosphorylated at their 5' ends, these nicks represent positions where a single phosphate group is missing from an otherwise continuous backbone. DNA of this composition will be referred to in the present study as 'nicked-DNA'. Similarly, a pair of 44-mer oligonucleotides was also generated in which two thymine residues were inserted into the middle of the 42-mer oligonucleotides (sequences G1 and G2, Materials and Methods). The annealing of these 44-mer oligonucleotides would be expected to produce duplex DNA with two-nucleotide gaps at 21 bp intervals along alternating strands (Figure 2.1). DNA of this composition will be referred to as

"gapped-DNA". By mixing one of the 42-mer oligonucleotides (i.e. N1) with its half-sliding complementary 44-mer (i.e. G2), it is possible to generate DNA duplexes with alternating nicks and gaps (Figure 2.1). DNA of this composition will be referred to as "nicked-gapped-DNA". In general, our approach allows for the incorporation of flexible points, in the form of nicks and/or gaps, at regular intervals into duplex polymers of significant length. This mode of nucleotide assembly also provides a means to assemble many copies of two or more oligonucleotide sequences into a volume that is defined by the persistence length of the resulting nicked/gapped-DNA polymer.

The length of nicked-DNA duplexes formed upon annealing of oligonucleotides N1 and N2 was examined by nondenaturing polyacrylamide gel electrophoresis. A 1:1 mixture of oligonucleotides N1 and N2 produced DNA assemblies with a distribution of lengths between approximately 200 bp and 2 kb, with the majority of these nicked-DNA duplexes being on the longer side of this range (Figure 2.2). The length of nicked-DNA duplexes was observed to vary directly with the stoichiometry of oligonucleotides N1 and N2. For N1:N2 ratios of 1:2, 1:3 and 1:4, where a significant excess of one strand was present, ladder-like bands appeared in the gel and the length of nicked-DNA duplexes decreased with the degree of deviation from a 1:1 ratio (Figure 2.2). The nicked-, gapped- and nicked-gapped-DNA assemblies formed from equal moles of monomer oligonucleotides, which in all cases yielded the longest assemblies (Figure 2.3), were used in the condensation experiments described below.

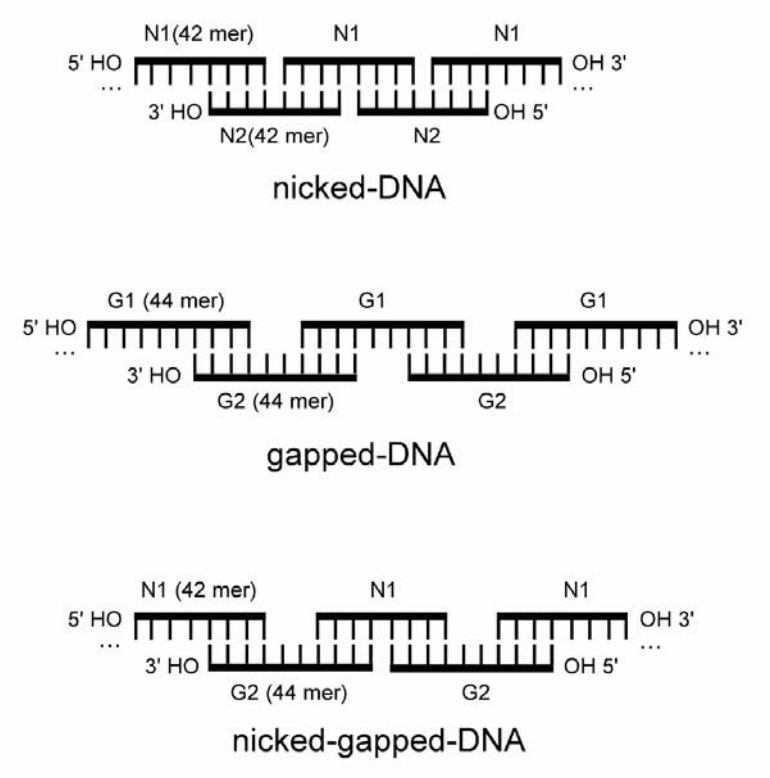

Figure 2.1. Schematic representations of DNA duplexes formed by oligonucleotides, which contain nicks and/or gaps at regular intervals. (**A**) The pairing of the 42-mer oligonucleotides N1 and N2 to produce a nicked-DNA duplex with nicks in the backbone at every 21 bp. (**B**) The formation of gapped-DNA, with 2-nt gaps at every 21 bp, by the pairing of the 44-mer oligonucleotides G1 and G2. (**C**) The formation of nicked-gapped-DNA, with alternating nicks and 2-nt gaps at every 21 bp, by the pairing of the 42-mer oligonucleotide N1 and the 44-mer oligonucleotide G2. Oligonucleotide sequences are given in Experimental and Procedures.

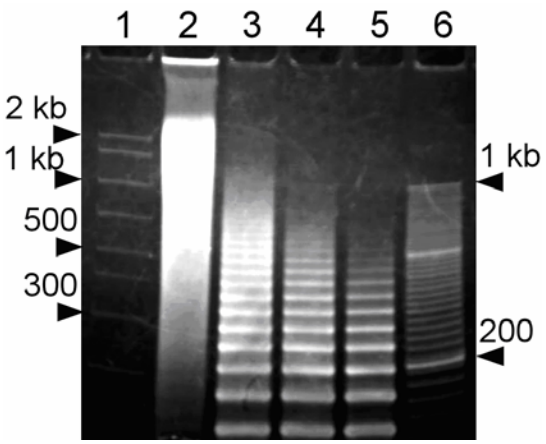

Figure 2.2. Characterization of nicked-DNA duplexes by non-denaturing polyacrylamide gel electrophoresis. Lane 1, AmpliSize molecular ruler (Bio-Rad); lanes 2-5, nicked-DNA from oligonucleotides N1 and N2 with N1:N2 strand stoichiometries of 1:1, 1:2, 1:3, 1:4, respectively; lane 6, 20 bp molecular ruler (Bio-Rad). The concentration of each oligonucleotide was 150 μM per strand. Gel was 3.5% polyacrylamide with a running buffer of 1× TBE (pH 7.9).

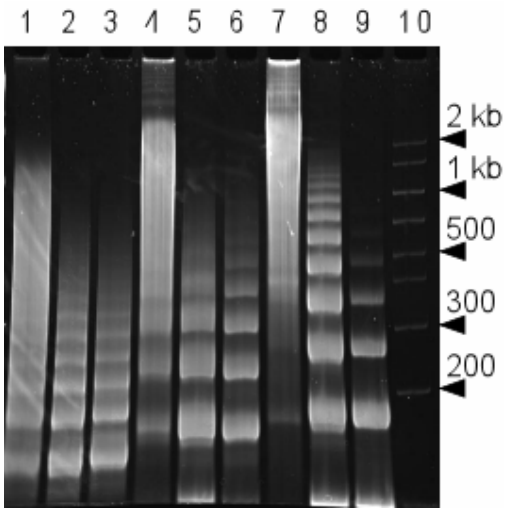

Figure 2.3. Characterization of nicked-DNA, nicked-gapped-DNA, gapped-DNA duplexes by non-denaturing polyacrylamide gel electrophoresis. Lanes 1-3, nicked-DNA from oligonucleotides N1 and N2 at strand stoichiometries of 1:1, 1:2, 1:4, respectively; lanes 4-6: nicked-gapped-DNA from oligonucleotides N1 and G2 at N1:G2 strand stoichiometries of 1:1, 1:2, 1:4, respectively; lanes 7-9: gapped-DNA from oligonucleotides G1 and G2 with G1:G2 strand stoichiometries of 1:1, 1:2, 1:4, respectively; lane 10, AmpliSize Molecular Ruler (Bio-Rad). Gel was 3.5% polyacrylamide with a running buffer of 1× TBE (pH 7.9).

2.3.2. Condensation of Nicked- and Gapped-DNA with Hexammine Cobalt Chloride

The condensation of nicked-DNA by hexammine cobalt chloride, a well-characterized DNA condensing agent [34], was compared to the condensation behavior of a short 21-mer duplex and a linear 3 kb plasmid DNA (*3kbDNA*). For this study, condensation reactions were performed by mixing hexammine cobalt chloride solutions of increasing concentrations with equal volume solutions of DNA at a constant concentration (7.5 μM in base pair after mixing). The process of DNA condensation was monitored by measuring the average light scattering intensity of the reaction mixture as a function of hexammine cobalt chloride concentration (Figure 2.4). When hexammine cobalt chloride was titrated into a solution of *3kbDNA* the average light scattering intensity of this sample increased rapidly in the low concentration regime and then reached a plateau at around 80 μM hexammine cobalt chloride (Figure 2.4). This increase in average light scattering can be attributed to the increased concentration of densely packed DNA particles [35,188-190]. The midpoint of *3kbDNA* condensation, under the conditions of our study, was at 49 μM hexammine cobalt chloride. This midpoint of condensation, and the shape of the titration profile, are consistent with earlier reports of DNA condensation under low salt conditions [89]. A similar titration of a 21-mer oligonucleotide duplex failed to produce a significant increase of light scattering intensity within the titration range, which indicates no appreciable formation of DNA condensates. This observation is consistent with earlier reports that DNA duplexes even as long as 140 bp in length are more difficult to condense with hexammine cobalt chloride than DNA that is thousands of bp in length [34]. In contrast, titration of nicked-DNA with

hexammine cobalt chloride produced a light scattering profile with a shape very similar to that of *3kbDNA*. A sigmoidal fit of scattered light intensity as a function of hexammine cobalt chloride concentration demonstrates that the nicked-DNA condenses with a midpoint of 37 μM (Figure 2.4, inset). Thus, nicked-DNA actually has a greater propensity to condense than linear duplex DNA of comparable length (i.e., *3kbDNA*), and dramatically different condensation properties when compared to the duplex 21-mer oligonucleotides. We note that the maximum light scattering intensity observed for condensed nicked-DNA is approximately half of that observed for *3kbDNA*. This result does not necessarily indicate that the nicked-DNA is in a less condensed state, as particle number and particle morphology also contribute to light scattering intensity. Hydrodynamic radius measurements based upon dynamic light scattering actually indicate that particles formed by nicked-DNA and hexammine cobalt chloride are larger than those formed by *3kbDNA* (Figure 2.5). Electron microscopy studies discussed below also confirm this to be the case. Light scattering measurements clearly indicate that the condensation of nicked-DNA by hexammine cobalt chloride is more similar to *3kbDNA* condensation than to the condensation of short duplex oligonucleotides.

The size and morphology of particles formed by the condensation of nicked-, gapped- and nicked-gapped-DNA DNA duplexes with hexammine cobalt chloride were directly analyzed using transmission electron microscopy (TEM) and compared with those formed by *3kbDNA*. Nicked-DNA condensed into ribbon-like aggregates that were around 75 nm in width, but frequently over 1 μM in length (Figure 2.6A). Gapped- and nicked-gapped-DNA duplexes produced similar ribbon-like structures when condensed by hexammine cobalt chloride (Figures 2.6B and 2.6C). Spherical particles of a size close

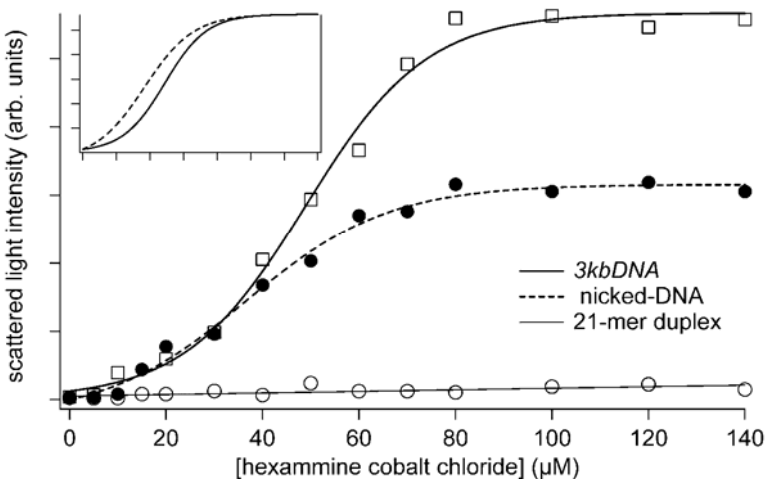

Figure 2.4. Condensation of *3kbDNA*, nicked-DNA and a 21-mer duplex by hexammine cobalt chloride, as monitored by light scattering. For each data point shown, DNA concentration was 7.5 μM in base pair (5 mM Bis-Tris, 50 μM EDTA, pH 7.0). Light-scattering intensities shown are averages from measurements taken over a 5 min period. (Insert) *3kbDNA* and nicked-DNA scattering intensities, as a function of hexammine cobalt chloride concentration, normalized to maximum observed intensity. Note: nicked-DNA condensation occurs at a lower hexammine cobalt chloride concentration than *3kbDNA*.

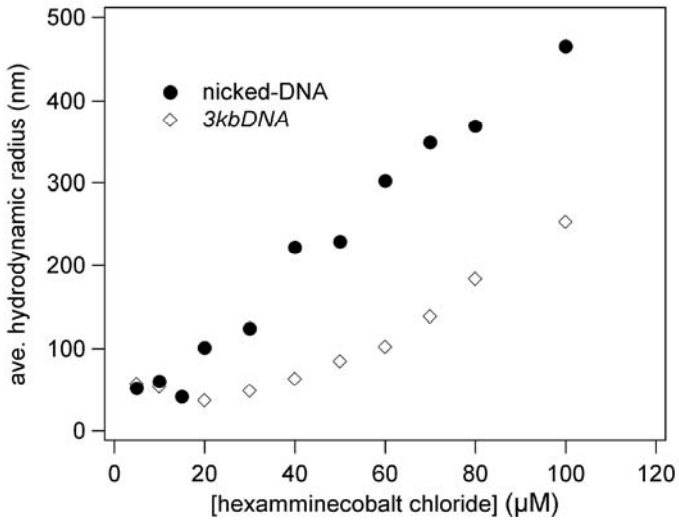

Figure 2.5. Hydrodynamic radius of nicked-DNA and *3kbDNA* condensate as a function of hexammine cobalt chloride concentration. The average hydrodynamic radius of the particles was calculated based on diffusion coefficients obtained by dynamic light scattering (Materials and Methods).

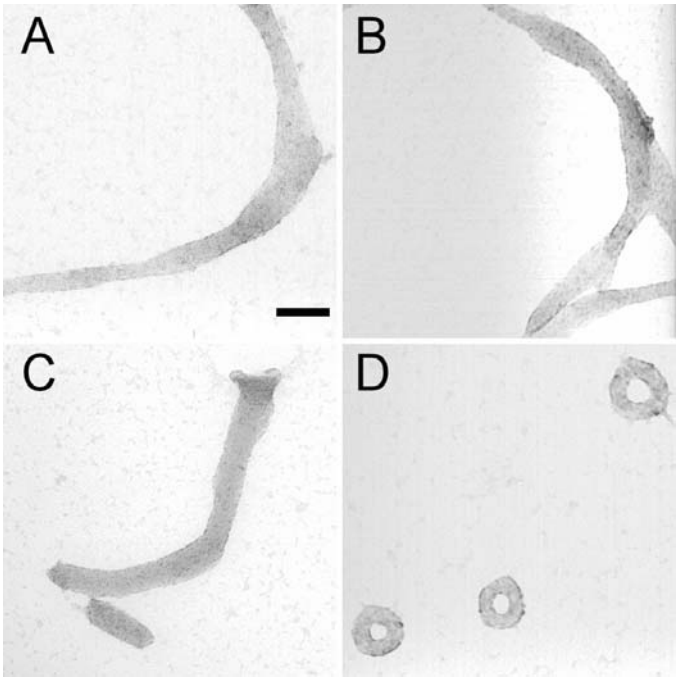

Figure 2.6. TEM images of particles formed by various DNA samples upon condensation with hexammine cobalt chloride. (**A**) Condensates formed by the nicked-DNA duplexes of oligonucleotides N1 and N2. (**B**) Condensates formed by the gapped-DNA duplexes of oligonucleotides G1 and G2. (**C**) Condensates formed by the nicked-gapped-DNA duplex of oligonucleotides N1 and G2. (**D**) Condensates formed by *3kbDNA*. For all samples, DNA was 15 μM in base pair, and condensed by mixing with an equal volume of 200 μM hexammine cobalt chloride in 5 mM Bis-Tris, 50 μM EDTA (pH 7.0). Scale bar is 100 nm.

to that typical of DNA toroids were occasionally found among the elongated ribbon-like aggregates. Under the same solution conditions, the condensation of *3kbDNA* by hexammine cobalt chloride produced toroids as the dominant morphology with a mean outer diameter of 85 nm (Figure 2.6D). This result for *3kbDNA* is consistent with the previous reports of linear plasmid DNA condensation from a low-salt buffer [95].

2.3.3. Condensation of Nicked- and Gapped-DNA by a Cationic Peptide

We also studied the condensation of DNA duplexes with multiple nicks and/or gaps by larger and more highly charged condensing agents. For these studies, condensing agents were chosen from molecules that had previously been shown to facilitate artificial gene delivery. Many cationic peptides have been reported as successful vectors for non-viral gene delivery [184,191]. Some of these peptides include naturally derived sequences that facilitate the translocation of DNA across biological membranes in the absence of any specific transporter or receptor. For example, a short peptide derived from the nuclear localization sequence (NLS) of the TAT protein, residues 47-57 (YGRKKRRQRRR), has been shown to promote the entry of nucleic acids into several different cell types [192-195]. Thus, we chose the Tat-NLS peptide as a model peptide to investigate if nicked- and gapped-DNA are condensed by a cationic peptide into a form that would be suitable for delivery.

Changing the condensing agent from hexammine cobalt chloride to the Tat-NLS peptide caused a dramatic alternation in the size and morphology of condensates formed by DNA duplexes containing nicks and/or gaps. Nicked-, gapped- and nicked-gapped-DNA duplexes all condensed into spherical particles, each with an average diameter of 45 nm (Figure 2.7A-C). The continuous *3kbDNA* was also condensed into spheres by the Tat-NLS peptide, but these particles were significantly larger with an average diameter of 65 nm (Figure 2.7D). Histograms of condensate particle diameters illustrate that distribution of particle sizes was also very similar among the three types of nicked- and gapped-DNA, and narrower for each than the distribution observed for *3kbDNA* (Figure 2.8A). We note that the 21-mer oligonucleotide duplexes (which did not condense with

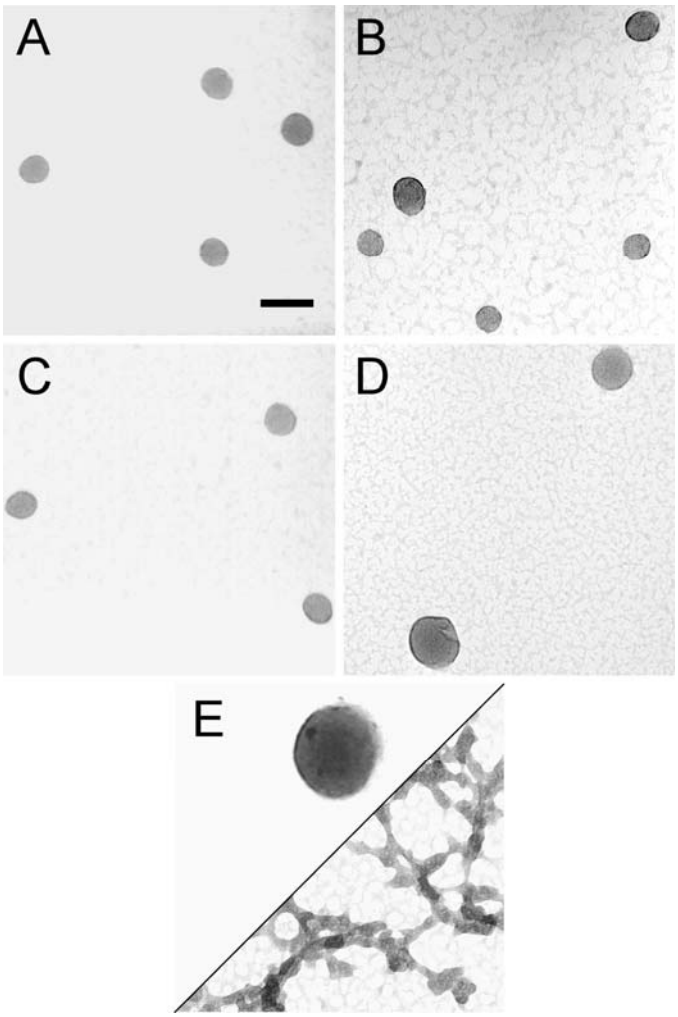

Figure 2.7. TEM images of particles formed by various DNA samples upon condensation with the Tat-NLS peptide. (**A**) Condensates formed by the nicked-DNA duplexes of oligonucleotides N1 and N2. (**B**) Condensates formed by the gapped-DNA duplexes of oligonucleotides G1 and G2. (**C**) Condensates formed by the nicked-gapped-DNA duplex of oligonucleotides N1 and G2. (**D**) Condensates formed by *3kbDNA*. (**E**) Condensates formed by 21-mer duplex. For all samples, DNA was 15 μM in base pair, and was condensed by mixing with the Tat-NLS peptide at a charge ratio of 1:2 (DNA phosphate:cationic charged group of the peptide) in 5 mM Bis-Tris, 50 μM EDTA (pH 7.0). Scale bar is 100 nm.

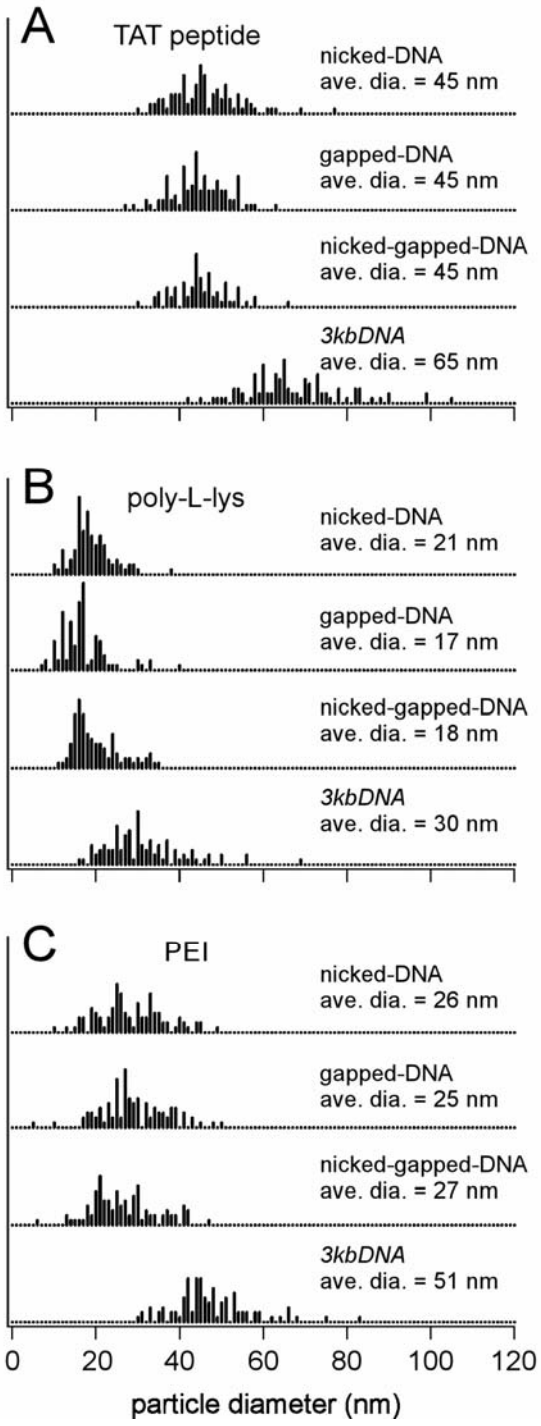

Figure 2.8. Histograms of DNA condensate diameters. Measurements were taken from TEM images similar to those shown in Figure 2.7. The DNA molecules associated with each histogram are given to the right of each. The condensing agents for the three sets of histograms are (A) Tat-NLS peptide (B) PEI and (C) PLL. The average particle diameters given in the figure are based upon measurements from at least 100 particles for each value reported. Experimental conditions for condensate formation are given in Materials and Methods.

hexammine cobalt chloride) were condensed by the Tat-NLS peptide, but much larger aggregates were observed compared to nicked- and/or gapped-DNA (Figure 2.7E). Thus, DNA with nicks and/or gaps can be condensed into smaller particles by the Tat-NLS peptide than either oligonucleotide duplexes or *3kbDNA*. The difference observed between the size and morphology of nicked- and gapped-DNA condensates when the condensing agent is changed from a trivalent cation to an eight-charged cationic peptide also illustrates the fundamental interplay between condensing agent type and DNA structure on DNA condensation.

2.3.4. Condensation of Nicked- and Gapped-DNA by PLL

We have also studied the condensation of DNA with multiple nicks and/or gaps by the much larger cationic peptide poly-L-lysine (PLL). PLL is of interest as a DNA condensing agent because it is known to enhance the cellular uptake of DNA and protect DNA from nuclease digestion [196,197]. All three types of nicked- and gapped-DNA duplexes were found to uniformly condense into small spherical particles with PLL (Figure 2.9). The average diameter of nicked-, gapped- and nicked-gapped-DNA-PLL condensates was essentially the same at 21 nm, 17 nm and 18 nm, respectively. However, *3kbDNA* under the same conditions produced appreciably larger spheres with an average diameter of 30 nm and with a somewhat greater size distribution (Figures 2.8B). Based upon an average length for our nicked- and gapped-DNA of 2 kb, the volume of a sphere with a 20 nm diameter and the previously determined packing density of condensed DNA [32], the spherical nicked- and gapped-DNA-PLL particles are the result of a single DNA polymer collapse. On the other hand, 30 nm PLL-*3kbDNA* particles are estimated to

contain 6 kb, or two strands of *3kbDNA*. The short 21-mer duplex was also condensed by PLL into well-defined spheres, but with a much greater degree of aggregation as compared to DNA with nicks and/or gaps (Figure 2.9).

2.3.5. Condensation of Nicked- and Gapped-DNA by PEI

Among the various polymeric DNA transfection agents described in the literature, polyethylenimine (PEI) has proven particularly efficient in a variety of *in vitro* and *in vivo* transfection studies [181-183]. Apart from DNA condensation and protection from nucleases, endosomal release of DNA is known to be essential for efficient transfection [198]. Among the different DNA carriers, PEI has been shown to effectively promote early release of DNA from the endosomal pathway [181]. Furthermore, additional chemical modifications can easily be introduced to the PEI molecule to enhance the target specificity without perturbing its bio-compatibility [199]. Thus, we have also investigated the condensation of DNA duplexes with multiple nicks and/or gaps by PEI. PEI condensed these DNA duplexes into spherical condensates with average diameters of 26 nm, 25 nm and 27 nm for nicked-, gapped- and nicked-gapped-DNA duplexes, respectively (Figure 2.8C). Thus, PEI condensates of nicked- and gapped-DNA are substantially smaller than condensates formed with hexammine cobalt chloride or the Tat-NLS peptide, but larger than those formed with PLL. PEI also condensed *3kbDNA* duplexes into spherical particles, however, the average diameter of the PEI-*3kbDNA* spheroids was 51 nm and with increased particle size distribution as compared to all three types of DNA duplexes with nicks and/or gaps (Figure 2.8C). Unlike PLL, PEI did not condense the duplex 21-mer oligonucleotides into discrete particles with a regular

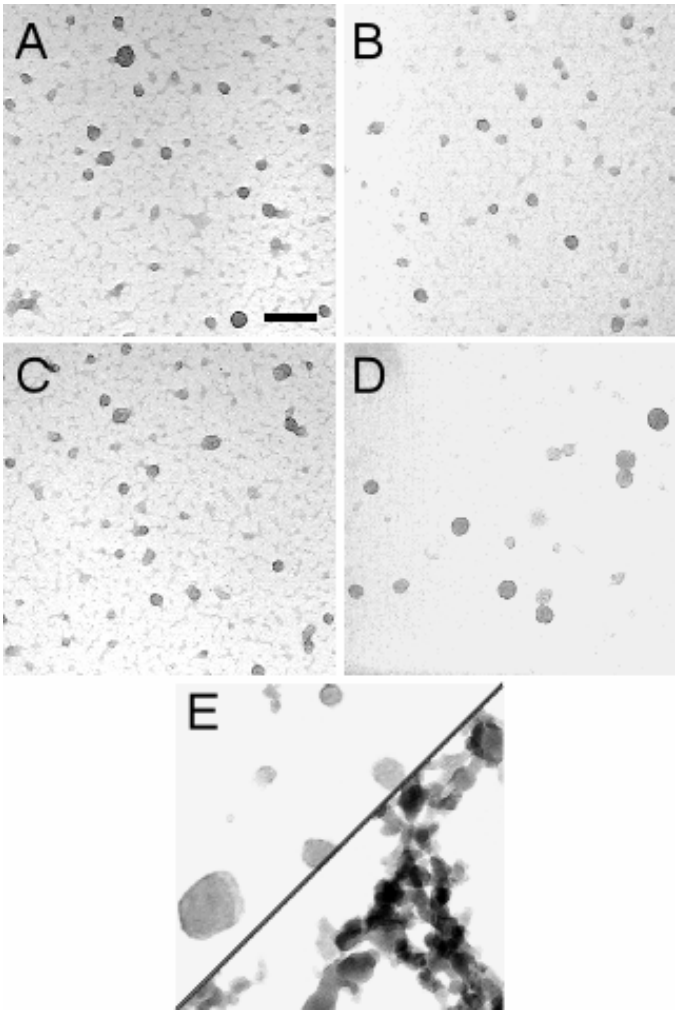

Figure 2.9. TEM images of particles formed by various DNA samples upon condensation with PLL. (**A**) Condensates formed by the nicked-DNA duplexes of oligonucleotides N1 and N2. (**B**) Condensates formed by the gapped-DNA duplexes of oligonucleotides G1 and G2. (**C**) Condensates formed by the nicked-gapped-DNA duplex of oligonucleotides N1 and G2. (**D**) Condensates formed by *3kbDNA*. (**E**) Condensates formed by 21-mer duplex. For all samples, DNA was 15 μM in base pair, and was condensed by mixing with PLL at a charge ratio of 1:2 (DNA phosphate:lysine) in 5 mM Bis-Tris, 50 μM EDTA (pH 7.0). Scale bar is 100 nm.

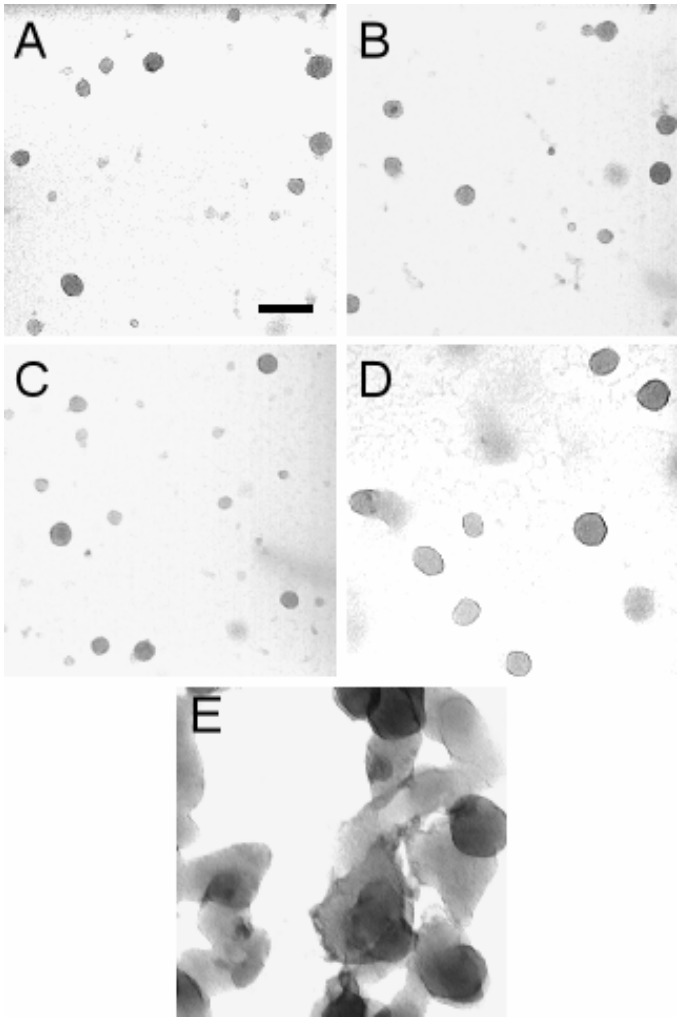

Figure 2.10. TEM images of particles formed by various DNA samples upon condensation with PEI. (**A**) Condensates formed by the nicked-DNA duplexes of oligonucleotides N1 and N2. (**B**) Condensates formed by the gapped-DNA duplexes of oligonucleotides G1 and G2. (**C**) Condensates formed by the nicked-gapped-DNA duplex of oligonucleotides N1 and G2. (**D**) Condensates formed by *3kbDNA*. (**E**) Condensates formed by 21-mer duplex. For all samples, DNA was 15 μM in base pair, and was condensed by mixing with PEI at a charge ratio of 1:2 (DNA phosphate:protonation site of PEI) in 5 mM Bis-Tris, 50 μM EDTA (pH 7.0). Scale bar is 100 nm.

morphology (Figure 2.10).

2.3.6 Nicked- and Gapped-DNA Are More Prone to Condensation than Continuous Duplex DNA

The light scattering studies reported here revealed that nicked-DNA condenses at a lower concentration of hexammine cobalt chloride than *3kbDNA* (Figure 2.4). This observation is consistent with nicked-DNA being intrinsically more prone to condensation than continuous duplex DNA of comparable length. The greater tendency of nicked-DNA to condense is most likely due to the ability of nicked-DNA to fold upon itself every 21 bp. The energetic cost associated with the introduction of sharp bends (i.e. kinks) at nicked sites would be considerably less than that associated with the tight kinking of continuous duplex DNA. In other words, the greater propensity for nicked-DNA to condense is likely due to the reduced rigidity or persistence length of nicked-DNA in comparison to continuous duplex DNA [149].

The large ribbon-like condensates produced by mixing nicked- or gapped-DNA with hexammine cobalt chloride clearly contain more DNA than a single 2 kb nicked/gapped-DNA duplex. As an illustration, if we approximate the ribbon-like structure shown in Figure 3A as a cylinder and assume hexagonal DNA packing with an inter-helix spacing of 2.8 nm [32], then this particle contains approximately 1 Mb of DNA. Given that the nicked-DNA duplexes used in this study are approximately 2 kb in length, this structure contains on the order of 50 nicked-DNA duplex molecules. The actual mechanism for the assembly of nicked- and gapped-DNA into ribbon-like structures is not clear. It is possible that the greater flexibility of nicked-DNA may allow

rearrangements to occur in the condensed state that lead to higher-order assemblies. In any case, this phenomenon is apparently particular to the condensation of nicked- and gapped-DNA when a trivalent cation, such as hexammine cobalt(III), is used as the condensing agent.

2.3.7 Nicked- and gapped-DNA Favors Small Condensates by Altering the Kinetics of Condensation

For all DNA samples of the current study, condensate size decreased as the net charge of the condensing agents increased from a trivalent to polyvalent cations. These results are consistent with the previous reports that DNA condensates tend to decrease in size as condensing agents increase in positive charge valency [200-202]. The trend to smaller particle size with greater condensing agent charge valency can be understood by considering the fact that DNA condensation is a nucleation-growth phenomenon [94,95]. Like crystal growth, if particle nucleation is rapid and the addition of molecules onto a growing particle is irreversible, then many small particles tend to form [203]. In such cases, particle growth is said to be "kinetically limited", because particle size is determined by the rate at which the bulk solution becomes depleted of free molecules from which the particles can grow. In contrast, if particle nucleation is slow and molecule addition is reversible, then a smaller number of particles grow to a much larger size. In terms of DNA condensation, condensing agents with greater charge valency are expected to more rapidly nucleate DNA condensation, and DNA condensed by such condensing agents is less likely to exchange back into solution than DNA condensed by a chemical agent of lower charge valency. Thus, like rapid crystal nucleation, condensing agents of

greater charge valency can favor the formation of smaller condensates by kinetically limiting DNA particle growth.

We have demonstrated that the condensates formed by nicked and gapped-DNA in presence of TAT peptide, PLL and PEI are smaller than those formed by continuous duplex *3kbDNA*. Our data also indicates that the spherical particles produced by nicked- and gapped-DNA in the presence of PLL result from the unimolecular collapse of nicked/gapped-DNA duplexes, whereas *3kbDNA* does not appear to form unimolecular particle under the same conditions. Together, these observations indicate that DNA with multiple nicks or gaps has a greater propensity to nucleate condensate formation than continuous duplex DNA. Single-stranded nicks and gaps in duplex DNA are known to effectively reduce the overall persistence length of a DNA polymer in solution by increasing the conformational freedom of the polymer through localized dynamic kinks [147-150,204,205]. These points of increased flexibility in nicked- and gapped-DNA would be expected to allow intra-polymer helix-helix associations that could act as nucleation sites for DNA condensate formation. As mentioned above, if DNA condensate nucleation is sufficiently rapid and essentially irreversible, then DNA condensate size can be limited by the kinetics of condensation. Since the condensates formed by nicked-, gapped- and nicked-gapped-DNA with the Tat-NLS peptide, PLL and PEI are smaller than the corresponding condensates of *3kbDNA*, the condensate nucleation sites provided by the flexible sites of nicked- and gapped-DNA apparently provide a mode of condensate nucleation that is kinetically more accessible than the nucleation structures formed by continuous duplex DNA.

The similar condensation of nicked-, gapped- and nicked-gapped-DNA is somewhat surprising, as the persistence length of nicked- and gapped-DNA duplexes have been reported to be significantly different [147,148,150,204,206,207]. Given the observation that these three types of DNA condense similarly, one might conclude that reduced persistence length does not fully account for the difference in the condensation of nicked- and gapped-DNA with respect to continuous DNA duplex. However, it is possible that the concept of DNA persistence length alone is not sufficient to describe what is observed and that the kinetics of nucleation must also be considered. Clearly, a common feature of our nicked-DNA and gapped-DNA is the propensity for sharp kinks to occur spontaneously along the helical axis [148,150,204,205]. We propose that that these kinks act as local nucleation sites for condensation and that at any given time a nicked-DNA duplex contains a sufficient number of these kinks to nucleate condensation. Gapped- and nicked-gapped-DNA may contain a larger number of these kinks, but because these sites principally act to nucleate condensation, having more kinks than nicked-DNA may not further alter DNA condensation.

2.4. CONCLUDING REMARKS

Our motivation to study the condensation of nicked- and gapped-DNA was two-fold: to acquire a more fundamental understanding of DNA condensation and to develop methods for the packaging of therapeutic oligonucleotides into discrete particles. We have described a new method for the efficient condensation of DNA oligonucleotides into discrete particles. By assembling oligonucleotides into long nicked or gapped duplexes, the condensation of short oligonucleotides into well-defined particles can be achieved

with various condensing agents. As noted above, efficient condensation of DNA into nanometer-scale particles correlates strongly with enhanced DNA delivery to living cells [166,200,208]. Thus, based on this criterion, the small particles produced by the self-assembly of oligonucleotides into long DNA duplexes with regularly spaced nicks or gaps represent promising vectors for oligonucleotide delivery. Nevertheless, we acknowledge that the utility of our approach for cellular delivery must still be proven by actual delivery studies.In addition, we have provided one more illustration of the interplay that exists between DNA structure and condensing agent structure on the size and morphology of condensates. The introduction of dynamic kinks in the nucleic acids structure represents a simple way to introduce nucleation sites that kinetically favor the formation of small, uniform condensates. The results presented also provide addition support to earlier proposals that nucleation can be a defining step in the determination of condensate size [54,81,95].

The simple strategy presented here should be readily amenable to further studies that aim to use short oligonucleotides to block viral or cellular disease-causing genes. In addition to facilitating the condensation of oligonucleotides, appending nicked- or gapped-DNA onto one end of a continuous gene-length DNA could provide nucleation sites for condensation. This might be a way to promote the condensation of gene-length DNA into small spherical particles, as we have previously shown that the incorporation of static loops into a 3 kb long DNA kinetically favors condensation into toroids with reduced dimensions [54,81,95]. Whether these improvements in DNA condensation result in enhanced gene/oligonucleotide transfer to target cells must ultimately be addressed directly by *in vitro* and *in vivo* gene delivery experiments.

CHAPTER 3

BACTERIAL PROTEIN HU DICTATES THE MORPHOLOGY OF DNA CONDENSATES PRODUCED BY CROWDING AGENTS AND POLYAMINES

3.1. INTRODUCTION

Multivalent cations and molecular crowding agents can cause DNA to collapse from solution into well-defined nanometer-scale particles [29,36,47,57,81]. This phenomenon of DNA condensation has been studied for many years as a model of high density DNA packing in living systems, particularly in sperm cells and viruses [3,22,25,28]. More recently, efforts to enhance artificial gene delivery for the improvement of gene therapies have generated substantial interest in the development of methods to control the size and shape of DNA condensates [151,153,154]. The principal morphologies of DNA condensates formed *in vitro* are toroids, rods and spheroids. Toroidal condensates are the predominant morphology observed under many experimental conditions, and have historically received the most attention.

We have recently demonstrated that the size of toroidal DNA condensates can be controlled by solution conditions and by static DNA loops that act as nucleation sites for toroid formation. Such loops can significantly decrease the average diameter of toroidal condensates [54,94,95]. Monovalent and divalent salt concentrations have also been shown to affect the size and thickness of DNA toroids [94,95]. In contrast, controlling the

morphology of DNA condensates between toroids and rods is largely an unexplored problem. Bloomfield and co-workers have demonstrated that condensation of DNA with me_8-spermidine (a derivative of spermidine with methylated amines), or with other condensing agents in water-alcohol mixtures, increases the population of rod-like condensates [1,41,47,86]. However, a general method for obtaining complete control over condensate morphology for a range of condensing agent structure and solution conditions has not been previously reported.

We have hypothesized that some natural proteins active in DNA condensation could be adapted to gain further control over DNA condensation *in vitro*. Protamines, which package DNA in vertebrate sperm cells, are obvious candidates because sperm cell chromatin represents one of the most highly condensed forms of DNA found in nature [16,209-211]. The DNA condensing properties of protamines have been the subject of numerous investigations [22,211-214], and have been used for artificial gene delivery [215-217]. Our laboratory has recently demonstrated that cysteine-rich mammalian protamines readily condense DNA into spherical particles that are salt-stable [218]. Nevertheless, sperm cell proteins represent only one possible class of proteins to aid the control of DNA condensation *in vitro*.

Prokaryotic cells contain a set of proteins that bind DNA and are associated with the nucleoid. Among these proteins, HU has been characterized as the most important protein for structural organization of the bacterial chromosome. For example, the lack of HU in the *hupAhupB* mutant results in decondensed nucleoids and anucleate cells [139,219-221]. In *E. coli*, HU exits predominantly as a 20 kDa heterodimer composed of two subunits, HUα and HUβ encoded by the *hupA* and *hupB* genes. While HU was

initially characterized as the bacterial equivalent of histones, more recent studies have revealed that the main role of HU in a number of cellular processes is that of a DNA architectural protein that bends DNA in a non-sequence specific manner [134,222-225]. Thus, HU appears to be more similar in function to the HMG proteins of eukaryotes than it is to histones [139,226-228]. The structure of *Anabaena* HU in a co-crystal with DNA revealed that conserved prolines of HU intercalate between the bases of DNA from the minor groove to induce pronounced kinks in the double helix [131]. The crystal structure reveals that the HU-induced bend angle in DNA is as great as 105º to 140º [131]. However, these HU-DNA co-crystals contained DNA with both mismatched and unpaired bases. Solution state studies with un-nicked DNA support a bend angle of approximately 60° [229,230]. Measurements of DNA bending by HU also vary because HU-DNA complexes form flexible hinges which can accommodate a range of different bend angles [131,133,231].

In the present study we have investigated the effects of HU on the process of DNA condensation *in vitro*. HU does not, by itself, cause DNA to condense into high density particles. Furthermore, HU has been shown previously by *in vitro* assays to only moderately decrease the concentration of macromolecular crowding agents required to condense DNA [232,233]. These previous experiments did not explore the potential role of HU in shaping the morphology of condensed DNA. Here we report that HU causes a substantial change in the preferred morphology of DNA condensates formed upon the addition of molecular crowding agents or polyamines. The results presented provide additional support that local alterations in nucleic acid structure can be used to control both the size and morphology of DNA condensates [54,95,234]. To the best of our

knowledge, this is the first report of controlling DNA condensation with a protein that does not by itself condense DNA into high density condensates. The results presented here are also suggestive of how HU may work in some capacity as an architectural protein in the compaction of the bacterial chromosome *in vivo*.

3.2. EXPERIMENTAL PROCEDURES

3.2.1. DNA Preparation

Bluescript II SK- (Stratagene) plasmid was isolated from the *E. coli* strain DH5-α (Life Technologies) using the Qiagen maxi-prep kit (Valencia, CA), and linearized by digestion with the restriction endonuclease *Hin*dIII (New England Biolabs). Following enzymatic digestion, the DNA was rinsed at least five times with 1× TE (10 mM Tris, 1 mM EDTA, pH 7.8) using a Microcon-YM 30 spin column (Millipore) to remove salts and buffers from the restriction digest. The DNA was finally resuspended from the spin column in 1× TE. DNA concentration was verified spectrophotometrically. Bluescript II SK- plasmid is abbreviated as "linear DNA" throughout the text. Supercoiled Bluescript II SK- plasmid, obtained directly from the plasmid isolation procedure, was determined to be more than 90% supercoiled based on agarose gel electrophoresis analysis. Supercoiled DNA was also rinsed at least five times with 1× TE to ensure that the buffer conditions of all DNA stock samples were identical.

3.2.2. HU Protein

HU protein was isolated and purified from *E. coli* strain RLM1078 following a procedure previously described by Wojtuszewski *et al*. [235]. To eliminate a

contaminating nuclease, isolated HU protein was further purified on an FPLC MonoS 5/5 or 10/10 cation exchange column (Amersham-Pharmacia). The column was developed with a 0.05 to 1.0 M linear NaCl gradient and HU eluted at 0.35 M NaCl. The lack of nuclease activity was verified by the absence of digested products after incubating plasmid DNA with the protein. The extinction coefficient at 230 nm of 37.5 $mM^{-1}cm^{-1}$ was used to calculate HU protein concentration [235].

3.2.3. Preparation of DNA Condensates

PEG-induced DNA condensates were prepared by mixing solutions of DNA and PEG 8000 to yield a final reaction mixture 5 μM DNA bp (given in units of base pair throughout), 125 mg/ml PEG 8000, 50 mM Tris-HCl (pH 7.8), 1 mM EDTA, 100 mM NaCl. The condensate reaction mixtures were allowed to equilibrate at room temperature for 20 min before depositing on grids. For PEG-induced condensates prepared in the presence of HU, HU was introduced to the DNA at three different points in the condensation process: (1) DNA was condensed with solutions of PEG containing HU for 20 min (HU during condensation); (2) DNA was incubated with HU for 10 min and then condensed with PEG for 10 min (HU before condensation); (3) HU was incubated for 10 min after DNA had been condensed by PEG for 10 min (HU after condensation). In all cases, the reaction mixtures were allowed to equilibrate at room temperature for 20 min before depositing on grids, and final condensate solutions were all 5 μM DNA bp, 125 mg/ml PEG 8000, 50 mM Tris-HCl (pH 7.8), 1 mM EDTA, 100 mM NaCl.

Spermidine-induced condensates were prepared by mixing solutions of DNA and spermidine to yield a condensation reaction mixture of 5 μM DNA, 700 μM spermidine,

0.33× TE (pH 7.8), 15 mM NaCl. The same protocol was followed for the preparation of spermine-induced condensates, in which DNA was mixed with spermine to yield a condensation reaction mixture of 5 μM DNA, 15 μM spermine, 0.33× TE (pH 7.8), 15 mM NaCl. For spermidine and spermine DNA condensation in the presence of HU, the same three protocols were followed as described above for the condensation of DNA by PEG in the presence of HU (i.e. HU before, during and after condensation).

3.2.4. Electron Microscopy and Analysis of DNA Condensates

A 5 μl aliquot of each DNA condensate reaction mixture was deposited directly onto a carbon-coated electron microscopy grid (Ted Pella, Redding, CA). After allowing condensates to settle onto the grid for 15 min, 2% uranyl acetate was added to the grid for 2 min, and then the grid was rinsed in 95% ethanol and air-dried. The condensates prepared with PEG 8000 were rinsed in 20% ethanol to reduce the deposition of PEG aggregates. The size and morphology of DNA condensates were examined using a JEOL-100C transmission electron microscope (TEM). To obtain the relative toroid and rod populations in each sample, the grid surface was randomly scanned and the number of unaggregated toroids and rods visible on the viewing screen were counted. Several hundred structures were counted for each grid. Each measurement reported is the average of the counts from three different grid preparations. Images were acquired at 100,000× magnification and film negatives were scanned into digital format at 300 pixels/inch. A computer graphics program was used to measure the dimensions of individual condensates for each sample.

3.3. RESULTS AND DISCUSSION

3.3.1. HU Governs the Morphology of Condensates Formed Under Molecular Crowding Conditions

The addition of PEG 8000 to a sample of linear DNA at physiological ionic strength causes the condensation of DNA into toroidal and rod-like particles (Figure 3.1A, B). The mean outer diameter of toroids was 199 nm (σ, ±94 nm) with a mean thickness of 71 nm (σ, ±39 nm). The average length of rods was 386 nm (σ, ±81 nm) with a mean thickness of 95 nm (σ, ±27 nm). The relative populations of rods and toroids measured under the PEG-induced condensation conditions were 83% toroids and 17% rods.

When the protein HU was added along with PEG to DNA a definitive shift was observed in condensate morphology from toroids to rods as a function of HU concentration (Figure 3.1C). A plateau in relative rod population was reached around 250 nM HU (in units of HU dimer). At this HU concentration, and up to at least 400 nM HU, rods represent 75% of the condensates tallied. The midpoint between the initial rod population and that of the plateau occurs at an HU concentration of 80 nM. Given that the DNA concentration for these experiments was 5 μM in bp, and that the binding site for HU is one HU dimer per 9 DNA bp, the concentration of HU required to cause the observed change in condensate morphology is less than that which would be required to fully load the DNA (ca. 560 nM HU). The number of HU molecules necessary to control DNA condensate morphology was actually found to be significantly less than full loading (*vide infra*).

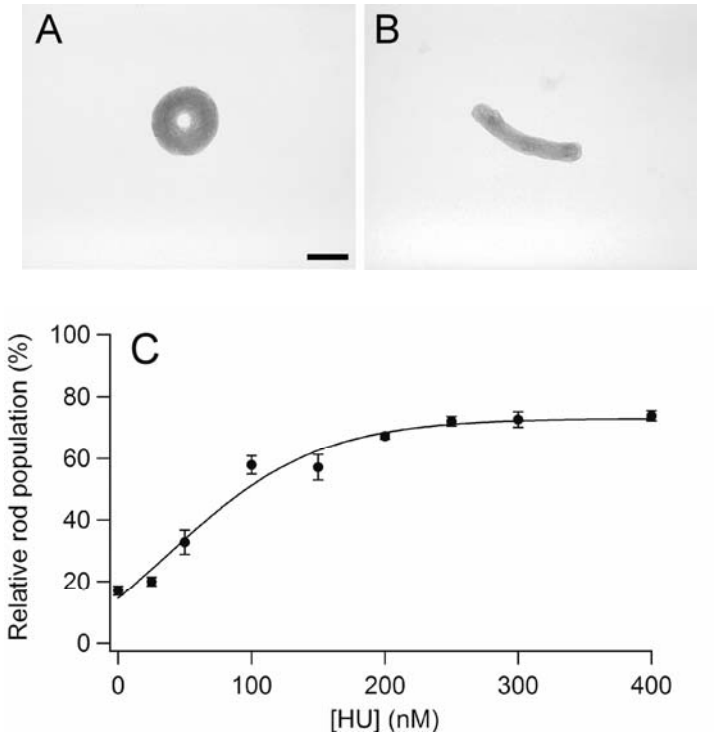

Figure 3.1. PEG-induced DNA condensate morphologies and morphology statistics as a function of HU concentration. (A) TEM image of a representative condensate of linear DNA condensed by PEG 8000 (no HU present). (B) TEM image of a representative condensate produced under identical conditions as in A, except in the presence of 200 nM HU. Scale bar is 100 nm. (C) Relative rod populations versus HU concentration for linear DNA condensed by PEG. Samples were 5 μM DNA bp, 125 mg/ml PEG 8000, 50 mM Tris-HCl, 1 mM EDTA (pH 7.8), 100 mM NaCl, and indicated concentrations of HU dimer. Each rod population measurement reported is the average of counts from three different EM grid preparations.

The addition of HU alone to DNA (i.e. in absence of PEG) was not observed to condense DNA into densely packed particles, even up to an HU concentration of 400 nM Furthermore, the DNA toroids and rods produced by PEG in the presence of HU are similar in size to those produced by PEG alone. Thus, HU apparently functions primarily as an architectural protein in condensation reactions rather than as either a strong protagonist or antagonist of DNA condensation, at least for the range of HU concentrations studied here.

We note that PEG 8000 (without DNA or HU) was observed to form globule structures under the same solution conditions and EM grid preparation procedure (Materials and Methods). PEG 8000 did not produce particles with toroidal or rod-like morphologies. Thus, the statistics reported for PEG-induced DNA condensate morphology accurately represent the relative populations of toroids and rods. However, it cannot be ruled out that the globule structures observed when DNA is condensed by PEG do not contain any condensed DNA. This caveat does not apply to the other condensation protocols presented below, because the polyamine condensing agents did not produce any particles on the EM grids when DNA was not present.

3.3.2. HU Governs the Morphology of Spermidine-DNA Condensates

When linear DNA of 3 kb in length or greater is condensed from solution by a wide variety of cationic molecules (e.g. polyamines, poly-lysine, protamines) the resulting condensate particles are mostly toroids, with the remaining particles being almost entirely rods [29,33,36,47,213,236]. Under our experimental conditions, spermidine condensed linear 3 kb DNA into 97% toroids and only 3% rods. To elucidate the effect of HU on DNA condensation by polyamines, the morphology of spermidine-induced condensates was examined as a function of HU concentration. As shown in Figure 3.2, HU also causes a significant increase in the population of rod-like condensates for linear DNA (5 μM bp) when condensed by spermidine (700 μM). Specifically, the relative population of rod-like condensates increases from 3% rods (in the absence of HU) to greater than 90% rods in the presence of 50 nM HU, with the half maximum rod population being observed at 15 nM HU (Figure 3.2E).

DNA toroids produced by spermidine-induced condensation were of similar dimensions to those produced by PEG-induced condensation, with a mean outside diameter of 250 nm (σ, ±22) and a mean thickness of 82 nm (σ, ±12 nm), but with smaller standard deviations in these dimensions. DNA rods produced by spermidine-induced condensation in the presence of HU exhibited an overall mean length of 450 nm and a mean width of 78 nm for all HU concentrations investigated. Rod length and thickness proved to be relatively insensitive to HU concentration. For example, rods formed in the presence 100 nM HU and 200 nM HU were the same size within experimental variation, i.e. mean rod length of 458 nm (σ, ±46 nm) vs. 450 nm (σ, ±61 nm), and mean rod thickness of 76 nm (σ, ± 4 nm) vs. 82 nm (σ, ±16 nm), respectively. We note that these mean thicknesses are also the same, within experimental error, for toroids and rods observed in absence and presence of HU. These observations demonstrate that HU does not significantly affect the dimensions of condensates produced by spermidine, only the relative population of rods. Thus, HU can act as a guide for DNA condensate morphology for both crowding-induced and polyamine-induced condensation. We note that HU causes a similar morphology shift for condensates formed by another commonly used tri-cationic DNA condensing agent, hexammine cobalt (III) (data not shown).

3.3.3. HU and Supercoiling Work Together to Promote the Formation of Rod-Like Condensates

It is known that supercoiling of DNA can provide high affinity binding sites for HU [237]. To explore the possibility that HU can work in conjunction with supercoiling

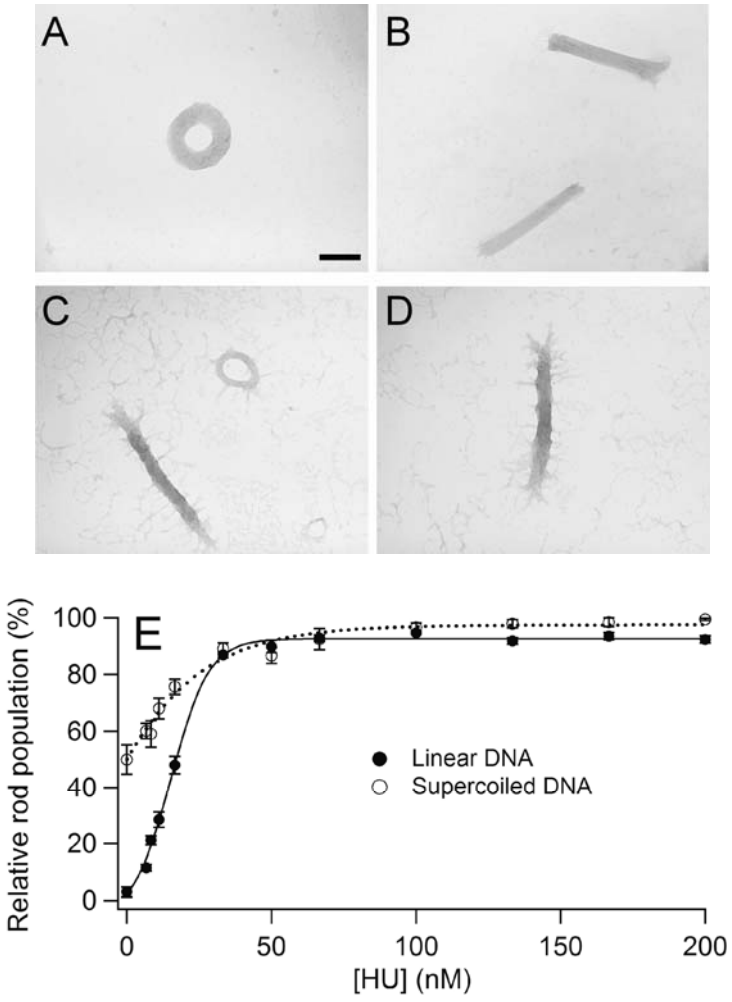

Figure 3.2. Spermidine-induced DNA condensates morphologies and morphology statistics as a function of HU concentration. (A) TEM image of a representative condensate of linear DNA condensed by spermidine (no HU present). (B) TEM image of representative condensates produced under identical conditions as in A, except in the presence of 50 nM HU. (C) TEM image of representative condensates of supercoiled DNA condensed by spermidine (no HU present). (D) TEM image of a representative condensate produced under identical conditions as in C, except in the presence of 50 nM HU. Scale bar is 100 nm. (E) Relative rod populations versus HU concentration for linear and supercoiled DNA condensed by spermidine. Samples were 5 μM DNA bp, 700 μM spermidine chloride, 0.33×TE (pH 7.8), 15 mM NaCl, and indicated concentrations of HU dimer.

to govern DNA condensate morphology, we investigated the condensation of supercoiled DNA as a function of HU concentration. For these particular studies we chose to use spermidine-induced condensation because, as mentioned above, the statistics for DNA condensate morphology were potentially more accurate than those obtained for PEG-induced condensation. Additionally, the dimensions of rods and toroids were more uniform for the spermidine condensation reaction, which arguably makes rod versus toroid population statistics more relevant with regards to the amount of DNA condensed into each of these two morphologies.

The condensation of supercoiled DNA by spermidine (in the absence of HU) produces a greater population of rods than linear DNA, i.e. 50% vs. 3%, respectively (Figure 3.2). The addition of HU along with spermidine to supercoiled DNA again resulted in a concentration-dependent increase in the population of rods (Figure 3.2E). We observed that this combination of HU and superhelical stress increases the population of DNA rods to at least 99% at 100 nM HU (5 μM DNA bp; 700 μM spermidine), which is greater than the maximum rod population observed with linear DNA. The half maximum rod population was observed at 15 nM HU dimer, which is similar to that observed for linear DNA condensed by spermidine. Thus, HU and superhelical stress apparently work together to increase the population of rod-like condensates, and the effect of HU on DNA condensation is not fundamentally different for linear versus supercoiled DNA.

The role of HU in controlling DNA condensate morphology, rather than as a true condensing agent, is again illustrated by the similar condensate structures observed for supercoiled DNA in the absence and presence of HU. Under the conditions of our study,

the rod-like condensates of supercoiled DNA condensed by spermidine exhibited thin fibril structures extending out from the main mass of the condensate (Figure 3.2C, D). We have previously shown that such structures indicate the existence of partially condensed DNA that collapses into fibrils upon preparation of EM grids [94]. Slight changes in condensation conditions (e.g. ionic strength, temperature, sample dilution) can cause the appearance or disappearance of such fibrils [94]. Thus, the coexistence of these fibrils on DNA condensates prepared in samples that only differ by the presence of HU is another strong indication that HU does not significantly promote or hinder DNA condensation at the protein concentrations used in this study. We note that fibrils extending from DNA condensates are not particular to supercoiled DNA, but are also observed for condensed linear DNA depending upon specific sample conditions [94].

3.3.4. HU Governs the Morphology of Spermine-DNA Condensates

Condensation reactions similar to those described above were also performed with linear DNA and the tetracation spermine to further explore the possibility that guiding DNA condensation is a general property of HU, regardless of condensing agent. Similar to spermidine, when linear DNA was condensed by spermine the majority of particles formed were well-defined toroids with a minor population of rods (97% toroids, 3% rods) (Figure 3.3).

DNA condensed by spermine also exhibited a gradual increase in the percentage of rod-like condensates as a function of HU (Figure 3.3C). A maximum plateau for rod population of approximately 90% was observed near 200 nM HU, with the half maximum population observed at 60 nM HU. Thus, HU is somewhat less effective in

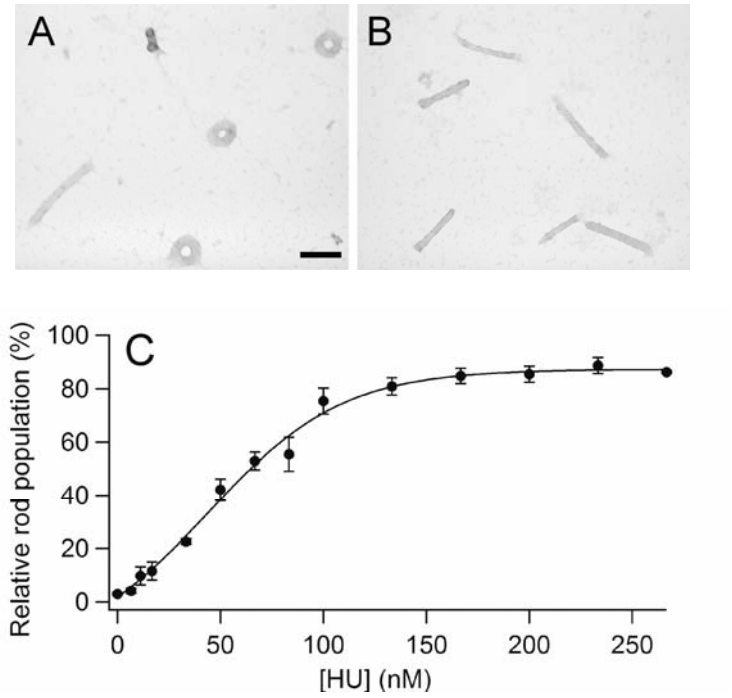

Figure 3.3. Spermine-induced DNA condensate morphologies and morphology statistics as a function of HU concentration. (A) TEM image of representative condensates of linear DNA condensed by spermine (no HU present). (B) TEM image of representative condensates produced under identical conditions as that shown in A, except in the presence of 100 nM HU. Scale bar is 100 nm. (C) Relative rod populations plotted as a function of HU concentration for linear DNA condensed by spermine. Samples were 5 μM DNA bp, 15 μM spermine chloride, 0.33×TE (pH 7.8), 15 mM NaCl and indicated concentrations of HU dimer.

controlling the condensates formed by spermine in comparison to spermidine (a polyamine with one less charge).

In contrast to the condensates formed in the presence of PEG or spermidine, the condensates formed by spermine are considerably smaller (Figure 3.3A, B). Toroids had a mean outside diameter of 102 nm (σ, ±12 nm) and a mean thickness of 34 nm (σ, ±6 nm). The overall mean length and thickness of spermine-DNA rods, 215 nm and 28 nm, respectively, for all samples was also considerably smaller than those produced by PEG or spermidine. These condensate dimensions did not change significantly with increasing

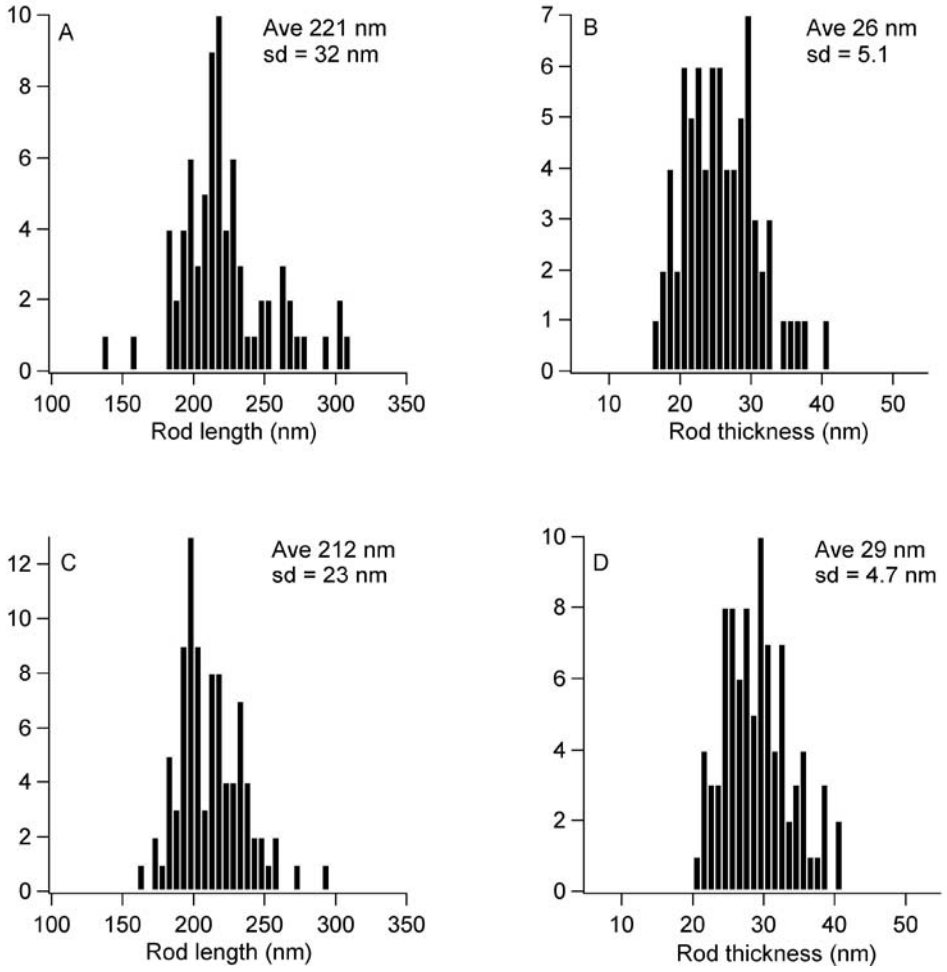

Figure 3.4. Histograms of spermine-induced rod dimensions formed in presence of different HU concentrations. Rod dimensions were compared after linear DNA (5 μM in base pair) were condensed by 15 μM spermine in 15 mM NaCl at (*A*-*B*), 100 nM of HU, (*C*-*D*) 200 nM HU. Rods at 100 nM HU: (*A*) length, average 221 ± 32 nm; (*B*) width, average 26 ± 5 nm. Rods at 200 nM HU: (*C*) length, average 212 ± 23 nm; (*D*) width, average 29 ± 5 nm.

HU concentration. For example, at 100 nM HU the mean rod length was 221 nm (σ, ±32 nm) and the mean rod thickness was 26 nm (σ, ±5 nm), compared to 212 nm (σ, ±23 nm) and 29 nm (σ, ±5 nm), respectively, at 200 nM HU (Figure 3.4). The similar dimensions for spermine-DNA condensates formed in the absence and presence of HU again demonstrates the general ability for HU to guide DNA condensate morphology without significantly altering condensate size. The small change observed in condensate size with increasing HU concentration is even less significant when one considers the much greater difference in rod lengths that are associated with different condensing agents.

3.3.5. How Many HU Proteins Are Necessary to Guide the Condensation of a DNA Molecule?

DNA condensed by spermidine appeared to be the most practical system of those presented here from which to determine the minimum number of HU proteins necessary to guide DNA condensation. A series of condensation experiments was conducted in which the concentration of linear DNA was increased above 5 μM bp (i.e. the concentration used in all other experiments). For these experiments HU concentration was fixed at 67 nM and spermidine concentration at 700 μM. This concentration of HU was chosen because it represents a point at which the rod population was within the plateau region (Figure 3.2E). At the initial concentrations of 5 μM DNA bp and 67 nM HU there is the potential to bind at most one HU dimer per 75 bp. Our analysis by EM did not reveal any reduction in rod population when DNA concentration was increased to 15 μM bp, at which point there could be no more than one HU dimer bound per 225 bp. In a condensation reaction where the DNA concentration was increased to 20 μM bp (i.e.

1 HU dimer per 300 bp), the rod population exhibited the first appreciable decrease to approximately 80%. However, at this concentration of DNA the condensates began to aggregate, which did not allow for the collection of precise morphology statistics. At DNA concentrations higher than 20 μM bp condensate aggregation became even worse. Thus, within the limits of these experiments, our results demonstrate that *at most* one HU dimer is required per 225 bp to guide spermidine-DNA condensates into rod-like structures. This ratio could be smaller, as this estimate assumes that all HU is bound to DNA that is condensed in the rod-like condensates.

For DNA rods 450 nm in length, one 180° bend occurs in the DNA helix approximately every 1300 bp. It is known that HU binds more tightly to bent DNA [229,238,239], so it is reasonable to hypothesize that HU proteins would be localized at the end regions of rods. As mentioned above, HU can stabilize DNA bend angles that range from 60 to 140° [131,133,229-231]. Thus, at most three HU dimers would be expected to localize at each DNA bend within a spermidine-DNA rod. This estimate translates to a maximum of one HU dimer per 430 bp. Our determination that not more than one HU dimer is required per 225 bp is within a factor of two of this simple theoretical estimate. Our observation that rod populations begin to decrease at a ratio of 1 HU per 300 bp (at 67 nM HU) is also in reasonable agreement with our estimate for the maximum number of HU dimers bound per rod.

Our determination that 67 nM HU will guide the condensation of DNA by spermidine into almost exclusively rod-like structures at a ratio of 1 HU dimer per 225 DNA bp also has important implications regarding the observed initial increase in rod population as a function of HU concentrations below 50 nM HU (Figure 3.2E). In

particular, the same ratio of HU to DNA bp does not result in the formation of more than 66% rods for a DNA concentration of 5 μM bp and an HU concentration of 22 nM (Figure 3.2E). Thus, for DNA samples 5 μM in bp and HU concentrations below approximately 50 nM the ability for HU to guide DNA condensation is not simply limited by the number of HU molecules present in the sample but apparently by the number of HU molecules actually bound to DNA (i.e. association constant limited). This conclusion is also supported by a set of experiments in which relative rod populations were measured for HU concentrations from 0 to 50 nM with a reduced DNA concentration was of 2.5 μM bp. Rod populations were found to be the same as those measured for DNA at 5 μM bp (data not shown), which also indicates that rod populations are governed by the HU-DNA association constant for HU concentrations below 50 nM, rather than simply the ratio of HU to DNA present in the samples.

The HU-DNA disassociation constant (K_d) for the salt conditions of the condensation experiments carried out with spermidine was previously determined to be 400 nM [240]. However, it is not currently possible to establish a complete equilibrium description of HU association with DNA in the presence of spermidine, as the possibility exists that HU binds more tightly to the sharp bends within a rod-like condensate than free DNA in solution.

3.3.6. Order of HU Addition Affects Condensation Morphology Statistics

We have previously shown that DNA condensate size and morphology is affected differently by chemical agents that alter DNA structure if these agents are added to DNA before, during (i.e. coincident) or after the addition of a condensing agent [94]. For

example, order-of-addition studies provided important clues regarding how Mg^{2+} (which promotes helix-helix contacts) influences the different stages of DNA condensation (i.e. nucleation, proto-toroid formation and equilibrium growth) [94]. The results presented above that reveal the effects of HU on DNA condensation were from experiments in which HU was added to DNA coincident with the condensing agents. As a means to gain insight into the stages at which HU controls the morphology of DNA condensates we have also performed experiments in which HU was added before or after the addition of each condensing agent.

When HU was incubated with DNA prior to condensing agent addition an increase in rod population was also observed for condensation by PEG/NaCl, spermidine and spermine (Figure 3.5). However, for all three condensing conditions, and for supercoiled DNA, a higher concentration of HU was required to achieve the same rod population measured when HU was added coincident with the condensing agent (Figure 3.5). The addition of HU to a PEG-DNA solution after condensation had occurred resulted in an even lower percentage of rod-like condensates. For example, an HU concentration of 400 nM resulted in an increase in rod population to 44% (data not shown), as compared to the 70% rod population observed when 400 nM HU was added before or during condensation by PEG (Figure 3.5). For condensates prepared with spermidine or spermine in the absence of HU, no apparent increase in rod population was observed when HU was added up to a concentration of 400 nM to solutions containing the pre-formed DNA-polyamine condensates.

The difference in rod populations observed for experiments in which the same concentration of HU was added before or coincident with condensation versus after

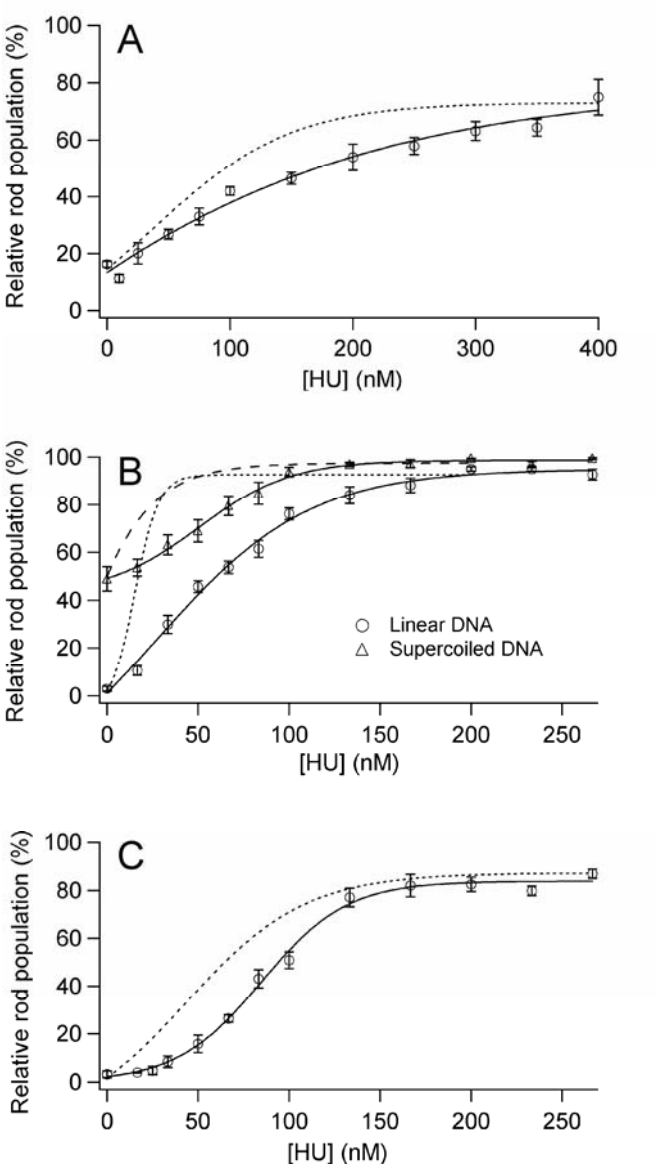

Figure 3.5. Condensate morphology statistics versus HU concentration for reactions with HU added to DNA before condensation. (A) Relative rod populations versus HU concentration for linear DNA condensed by PEG. Samples were 5 μM DNA bp, 125 mg/ml PEG 8000, 100 mM NaCl, 50 mM Tris-HCl, 1 mM EDTA (pH 7.8), and indicated concentration of HU dimer. (B) Relative rod populations versus HU concentration for linear (circle) and supercoiled DNA (triangle) condensed by spermidine. Samples were 5 μM DNA bp, 700 μM spermidine chloride, 0.33×TE (pH 7.8), 15 mM NaCl and indicated concentrations of HU dimer. (C) Relative rod populations versus HU concentration for linear DNA condensed by spermine. Samples were 5 μM DNA bp, 15 μM spermine chloride, 0.33×TE (pH 7.8), 15 mM NaCl and indicated concentrations of HU dimer. Dashed curves are best-fit curves from rod populations measured for corresponding experiments in which HU was added coincident with the condensing agent (see Figures 1-3 for details).

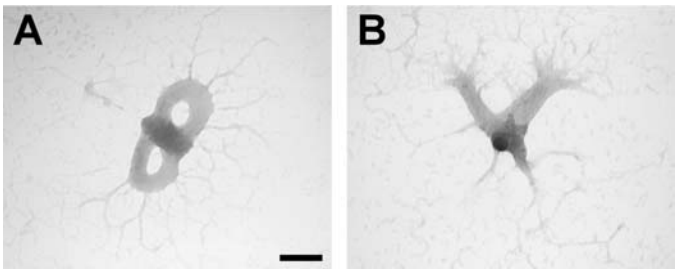

Figure 3.6. TEM images of representative condensates of (A) linear DNA and (B) supercoiled DNA condensed by spermidine, followed by addition of HU. Samples were 5 μM DNA bp, 700 μM spermidine chloride, 400 nM HU, 0.33×TE (pH 7.8), 15 mM NaCl. Scale bar is 100 nm.

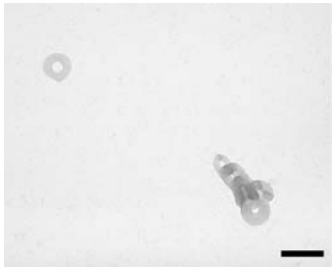

Figure 3.7. TEM image of representative condensates of linear DNA condensed by spermine, followed by addition of HU. Samples were 5 μM DNA bp, 15 μM spermine chloride, 400 nM HU, 0.33×TE (pH 7.8), 15 mM NaCl. Scale bar is 100 nm.

condensation clearly demonstrates that HU influences condensate morphology during the process of DNA particle formation (i.e. nucleation and initial growth). On the other hand, the ability of HU to significantly increase the population of rods formed in the presence of PEG after condensation has occurred demonstrates that the ability for HU to increase the relative populations of rod-like condensates is also thermodynamic in nature. We note that the addition of HU to DNA condensed by spermidine and spermine caused a substantial increase in condensate aggregation, which may have limited DNA re-arrangement into rods (Figure 3.6 and Figure 3.7).

3.3.7. A Model for How HU Guides DNA Condensation *In Vitro*

The co-existence of rods and toroids as products of *in vitro* DNA condensation reactions reflects the nearly equivalent energetics of DNA packing within these two distinct morphologies, including the energy required for the smooth bending of DNA within toroids versus that required to produce sharp bends at the ends of rods [1,85,117]. When DNA is condensed in the presence of high concentrations of alcohol, or condensing agents with hydrophobic groups (e.g. permethylated spermidine), rod populations increase with respect to toroid populations [41,86,112,241,242]. Under such conditions hydrophobic groups of the solvent or condensing agent interact favorably with unstacked DNA bases. These interactions lower the free energy penalty associated with sharp bending at the ends of rods, which renders rod formation more energetically favorable [41,86,243]. The higher population of rods observed with supercoiled DNA versus linear DNA can be attributed to torsional strain, which also makes DNA more prone to the formation of sharp bends [83,120]. These correlations between the promotion of sharp bends and increased rod populations inspired us to investigate the possibility that DNA bending proteins could be used to control the morphology of DNA condensates.

To understand the origin of the increase in rod populations observed in the presence of HU we must consider both what is known about HU binding to DNA and the state of DNA within rods and toroids. DNA condensed into a rod exists in two states, in a sharply bent state in the end regions, and presumably unbent state in the linear region between the two ends. HU has been shown to preferentially bind pre-bent DNA, and to bend linear DNA [229,230,238,239]. Therefore, HU binding is expected at the ends of

rods, where binding would increase rod stability, and not in the linear regions, at least not at the HU concentrations used in the present study. DNA condensed within toroids is smoothly bent over a radius of curvature that is much greater than that of the sharp bends induced by HU [32]. Thus, HU would not be expected to stabilize toroids, and may even suppress toroid formation, by introducing bends that are incompatible with DNA packing within a toroid.

DNA condensation *in vitro* is a nucleation-growth process that includes rod/toroid nucleation, proto-rod/proto-toroid formation (i.e. intramolecular condensation) and particle growth by intermolecular condensation [85]. In Figure 5 we present a schematic diagram of this process for DNA condensed in the presence of HU. Steps involving rod nucleation and growth are indicated by bold arrows as being more favorable in the presence of HU, as our data indicates that DNA condensation steps under both kinetic and thermodynamic control are more favorable towards rod formation in the presence of HU.

The apparent kinetic advantage provided to rods by HU can be understood in terms of how HU binding would preferentially promote rod nucleation. The nucleation structure for rods has not been investigated by experiment as it has been for toroids [54,95]. However, Langevin dynamics simulations of DNA condensation indicate that rods are also nucleated by DNA loops, with toroids being nucleated by loops with an obtuse internal contact angle and rods being nucleated by loops with an acute internal contact angle [117]. We propose that the binding of HU to either type of DNA loop would increase the probability for the loop to collapse on itself (Figure 3.8), forming a condensed oval structure that would nucleate rod formation. This proposed path to rod

nucleation would simultaneously increase the probability of rod nucleation and reduce the probability of toroid nucleation. Creation of rod nucleation sites, by this or an alternative route, can also be viewed as a reduction in the activation energy required for rod nucleation as a result of DNA binding and bending by HU.

The intramolecular condensation of a single 3kb DNA molecule gives rise to a proto-rod or a proto-toroid, depending upon nucleation structure (Figure 3.8). HU binding is again expected to be most favored at the ends of a proto-rod, which would increase the stability of the proto-rod. HU-stabilized proto-rods would then be more likely to grow into full size rods by the addition of DNA from solution (Figure 3.8), versus proto-rods in the absence of HU. Finally, the binding of HU to DNA within a rod at any stage of growth would also be expected to provide additional stability to the rod structure versus DNA condensed into a toroid, and thereby provide a thermodynamic advantage to rods under equilibrium conditions (i.e. after the kinetically-controlled stages of condensation).

While the model describe above explains our observation that rod populations increase in the presence of HU, this model does not explain the reduced effectiveness of HU in promoting rod formation when HU is added prior to a DNA condensing agent, as compared to coincident addition. However, this observation can be understood considering what is known about the bound lifetime of HU on DNA versus the time scale of DNA condensation. HU-DNA complexes have a dissociation half-life of 0.6 min and 6.3 min in 50 mM NaCl and 5 mM NaCl, respectively [244]. The initial stages of DNA condensation, including nucleation and intramolecular collapse of a DNA strand, are complete within milliseconds [245,246]. Thus, HU molecules preassociated with DNA may not be able to completely redistribute within the time frame of condensate formation

to maximize their influence on the nucleation of rods or the stabilization of proto-rods. In contrast, HU added coincident with a condensing agent would be more efficient in guiding condensate structure if the on-rate of binding to DNA is faster for bent DNA, in which case HU would preferentially bind at the ends of nucleated rods rather than in the linear region of a rod or along a DNA strand that has nucleated a toroid.

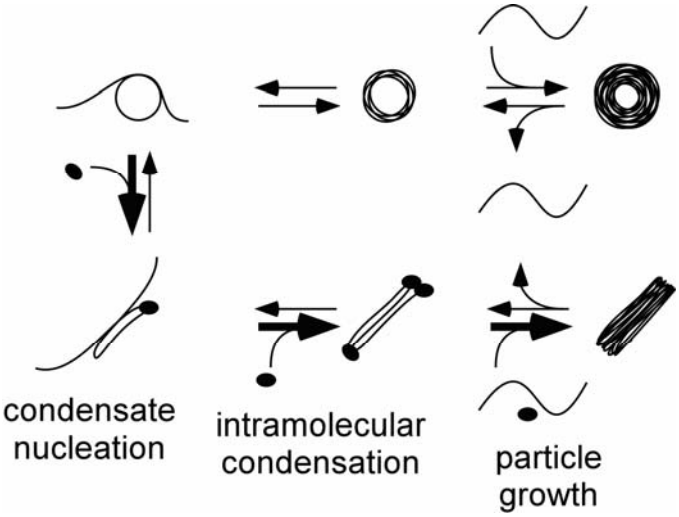

Figure 3.8. A model for how HU affects the process of DNA condensation in which rods and toroids are formed. The three stages of DNA condensation *in vitro*, as described in text, are: rod/toroid nucleation; proto-rod/proto-toroid formation (intramolecular condensation); and condensate growth (intermolecular condensation), which includes strand exchange between condensates (under some conditions). Bold arrows indicate steps that apparently become more favorable in the presence of HU. Black ellipsoids represent HU molecules.

We have observed that the relative rod population of DNA condensates formed in the presence of PEG/NaCl increases when HU is added even after condensation has taken place. In contrast, HU did not significantly increase rod populations when added after DNA was condensed by spermidine or spermine. We have previously presented evidence that the conversion between fully-formed toroids and rods takes place through the

exchange of condensed DNA with solution [85]. The ability for HU to cause the conversion of toroids formed in the presence of PEG/NaCl into rods suggests that appreciable strand exchange occurs between toroids and solution after condensation is complete. In contrast, our observation that HU does not promote rod formation after condensation by spermidine or spermine, suggests that strand exchange in these preparations is minimal, and that the observed effects of HU on spermidine and spermine condensate morphology occurs during the earlier stages of condensation (i.e. nucleation, proto-structure formation and initial growth). Nevertheless, it is likely that HU can alter the morphology of condensates formed by polyamines under equilibrium conditions if conditions are used that allow DNA strand exchange with solution after initial condensation (e.g. higher monovalent ionic strength). This possibility is currently being explored. We also note that the amount of HU bound to DNA within HU-induced rods has not been determined directly for any of the condensate preparations reported here. It is possible that less HU may be necessary to maintain the rod morphology than is initially required to guide the condensation of DNA into rods. Experimental conditions may even exist for which it is possible to completely remove HU from rods without reverting to alternative condensate morphologies.

3.3.8. Implications Regarding the Functionality of HU in DNA Condensation

Our present study of controlling DNA condensation with the protein HU also suggests a possible functionality of this nucleoid-associated protein within bacteria cells. The bacterial nucleoid is a highly compact structure containing chromosomal DNA and nucleoid-associated proteins. A combination of factors has been suggested to contribute

to the compaction of the bacterial chromosome. Two principle levels of organization are known to facilitate bacterial chromosome packing: long-range structural organization that involves the folding of a single chromosome into multiple independent supercoiled domains, and short-range organization of these negatively supercoiled regions by nucleoid-associated proteins [247,248]. Polyamines and macromolecular crowding forces are also known to play an indispensable role in bacterial chromosome condensation [12,249,250]. However, the details concerning how these factors work together to condense the bacterial chromosome is not well understood.

The 4.6 Mb circular chromosome of *E. coli* is organized into topologically independent domains of approximately 10 kb in size [251-257]. The introduction of negative supercoils, interwound and highly branched structures within these domains produce a more compacted form of DNA than that adopted by free DNA in solution [258,259]. Nevertheless, supercoiling alone is unable to account for the 1000-fold or greater degree of condensation of the bacterial chromosome in the nucleoid. Therefore, other cellular factors must also play a significant role in bacterial chromosome condensation.

Prokaryotic cells contain a set of basic proteins that bind DNA and are associated with the nucleoid. Among these nucleoid-associated proteins, the protein HU has been characterized as the most important protein in structural organization of the bacterial chromosome. Although HU is one of the most abundant nucleoid-associated proteins and has often been referred to as a 'histone-like' protein, the role of HU in *condensing* the bacterial chromosome is not understood [134,230,231,260-263]. Our use of spermidine (one of the major polyamines in bacteria) and PEG (a macromolecular crowding agent) is

clearly far too simplistic to be considered a reasonable model of the bacterial cytoplasm. Nevertheless, we have demonstrated that HU guides the condensation of DNA into structures with linear bundles (i.e. rods) when DNA is condensed by two very different solution conditions, polyamines and a crowding environment. Thus, the ability to control DNA condensate morphology appears to be an intrinsic property of HU. These combined results indicate that HU is much more effective in controlling the morphology of DNA condensation than it is in promoting DNA condensation, which may reflect how HU plays an architectural role in the condensation of bacterial chromosomal DNA.

Azam *et al.* have estimated that 30,000 HU dimers exist per *E. coli* cell during the exponential growth phase [264]. If HU is evenly distributed throughout the chromosomal DNA of an *E. coli* cell in this phase, then HU loading of DNA would be on average only 1 HU dimer per ~300 to 400 bp [264]. Our results demonstrate that HU can act as an architectural protein for guiding DNA condensing at such low loading levels (≤ 1 HU dimer per 225 bp). As HU is believed to be somewhat evenly distributed throughout the bacterial chromosome, our experimental evidence of the architectural role of HU in guiding DNA condensation is definitely of physiological relevance [265].

Mutational and biochemical analyses have implicated HU as a determinant protein in packaging the bacterial chromosome [139,219-221,266]. Zimmerman and coworkers demonstrated that HU reduces the concentration of crowding agents (i.e. PEG 8000, albumin) required to condense DNA *in vitro* [232,233]. However, more recent studies question the exact role of HU in chromosome condensation. Single molecule investigations of HU binding to DNA have revealed that HU has a dual mode of binding to DNA. At low HU to DNA ratios, (e.g. less than 1 HU dimer per 150 bp), HU-induced

bends decrease the persistence length of DNA [230,231,262]. In contrast, at high HU to DNA ratios (e.g. 1 HU dimer per 9 bp) HU actually increases the stiffness of DNA [230,231,261,262]. While the high-loading mode of HU is intriguing, it is still unknown why such a mode exists for a protein that is believed to facilitate DNA compaction. In the present study we have observed a dramatic effect of HU on DNA condensation at much lower HU concentrations and at much lower DNA loading levels than those of the above mentioned studies.

We propose that HU can function *in vivo* as an architectural protein during chromosomal condensation. Over the range of HU concentrations we have investigated, HU primarily functions as an architectural protein but not as an antagonist to DNA condensation, as has been suggested in recent reports [10,231,250,261,262]. We hypothesize that HU could locally organize bacterial chromosome DNA in the presence of polyamines and a crowded environment to facilitate DNA condensation into a more ordered, bundle-like state. We emphasize that the rod-like DNA structures observed with HU and DNA condensing agents are not likely the same dimensions as condensed domains of DNA within bacterial cells, which will be restricted by higher levels of chromosome structure and domain supercoiling. Nevertheless, the morphology of DNA condensates produced *in vitro* appears to be useful means for monitoring the conditions under which HU affects DNA condensation, which could prove valuable for further exploration of HU-controlled condensation within more sophisticated models of the bacterial cytoplasm.

3.4. CONCLUDING REMARKS

In conclusion, our demonstration that the morphology of DNA condensates, formed under a variety of conditions, is shifted completely from toroids to rods if the bacterial protein HU is present during condensation has important implications for controlling DNA condensates for gene delivery, as well as potential implications concerning the mechanism of packaging of chromosomal DNA in bacteria. HU is a nonsequence-specific DNA binding protein that sharply bends DNA, but alone does not condense DNA into densely packed particles. Less than one HU dimer per 225 bp of DNA is sufficient to completely control condensate morphology when DNA is condensed by spermidine. We propose that rods are favored in the presence of HU because rods contain sharply bent DNA, whereas toroids contain only smoothly bent DNA. The results presented illustrate the utility of naturally derived proteins for controlling the shape of DNA condensates formed *in vitro*. HU is a highly conserved protein in bacteria that is implicated in the compaction and shaping of nucleoid structure. However, the exact role of HU in chromosome compaction is not well understood. Our demonstration that HU governs DNA condensation *in vitro* also suggests a mechanism by which HU could act as an architectural protein for bacterial chromosome compaction and organization *in vivo*.

CHAPTER 4

INTEGRATION HOST FACTOR (IHF) ALTERS DNA CONDENSATION IN VITRO: IMPLICATIONS FOR THE ROLE OF IHF IN THE COMPACTION OF BACTERIAL CHROMATIN

4.1. INTRODUCTION

The bacterial nucleoid is a highly compacted structure containing chromosomal DNA and nucleoid-associated proteins. Two principle levels of organization are known to facilitate bacterial chromosome packing. In *E. coli* long-range structural organization involves the folding of the 4.6 Mb circular chromosome into multiple, topologically independent domains of approximately 10 kb in average length [251-257]. Short-range organization involves DNA domains which are negatively supercoiled and stabilized by the interaction of the major chromosome-associated proteins [247,248]. Thus, these proteins are believed to function in compaction of the chromosomal DNA. In addition to these factors, polyamines and macromolecular crowding effects, exerted by RNA and cellular proteins are also known to play an indispensable role in bacterial chromosome condensation [10-12,249].

Among the ten nucleoid-associated proteins, IHF is one of the major proteins that alter local DNA structure by bending the DNA helix upon binding. IHF acts as an architectural protein in many cellular processes, including replication, transposition, regulation of transcription initiation, site specific recombination of λ phage, packaging of phage DNA [12,267-269]. IHF is a highly abundant protein within the *E. coli* cell, with a

concentration that varies as a function of the growth phase [264]. In *E. coli*, IHF is primarily a heterodimeric protein composed of two subunits α- and β-, approximately 11 kDa and 9.5 kDa in size, respectively, with 30% sequence homology [12]. In contrast to HU, a protein which shares 40% sequence homology with IHF, IHF binds to specific DNA sequences with very high affinity; K_d ranges from 0.3 to 20 nM [270-272]. A typical sequence-specific IHF binding site is 30 to 35 bp in length. The 3' region of these sequences are highly conserved, IHF binds to a consensus sequence WATCAANNNNTTR (W = A/T; R = G/A; and N = all bases) [273]. The 5' domain, which is composed of ~20 bp, has no consensus sequence but is commonly A/T rich. Many IHF binding sites have an A-tract containing three to six consecutive adenines in the 5' region [274,275]. In addition to binding sequence-specific DNA sites, IHF also binds to DNA in a sequence-independent manner, but with 1,000 to 10,000-fold lower affinity [270-272].

The x-ray crystal structure of the *E. coli* IHF protein bound to a 35 bp DNA fragment containing the λ phage H' IHF binding site showed that the fold of IHF is almost identical to that of HU [131,132,276-278]. The two subunits of IHF form an intertwined compact α-helical core from which β-sheet strands extend. These two flexible β-sheet "arms" of IHF wrap around the DNA and inserted into the minor groove [132]. The intercalation of conserved proline residues (residues 65 and 64 of the α and β subunits, respectively) located at the tip of the β-ribbon arms induce two sharp kinks that are separated by 9 bp, which causes a sharp bend of 160-180° over only ~35 bp. This DNA bend is stabilized by both the minor groove IHF-base interactions described above, as well as electrostatic interactions between IHF and the sugar phosphate backbone of

DNA [132]. Solution state studies of IHF-DNA complex using single-pair FRET measurements also corroborate the crystallographic data that IHF induces a bend angle of approximately 160° in the DNA [230,279].

The *E. coli* genome is estimated to contain approximately 1,000 specific binding sites for IHF [280]. In the exponential phase, *E. coli* cells contain approximately 6,000 IHF dimer molecules per cell [264]. The numbers are even higher for cells in stationary-phase, the IHF concentration increases to approximately 30,000 dimers per cell. Recent *in vivo* measurements estimate that during the exponential phase only ~1 nM of IHF proteins remain free inside the cell, and only 5 nM in the stationary phase [272]. Therefore, essentially all IHF specific binding sites are continuously occupied. This high concentration of DNA bound IHF proteins, is far beyond that necessary to fully load all the high-affinity IHF binding sites known to present in *E. coli* genome. These conclusions indicate that most of the IHF in *E. coli* is bound nonspecifically to chromosomal DNA, which suggests that nonspecific binding of IHF has an important biological role, such as chromosome compaction.

The single molecule experiments conducted by Ali *et al*. using λ-DNA provide evidence for the possibility that IHF facilitates DNA compaction in bacterial cells, as DNA is compacted ~30% upon binding by IHF [281]. This compaction was concluded to result from the sequence independent binding of IHF to multiple sites on λ-phage DNA because of the large concentration of IHF that is required to obtain the observed effect. Furthermore, the same degree of compaction was achieved with DNA molecules with and without a sequence-specific IHF binding site, and that the compaction of λ-phage

DNA was reduced in the presence of DNA that did not contain any sequence-specific IHF binding sites.

The combined results of the experiments discussed above and the intracellular concentration of IHF strongly suggest that the nonspecific binding of IHF to DNA plays a significant role in the compaction of the bacterial chromosome. There is some evidence that IHF can also bind nonspecifically in a side-by-side manner along DNA, which might give rise to stiff IHF-DNA filaments, as previously observed with high concentration of HU [231,282]. However, there is no evidence of such rigidification of DNA in the single-molecule elasticity measurements reported by Ali *et al*. [281]. Overall, experiments with IHF strongly suggest a role in bacterial chromosome packaging, but its exact role is still not well understood.

While nucleoid-associated proteins, DNA supercoiling and cellular crowding effects have all been implicated in bacterial chromosome condensation, no single factor is sufficient to achieve full condensation at the level observed *in vivo*. Previous experiments have provided evidence for the functional involvement of multiple cellular factors in shaping the bacterial nucleoid [232,233]. Furthermore, we have shown that HU functions as an architectural protein that guides DNA to condense into linear rod-like structures in the presence of polyamines and macromolecular crowding agents, but does not act as a condensing agent *per se* [283]. We have also suggested that HU could work in a similar manner *in vivo* with other cellular condensing factors to locally organize the bacterial chromosome. As discussed above, HU and IHF are closely related DNA bending proteins. The studies presented in this chapter were designed to investigate the effects of IHF on *in vitro* DNA condensation. Like our studies of HU presented in the previous

chapter, our goal was to understand the interplay between IHF, DNA supercoiling, and polyamines as a means to gain insights into role of IHF in DNA compaction within the bacterial nucleoid.

In this chapter a systematic study is presented regarding the effects of sequence specific and sequence independent IHF binding on DNA condensation. Using transmission electron microscopy we demonstrate that IHF causes DNA to compact into bundle-like structures upon condensation by polyamines, which suggests functional similarity of HU and IHF during DNA compaction. Our results support the view that IHF plays an active role in shaping the local structure of the bacterial chromosome in the compact state of the nucleoid.

4.2. EXPERIMENTAL PROCEDURES

4.2.1. DNA Preparation

λ phage DNA (λ DNA) was purchased from Invitrogen. Another DNA substrate YEp13 yeast episomal vector (10.7 kb circular DNA) was isolated from the *E. coli* strain DH5-α using the Qiagen maxi-prep kit (Valencia, CA), and linearized by digestion with the restriction endonuclease *Bam*HI (New England Biolabs). Shorter plasmid DNA molecules (3.4 kb and 3.9 kb) were also used in our experiments with and without sequence-specific binding sites for IHF. A series of DNA plasmids were constructed that contain one or two specific sites for IHF binding where specific sites are separated by varied lengths of DNA. The parent plasmid used was pBluescript II SK-. The *Eco*RI site of Bluescript II SK- was destroyed by insertion of a 14 bp linker containing a *Bgl*II site (GGTGAGATCTCACC) at position 706 to create a modified pBluescript II SK-. A 209

bp fragment (derived from a portion of the RhoA DNA sequence) with *BamH*I and *Bgl*II restriction sites at the two ends was inserted into the compatible cohesive *BamH*I site in the multiple cloning region of the modified Bluescript II SK- vector. Then the 242 bp insert (present between *BamH*I/*Bgl*II restriction fragment) was isolated from the modified vector and unidirectionally subcloned once and three times into the modified Bluescript II SK- vector containing one 242 bp insert. Subcloning was accomplished by first linearizing the modified Bluescript II SK- vector with *Bgl*II and then dephosphorylated with calf intestinal alkaline phosphatase (CIAP), followed by ligation in the presence of the desired RhoA-derived insert. The orientation of the inserts in the vector was verified using *BamH*I/*Bgl*II co-digestion [284]. The resultant plasmid, which contained two tandem repeats (242 bp each repeat; 484 bp total insert), was named pBD (3.4 kbp) [284]. Another plasmid containing four tandem repeats (242 bp each repeat; 968 bp total insert) was named pBQ (3.9 kbp) [284]. A 30 bp duplex with sticky ends (formed by annealing two synthetic oligonucleotides, sequences given below as oligo1 and oligo2) containing the H' site of phage λ, one of the best characterized and highest affinity IHF binding sites [132,270], was used to insert IHF binding sites into pBD. This 30 bp duplex was ligated into the pBD plasmid between the two restriction sites *Hind*III and *Bgl*II. The resultant plasmid, named pBDIHF, was used in the transformation of *E. coli* K12 strain ER2925 (dam^-/dcm^-) (New England Biolabs). The sequences around the IHF binding site were confirmed by the dideoxy-NTP sequencing method. To insert a second specific IHF binding site in the plasmid pBDIHF, another 32 bp duplex (sequences given below as oligo3 and oligo4) containing the H' site of phage λ was ligated into the plasmid pBDIHF between the two restriction sites *Xba*I and *Sac*I. The ligation reaction was used

to transform *E. coli* K12 strain DH5-α and the resultant plasmid was named as pBD2IHF. The sequences around the IHF binding sites were confirmed by the dideoxy-NTP sequencing method. In the plasmid pBD2IHF, two IHF sites are 497 bp apart. We also constructed another plasmid where two IHF sites are separated by 956 bp DNA length.

The synthetic 30 bp duplex containing the H' site of phage λ was also ligated into the plasmid pBQ between the two restriction sites *Hind*III and *Bgl*II. This modified plasmid, named pBQIHF, was transformed into *E. coli* K12 strain ER2925 (dam^-/dcm^-). To insert second a IHF specific binding sites in the plasmid, the 32 bp duplex formed by annealing oligo3 and oligo4, was ligated into the plasmid pBQIHF between the two restriction sites *Xba*I and *Sac*I and the ligation reaction was used to transform *E. coli* K12 strain DH5-α, the resultant plasmid was named pBQ2IHF. The sequences around the IHF binding sites were confirmed by dideoxy-NTP sequencing.

oligo1 5'-AGCTTAAAAAAGCATTGCTTATCAATTTGTTGCA-3'
oligo2 3'-ATTTTTTCGTAACGAATAGTTAAACAACGTCTAG-5'
[**A]**

oligo3 5'-CTAGATAAAAAAGCATTGCTTATCAATTTGTTGCAGAGCT-3'
oligo4 3'-TATTTTTTCGTAACGAATAGTTAAACAACGTC-5'
[**B]**

Plasmids pBD, pBQ, pBD2IHF and pBQ2IHF were isolated from the *E. coli* strain DH5-α and plasmids pBDIHF and pBQIHF were isolated from the *E. coli* strain ER2925 using the Qiagen maxi-prep kit (Valencia, CA). To remove any IHF proteins bound to in the plasmids after isolation, purified plasmids (pBDIHF, pBQIHF, pBD2IHF

and pBQ2IHF) were treated with Proteinase K and later Proteinase K was removed by heat inactivation at 65°C and the Qiagen PCR purification kit (Valencia, CA).

The purity of the isolated DNA plasmids was verified spectrophotometrically (UV absorbance ratio A_{260}/A_{280} >1.8). All plasmids were linearized by digestion with the restriction endonuclease *Sca*I (New England Biolabs). Following enzymatic digestion, the DNA was rinsed at least five times with 1×TE (10 mM Tris, 1 mM EDTA, pH 7.8) using a Microcon-YM 30 spin column (Millipore) to remove salts and buffers from the restriction digest. The DNA was finally resuspended from the spin column in 1×TE. DNA concentration was determined spectrophotometrically. Supercoiled plasmids, obtained directly from the plasmid isolation procedure, were determined to be more than 90% supercoiled based on agarose gel electrophoresis analysis. Supercoiled DNA was also rinsed at least five times with 1×TE to ensure that the buffer conditions of all DNA stock samples were identical.

Plasmid pBD, pBQ and YEp13 are designated as 3.4 kb DNA, 3.9 kb DNA, and 10.7 kb DNA, respectively, throughout the chapter. Plasmid DNA containing one specific IHF binding site pBDIHF and pBQIHF are designated as 3.4 kb DNA with one IHF specific binding site, 3.9 kb DNA with one IHF specific binding site, respectively, throughout the text. Plasmid DNA containing two specific IHF binding sites pBD2IHF and pBQ2IHF are designated as 3.4 kb DNA with two IHF specific binding sites 500 bp apart, 3.9 kb DNA with two IHF specific binding sites 950 bp apart, respectively, throughout the chapter.

4.2.2. IHF Protein

IHF protein was provided by the laboratory of Prof. Ishita Mukerji, Wesleyan University, as part of a collaboration with the Hud laboratory at Georgia Tech.

4.2.3. Preparation of DNA Condensates

Spermidine-induced condensates were prepared by mixing solutions of DNA and spermidine to yield a final condensation reaction mixture of 5 μM DNA in bp (given in units of base pair throughout), 700 μM spermidine, 0.33×TE (pH 7.8), 15 mM KCl. The condensate reaction mixtures were allowed to equilibrate at room temperature for 10 min before depositing on grids. The same protocol was followed for the preparation of spermine-induced condensates, in which DNA was mixed with spermine to yield a condensation reaction mixture of 5 μM DNA, 15 μM spermine, 0.33×TE (pH 7.8), 15 mM KCl. For spermidine-induced condensates prepared in the presence of IHF, DNA was incubated with IHF for 10 min and then condensed with spermdine for 10 min before depositing on grids, and final condensate solutions were all 5 μM DNA, 700 μM spermidine, 0.33×TE (pH 7.8), 15 mM KCl. For spermine DNA condensation in the presence of IHF, the same protocol was followed as described above for the condensation of DNA by spermidine in the presence of IHF, where all final condensate solutions were all 5 μM DNA, 15 μM spermine, 0.33×TE (pH 7.8), 15 mM KCl.

4.2.4. Electron Microscopy and Analysis of DNA Condensates

A 10 μl aliquot of each DNA condensate reaction mixture was deposited directly onto a carbon-coated electron microscopy grid (Ted Pella, Redding, CA). After allowing

condensates to settle onto the grid for 15 min, 2% uranyl acetate was added to the grid for 2 min, and then the grid was rinsed in 95% ethanol and air-dried. The size and morphology of DNA condensates were examined using a JEOL-100C transmission electron microscope (TEM). To obtain the relative toroid and rod populations in each sample, the grid surface was randomly scanned and the number of unaggregated toroids and rods visible on the viewing screen were counted. Several hundred structures were counted for each grid. Each measurement reported is the average of the counts from three different grid preparations. Images were acquired at 100,000× magnification. A computer graphics program was used to measure the dimensions of individual condensates for each sample.

4.3. RESULTS AND DISCUSSION

4.3.1. Effects of IHF on Spermidine Induced Condensation of λ-Phage DNA and Linear Plasmid DNA with and without Specific IHF-Binding Sites

λ-phage DNA condensed by spermidine is compacted into toroidal condensates with a mean outside diameter of 200 nm (σ, ±16 nm) and a mean thickness of 66 nm (σ, ±8 nm). Along with the toroids, approximately 10% of observed condensates are bundle-like or rod-like structures with a mean length of 415 nm (σ, ±30 nm) and a mean thickness of 62 nm (σ, ±6 nm). To examine the effects of IHF on a λ-phage DNA condensation, spermidine-induced DNA condensates were examined using electron microscopy, as a function of IHF concentration. IHF causes a significant increase in the population of rod- like condensates that increases with IHF concentrations, as shown in Figure 4.1 and 4.2. The relative population of rod-like condensates increases from ~10%

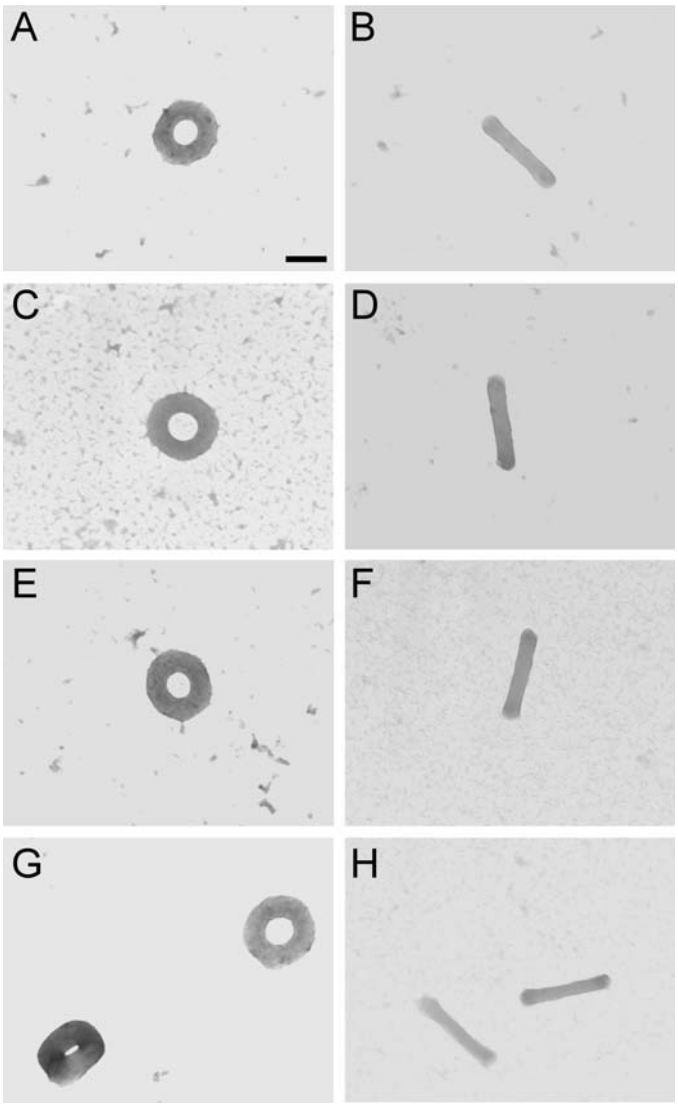

Figure 4.1. Transmission electron microscopy (TEM) images of spermidine-induced linear DNA condensates produced in the presence and absence of IHF. (A) DNA condensates produced by the addition of spermidine to λ-DNA. (B) DNA condensates produced by the addition of spermidine to λ-DNA in the presence of 75 nM IHF. (C) DNA condensates produced by the addition of spermidine to linear 3.4kbDNA. (D) DNA condensates produced by the addition of spermidine to linear 3.4kbDNA in the presence of 75 nM IHF. (E) DNA condensates produced by the addition of spermidine to linear 3.4kbDNA containing two specific IHF binding sites 500 bp apart. (F) DNA condensates produced by the addition of spermidine to linear 3.4kbDNA having two specific IHF binding sites 500 bp apart in the presence of 75 nM IHF. (G) DNA condensates produced by the addition of spermidine to linear 3.9kbDNA containing two specific IHF binding sites 950 bp apart. (H) DNA condensates produced by the addition of spermidine to linear 3.9kbDNA having two specific IHF binding sites 950 bp apart in the presence of 75 nM IHF. All reactions contained final concentration of 5 μM DNA bp, 700 μM spermidine chloride, 0.33×TE (pH 7.8) and 15 mM KCl. Scale bar is 100 nm

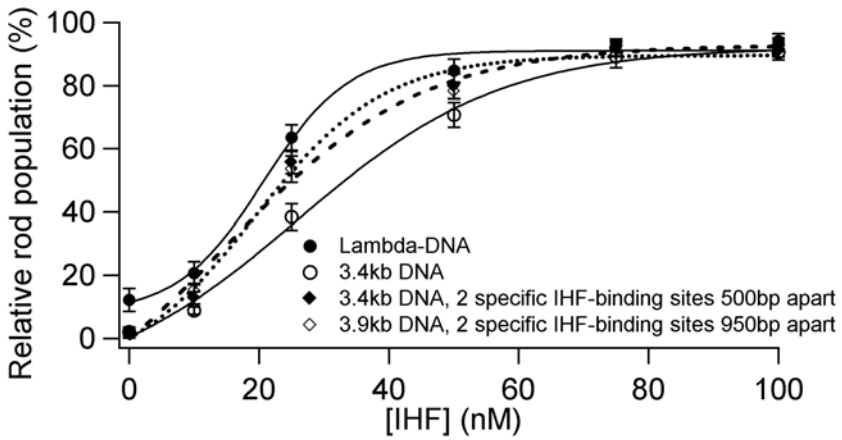

Figure 4.2. Spermidine-induced DNA condensates morphology statistics for DNA samples having specific IHF-binding sites or without a binding site, as a function of IHF concentration. All reactions contained final concentration of 5 μM DNA bp, 700 μM spermidine chloride, 0.33×TE (pH 7.8), 15 mM KCl and indicated concentrations of IHF dimer.

rods (in the absence of IHF) to greater than 90% rods in the presence of 75nM IHF, whereas above this IHF concentration further increases in rod percentages are not observed (Figure 4.2).

DNA rods produced by spermidine-induced condensation in the presence of IHF exhibited an overall mean length of 396 nm and a mean width of 58 nm at a IHF concentration of 75 nM. Rod length and thickness proved to be relatively insensitive to IHF concentration at the point where the relative rod population almost reaches a plateau. For example, rods formed in the presence 75 nM IHF and 100 nM IHF were of similar dimensions, i.e. mean rod length of 396 nm (σ, ±36 nm) vs. 386 nm (σ, ±41 nm), and mean rod thickness of 58 nm (σ, ± 9 nm) vs. 61 nm (σ, ±10 nm), respectively. These observations demonstrate that IHF does not significantly alter the dimensions of condensates produced by spermidine, only the relative population of rods. Thus, IHF can act as a guide for formation of bundle like condensate structure for spermdine-induced

Table 4.1 Dimensions of rods produced from linear DNA having specific IHF-binding sites or without a binding site in presence of IHF protein

Linear DNA	Condensing Agent	Length (nm)	Thickness (nm)
3.4kbDNA	spermidine	383±32	57±8
3.4kbDNA with one specific IHF site	spermidine	373±24	56±8
3.4kbDNA with two specific IHF sites 500 bp apart	spermidine	394±33	58±9
3.9kbDNA with one specific IHF site	spermidine	391±25	57±11
3.9kbDNA with two specific IHF sites 950 bp apart	spermidine	373±46	57±7
10.7 kb DNA	spermidine	406±27	59±9
λ-DNA	spermidine	396±36	58±9
3.4kbDNA	spermine	206±35	34±3
3.4kbDNA with one specific IHF site	spermine	227±29	31±4
3.4kbDNA with two specific IHF sites 500 bp apart	spermine	203±26	34±5
3.9kbDNA with one specific IHF site	spermine	202±24	34±7
3.9kbDNA with two specific IHF sites 950 bp apart	spermine	202±24	34±7
10.7 kb DNA	spermine	231±31	32±5
λ-DNA	spermine	248±32	30±3

Table 4.2 Dimensions of rods produced from supercoiled DNA having specific IHF-binding sites or without a binding site in presence of IHF protein

Supercoiled DNA	Condensing Agent	Length (nm)	Thickness (nm)
3.4kbDNA	spermidine	352±41	51±7
3.4kbDNA with two specific IHF sites	spermidine	340±43	48±8
10.7kbDNA	spermidine	375±40	50±8
3.4kbDNA	spermine	206±35	32±6
3.4kbDNA with two specific IHF sites	spermine	200±27	34±5
10.7kbDNA	spermine	231±32	35±4

condensation in a similar fashion as we have observed previously in presence of DNA bending protein HU (Chaper 3).

The λ-phage genome contains a small number of high affinity specific binding sites for IHF that are highly clustered. Therefore, the effect of IHF on spermidine induced DNA compaction could be due to the binding of IHF protein to both sequence-specific and non-specific binding to λ-phage DNA. To determine whether the effect on condensation is caused by specific or non-specific binding, we conducted similar experiments with comparatively shorter linear plasmid DNA (3.4 kb) with and without specific IHF binding sites. For this purpose, DNA molecules 3.4 kb long without a specific site, 3.4 kb long with two high affinity binding sites and another DNA molecule 3.9 kb long with two high affinity binding sites were studied. In the former case, two IHF sites were 500 bp apart, whereas in the later case 950 bp apart. All three DNA molecules were preincubated with IHF protein and then condensed by spermidine. DNA condensate morphology as a function of IHF concentration was determined by TEM. Representative TEM images of condensates formed from all three DNA molecules are shown in Figure 4.1. A definite shift in the DNA condensate morphology from toroid to rod was observed with the increasing IHF concentration, irrespective of whether or not IHF specific sites were present in the DNA (Figure 4.2).

The similar magnitude increase in relative rod populations of linear DNA molecules with specific IHF-binding sites and without specific sites, as a function of IHF concentration, indicates that the effect of IHF on DNA condensation is due to the non-sequence specific binding of IHF to the DNA (Figure 4.2). The half-maximum of rod population was observed at 21 nM IHF dimer for λ-phage DNA, which is similar to that

observed for 3.4 kb linear DNA containing two specific IHF sites (24 nM IHF dimer) and 3.9 kb linear DNA containing two specific IHF sites (25 nM IHF dimer) condensed by spermidine. However, the half-maximum of rod population was found to be at 34 nM IHF dimer for 3.4 kb linear DNA containing no sequence specific IHF-binding sites (Figure 4.2). Thus, in the λ-phage DNA and plasmid length DNA with specific IHF-binding sites, the high-affinity (sequence specific) and low-affinity (sequence independent) binding apparently work together to increase the population of rod-like condensates.

The dimensions of the spermidine-induced rod condensates formed in presence of 75 nM IHF, where relative rod populations were greater than 90% for all above mentioned linear DNA, are shown in the Table 4.1. Rods formed by the condensation of the λ-phage DNA and 3.4 kb linear DNA containing no IHF specific sites, linear DNA containing two specific IHF binding sites 500 bp apart, 3.9 kb linear DNA containing two specific IHF binding sites 950 bp apart were similar in size. For example, the mean rod length of 3.4 kb linear DNA containing no IHF specific sites was 383 nm (σ, ±32 nm) and thickness 57 nm (σ, ±8nm), whereas rod length of 3.4 kb linear DNA containing two specific IHF binding sites was 394 nm (σ, ±33 nm) and thickness 58 nm (σ, ±9nm). 3.9 kb DNA containing two specific IHF binding sites, but separated by 950 bp, condensed into rod-like structure with mean length 373 nm (σ, ±46 nm) and mean thickness of 57 nm (σ, ±7nm).

3.4 kb and 3.9 kb linear DNA containing only one specific IHF-binding site, and 10.7 kb linear plasmid DNA (which contains one natural IHF specific site) were condensed by spermidine in the presence of 75 nM IHF and found to produce rod-

populations that were over 90% in all cases. The dimensions of the rod condensates formed from these DNA samples were determined to be very similar in size as the samples reported in Table 4.1. Thus, the dramatic increase in the relative rod population and similar dimensions for spermidine-DNA condensates formed in the presence of IHF for 3.4 kb to 48.5 kb linear DNA, including 10.7 kb DNA with and without IHF specific sites, demonstrate the general ability of IHF to guide bundle like morphology, which is irrespective of the absence or presence of IHF specific binding sites and also independent of the DNA length.

4.3.2. Effects of IHF on Spermine Induced Condensation of λ-Phage DNA and Linear Plasmid DNA with and without Specific IHF-Binding Sites

The 48 kb λ-phage DNA and other plasmid-length linear DNA, including plasmids with one and two specific IHF-binding sites, were condensed with the tetracation polyamine spermine in absence and presence of IHF proteins. Similar to the spermidine results presented in the previous section, when linear DNA was condensed by spermine the majority of particles (over 95%) formed were well-defined toroids with a minor population of rods (Figure 4.3). DNA condensed by spermine in presence of IHF (125 nM) also exhibited a striking increase in the percentage of rod-like condensates to approximately 85% from less than 5% in absence of IHF (Figure 4.3). These results suggest that guiding DNA condensate morphology is a general property of IHF, regardless of condensing agent.

In contrast to the condensates formed in the presence of spermidine, the condensates formed by spermine are considerably smaller (Figure 4.1, 4.3). Toroids

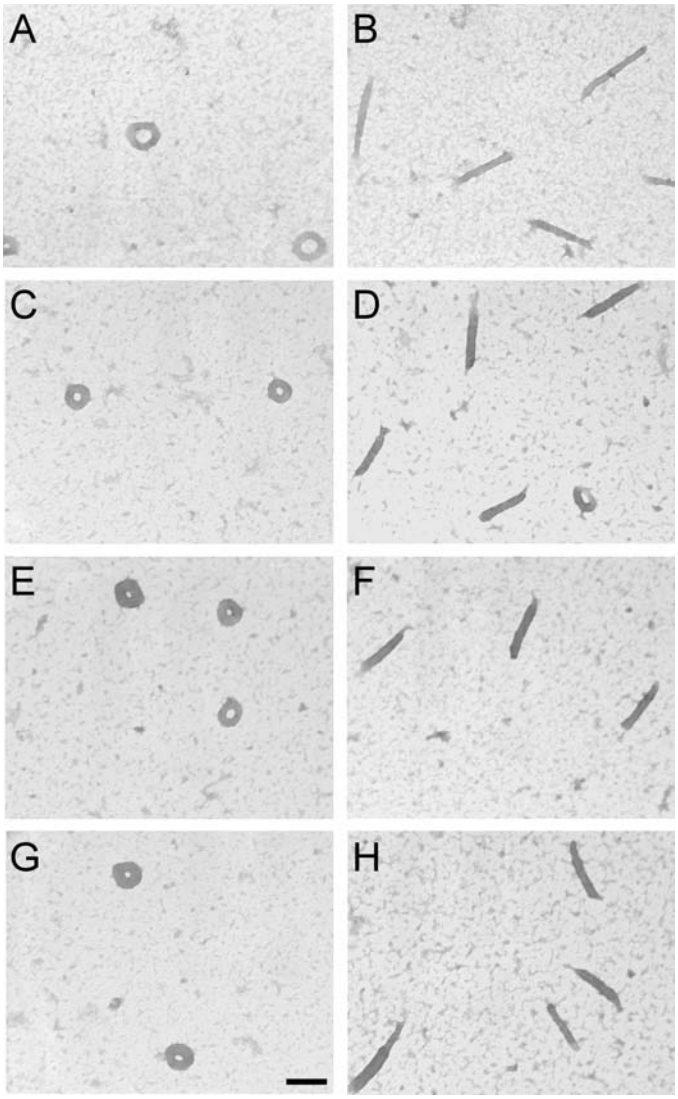

Figure 4.3. Transmission electron microscopy (TEM) images of spermine-induced linear DNA condensates produced in the presence and absence of IHF. (A) DNA condensates produced by the addition of spermine to λ-DNA. (B) DNA condensates produced by the addition of spermine to λ-DNA in the presence of 125 nM IHF. (C) DNA condensates produced by the addition of spermine to linear 3.4kbDNA. (D) DNA condensates produced by the addition of spermine to linear 3.4kbDNA in the presence of 125 nM IHF. (E) DNA condensates produced by the addition of spermine to linear 3.4kbDNA containing two specific IHF binding sites 500 bp apart. (F) DNA condensates produced by the addition of spermine to linear 3.4kbDNA having two specific IHF binding sites 500 bp apart in the presence of 125 nM IHF. (G) DNA condensates produced by the addition of spermine to linear 3.9kbDNA containing two specific IHF binding sites 950 bp apart. (H) DNA condensates produced by the addition of spermine to linear 3.9kbDNA having two specific IHF binding sites 950 bp apart in the presence of 125 nM IHF. All reactions contained final concentration of 5 μM DNA bp, 15 μM spermine chloride, 0.33×TE (pH 7.8) and 15 mM KCl. Scale bar is 100 nm.

formed by the condensation of λ-phage DNA with spermine had a mean outside diameter of 110 nm (σ, ±14 nm) and a mean thickness of 31 nm (σ, ±3 nm). The overall dimensions of the spermine-DNA rod condensates formed in presence of 75 nM IHF, for all DNA samples were also considerably smaller than those produced by spermidine, as shown in Table 4.1. For example, the mean rod length of the spermine-induced λ-phage DNA condensate was 248 nm (σ, ±32 nm) and the mean rod thickness was 30 nm (σ, ±3 nm) at 125 nM IHF, compared to 396 nm (σ, ±36 nm) and 58 nm (σ, ±9 nm), respectively, of spermidine-induced λ-phage DNA condensate at 75 nM IHF. However, similar to spermidine, the dimensions of spermine induced rod-like condensate formed in presence of IHF did not change significantly with the DNA length or presence and absence of specific IHF-binding sites, as illustrated in Table 4.1. The 48 kb λ-phage DNA condensed into rod-like condensate at 125 nM IHF with a mean length of 248 nm (σ, ±32 nm) and a mean thickness of 30 nm (σ, ±3 nm), whereas under similar condition linear plasmid DNA size 3.4 kb and 10.7 kb 212 nm condensed into rod-like condensate with the mean length of 206 nm (σ, ±35 nm) and 231 nm (σ, ±5 nm), the mean thickness of 34 nm (σ, ±3nm) and 32 nm (σ, ±5 nm), respectively (Table 4.1). The dimensions of spermine-DNA rods were also found to be insensitive to the presence and absence of specific IHF-binding sites. For example, rods formed from the 3.4 kb linear DNA containing no specific IHF sites and the same DNA containing one and two specific IHF sites were the same size within experimental variation, i.e. mean rod length of 206 nm (σ, ±35 nm) for non specific sites vs. 227 nm (σ, ±29 nm) and 203 nm (σ, ±26 nm) for one and two specific sites, respectively, and mean rod thickness of 34 nm (σ, ±3 nm) vs. 31 nm (σ, ±4 nm) and 34 nm (σ, ±5 nm), respectively (Table 4.1). These results also

suggest an architectural role of IHF in DNA condensation, and implicate an underlying similarity in function of IHF and another architectural protein HU which is known to bind and bend the DNA without any sequence specificity in DNA condensation.

When the linear plasmid DNA molecules containing two specific IHF-binding sites separated by 500 and 950 bp DNA length were condensed by spermine in presence of 125 nM IHF, the bundle or rod-like structures produced were very similar in dimensions (Figure 4.3E-H). The mean rod length and thickness of 3.4 kb DNA with two IHF sites separated by 500 bp DNA length were measured to be 203 nm (σ, ±26 nm) and 34 nm (σ, ±5 nm) and of 3.9 kb DNA with two IHF sites separated by 950 bp DNA length 202 nm (σ, ±24 nm) and 34 nm (σ, ±7 nm), respectively (Table 4.1). This finding is also consistent with the condensation studies done with the same DNA molecules in presence of 75 nM IHF and spermidine, as shown in Figure 4.1(E-H) and Table 4.1. The mean rod length and thickness of 3.4 kb DNA with two IHF sites 500 bp apart were measured to be 394 nm (σ, ±33 nm) and 58 nm (σ, ±9 nm) and of 3.9 kb DNA with two IHF sites 950 bp apart 373 nm (σ, ±46 nm) and 57 nm (σ, ±7 nm), respectively. These findings indicate that the bundle lengths are less dependent on the separation between the specific IHF binding sites as compared to the nature of the condensing agents. These results may indicate that the sequence specific IHF binding sites do not dictate the size of a DNA bundle produced upon condensation. However, the phasing of the sites incorporated may not be optimal for controlling rod formation, and we therefore cannot conclude that IHF sites found in the *E. coli* genome do not facilitate the local condensation of DNA into linear bundles.

4.3.3. Effects of IHF on Spermidine and Spermine Induced Condensation of Supercoiled DNA with and without Specific IHF-Binding Sites

We have also investigated the effects of IHF on the condensation of supercoiled DNA by spermidine. Supercoiled DNA is the natural substrate of IHF in the bacterial cell, and supercoiling of DNA within topologically independent domains (~10 kb in average size) is known to facilitate bacterial chromosome compaction *in vivo* [257,285]. We investigated the spermidine-induced condensation of 10.7 kb supercoiled DNA (which contains one natural high affinity specific binding site) and 3.4 kb supercoiled DNA lacking a specific IHF-binding site in absence and presence of IHF. We also studied the condensation of 3.4 kb supercoiled DNA containing two IHF sites under identical condition.

The condensation of supercoiled DNA by spermidine (in the absence of IHF) produces a greater population of rods than linear DNA, due to the torsional strain of the supercoiled DNA (Figure 4.4). The incubation of supercoiled DNA with 75 nM IHF before condensation with spermidine again resulted in an increase in the population of rods to greater than 95%, compared to 40% in the absence of IHF (Figure 4.4). The spermidine induced rod condensates formed from the condensation of supercoiled DNA of two different lengths 10.7 kb and 3.4 kb in presence of IHF were observed to be similar in dimensions. The mean rod lengths were 375 nm ($\sigma, \pm 40$ nm) and 352 nm ($\sigma, \pm 41$ nm) and the mean thickness were 50 nm ($\sigma, \pm 8$ nm) and 51 nm ($\sigma, \pm 7$ nm), respectively (Table 4.2). These results illustrate that the effects of IHF on DNA condensation are fundamentally similar for linear and supercoiled DNA. The 3.4 kb supercoiled DNA containing two specific IHF-binding sites when condensed by

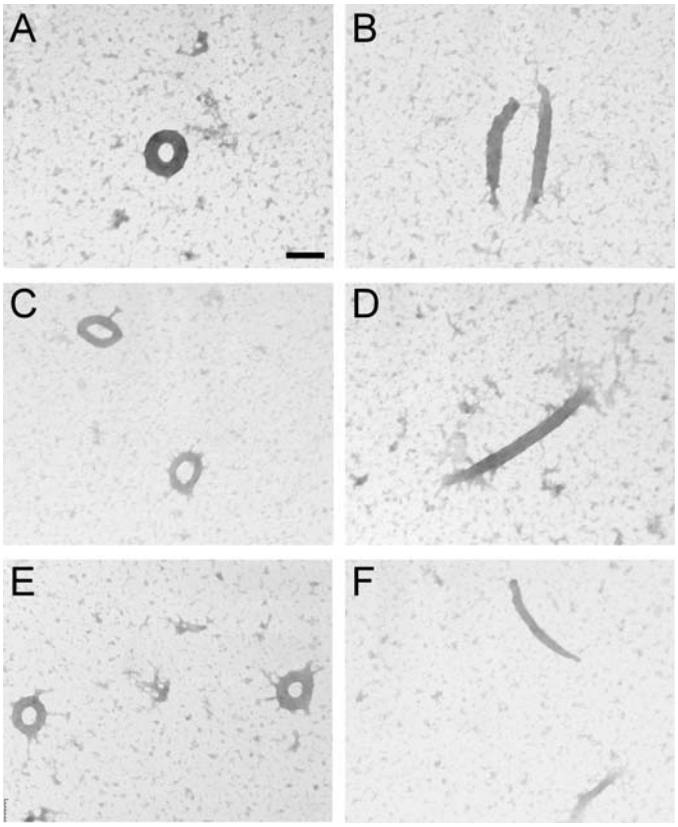

Figure 4.4 Transmission electron microscopy (TEM) images of spermidine-induced supercoiled DNA condensates produced in the presence and absence of IHF. (A) DNA condensates produced by the addition of spermidine to supercoiled 10.7kbDNA. (B) DNA condensates produced by the addition of spermidine to supercoiled 10.7kbDNA in the presence of 75 nM IHF. (C) DNA condensates produced by the addition of spermidine to supercoiled 3.4kbDNA. (D) DNA condensates produced by the addition of spermidine to supercoiled 3.4kbDNA in the presence of 75 nM IHF. (E) DNA condensates produced by the addition of spermidine to supercoiled 3.4kbDNA containing two specific IHF binding sites 500 bp apart. (F) DNA condensates produced by the addition of spermidine to supercoiled 3.4kbDNA containing two specific IHF binding sites 500 bp apart in the presence of 75 nM IHF. All reactions contained final concentration of 5 μM DNA bp, 700 μM spermidine chloride, 0.33×TE (pH 7.8) and 15 mM KCl. Scale bar is 100 nm.

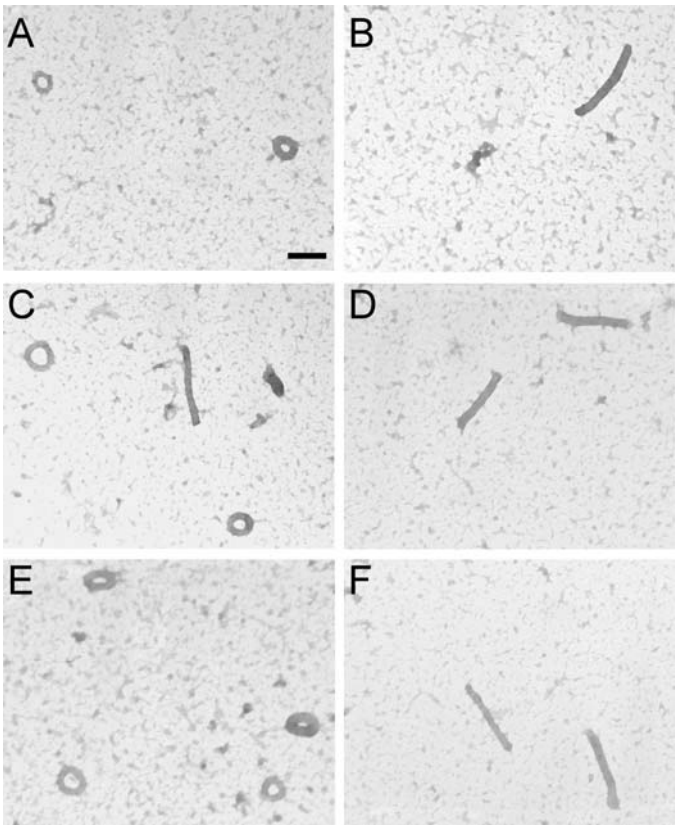

Figure 4.5. Transmission electron microscopy (TEM) images of spermine-induced supercoiled DNA condensates produced in the presence and absence of IHF. (A) DNA condensates produced by the addition of spermine to supercoiled 10.7kbDNA. (B) DNA condensates produced by the addition of spermine to supercoiled 10.7kbDNA in the presence of 125 nM IHF. (C) DNA condensates produced by the addition of spermine to supercoiled 3.4kbDNA. (D) DNA condensates produced by the addition of spermine to supercoiled 3.4kbDNA in the presence of 125 nM IHF. (E) DNA condensates produced by the addition of spermine to supercoiled 3.4kbDNA containing two specific IHF binding sites 500 bp apart. (F) DNA condensates produced by the addition of spermine to supercoiled 3.4kbDNA containing two specific IHF binding sites 500 bp apart in the presence of 125 nM IHF. All reactions contained final concentration of 5 μM DNA bp, 15 μM spermine chloride, 0.33×TE (pH 7.8) and 15 mM KCl. Scale bar is 100 nm.

spermidine in presence of IHF produced rods with the average length of 340 nm (σ, ±43 nm) and the average thickness of 48 nm (σ, ±8 nm). Thus, rod dimensions appear to also be independent of the presence of specific IHF-binding sites in supercoiled DNA.

Supercoiled DNA 10.7 kb, 3.4 kb lacking a specific IHF-binding site and 3.4 kb DNA with two specific sites condensed by spermine formed toroids and rods (toroids 55%, rods 45%). When supercoiled DNA was condensed in presence of 125 nM IHF an increase in the relative rod populations to over 90% were observed for all three DNA molecules (Figure 4.5). The rod condensates formed by spermine in presence of IHF were ~200 nm in length and ~30 nm in thickness (Table 4.2). Rod dimensions did not change significantly with the length of the supercoiled DNA or with the introduction of specific IHF-binding sites, as shown in Table 4.2.

Significant differences in condensate dimensions were observed for the different condensing agents (trivalent spermidine or tetravalent spermine). As an example, when 3.4 kb supercoiled DNA with two specific IHF sites was condensed by spermine in presence of 125 nM IHF rods were formed with a mean length of 200 nm (σ, ±27 nm) and a mean thickness of 34 nm (σ, ±5 nm), while rods formed by the addition of spermidine had a mean length of 340 nm (σ, ±43 nm) and a mean thickness of 48 nm (σ, ±8 nm), in presence of 75 nM IHF. Our findings illustrate that supercoiled DNA of different length, and with and without specific IHF sites, are compacted by polyamines into linear bundles in presence of IHF proteins with bundle length being dictated mostly by the nature of the condensing agent.

4.3.4. Model for Enhanced Bundle-Like DNA Condensate Formation in the Presence of IHF

The co-existence of both condensate morphologies reflects the isoenergetics of DNA packing within rods and toroids, including the energy required for the smooth bending of DNA within a toroid versus that required to produce sharp bends at the ends of a rod [1]. It has also been demonstrated that DNA condensation under conditions that make base pair destacking less energetically unfavorable (e.g. in mixed alcohol-water solvents, hydrophobic ligands, superhelical stress) increases the population of rod-like condensates by lowering the energetic penalty associated with sharp bends [41,83,86,112,241,242]. In the previous chapter it was demonstrated that DNA condensate morphology can be controlled by HU protein which can significantly bend the DNA and stabilize the rod-like condensate structure. We demonstrated that HU alone does not condense DNA into ordered densely packed particles, but kinetically and thermodynamically stabilized rod-like DNA condensate structures by acting as a DNA bending protein during *in vitro* DNA condensation. The experiments presented in this chapter for an another DNA bending protein, IHF, confirm and extend these conclusions. We have demonstrated that IHF can guide the condensation of DNA into structures with linear bundles (i.e. rods) when DNA is condensed from two different condensing agents, trivalent spermidine and tetracation spermine. Thus, the ability to control DNA condensate morphology appears also to be an intrinsic property of IHF. Together our results suggest that the primary function of IHF and HU in DNA compaction appears to an architectural function.

As discussed in Chapter 3 for HU, the bends created by IHF in DNA will effectively facilitate the rod formation in the presence of a condensing agent that promotes DNA helix-helix contacts because the ends of the rod condensates contain sharply bent DNA. In contrast, DNA condensed within toroids is smoothly bent over a radius of curvature that is much greater than that of the sharp bends induced by IHF. Thus, IHF should not be expected to promote toroid formation, but should be expected to suppress toroid formation by introducing bends that are incompatible with DNA packing within toroids.

4.4. SUMMARY AND IMPLICATIONS

The structure of the bacterial nucleoid is not well-established. Furthermore, even the roles of major nucleoid proteins in modulating the structure of the bacterial nucleoid remain to be understood in detail. The nucleoid-associated proteins are classified as DNA bending proteins (HU, IHF) and DNA bridging proteins (H-NS, SMC) [286]. We have used *in vitro* DNA condensation as a means to elucidate the effects of DNA bending proteins (IHF, HU) on the compaction of bacterial chromosome into the nucleoid. We have shown that IHF strongly influences condensate morphology when DNA is condensed by polyamines. The non-sequence specific DNA bending protein HU showed similar effects when present during condensation of DNA by polyamines and crowding agents. In contrast to HU, IHF binds DNA both sequence specifically (high-affinity) and non-sequence specifically (low affinity). We show that sequence specific binding by IHF is not required for IHF to strongly influence condensate morphology. However, for DNA containing the IHF sequence specific binding sites, the effect of IHF may be due to the

both, sequence specific and non-sequence specific binding of IHF proteins. We also demonstrate that the positions of IHF sequence specific binding sites do not generally correlate with the dimensions of the bundle-like DNA condensates. However, we cannot rule out that IHF specific sites inserted may not be in proper phase for dictating the size of the rod condensates.

The increase in the relative population of rod-like DNA condensates is independent of DNA length over the range 3.5–48.5 kbp for linear and supercoiled DNA. These results demonstrate that IHF can guide the morphology of DNA condensates without significantly altering condensate dimensions. The ability of the IHF to guide DNA into bundle like structure *in vitro*, as observed with HU previously, suggests that IHF can act as an architectural factor during DNA condensation by providing the bending energy required for rod-formation through the binding energy offered from IHF-DNA interactions. The similar effects on DNA condensation of IHF and HU suggest that both the proteins have related general functions in the modulation of chromosome structure in bacteria. IHF and HU, as architectural factors, could locally organize chromosomal DNA in the presence of cellular condensing environment to facilitate its condensation into a more ordered, bundle-like state *in vivo*.

CHAPTER 5

CONCLUSIONS AND FUTURE WORK

5.1. IMPLICATIONS OF DNA CONDENSATION ON THE DEVELOPMENT OF GENE DELIVERY SYSTEMS

In the past few years major advances have been made in the fields of oligonucleotide therapy [167-170,172,174-176,287]. Among these, siRNAs have emerged with great promise for effective therapies for a wide variety of diseases, like cardiovascular diseases, viral infections, and cancer, as well as providing a functional genomics tool for modulating gene expression through RNA interference (RNAi) [171-176]. Effective implementation of oligonucleotide technology in biology and medicine largely depends on the transfection efficiencies of the oligonucleotides. However, poor permeability of the cell membrane is the critical barrier to the development of oligonucleotides therapeutics [154,161]. Most non-viral DNA delivery systems developed to date involve charge-neutralization and condensation of DNA into small particles that facilitate DNA entry into the cells by endocytosis and escape into the cytoplasm before endosomal degradation [154]. Finally, the entry of the DNA into the nucleus is believed to occur by transport through the nuclear pores (~10 nm diameter) or during cell division [154]. Thus, many oligonucleotide delivery systems that are very potent for *in vitro* transfection, fail to exhibit the same level of potency in nondividing cells, such as hepatocytes *in vivo*. The efficiency of cellular uptake and transgene

expression has shown to be greatly improved by the packaging of DNA into particles with dimensions smaller than 50 nm [151,154,161,165,166].

Efforts to improve oligonucleotide delivery system have driven the development of novel reagents for DNA condensation and their physiochemical characterization. The potential for nucleic acid structure and topology to improve DNA compaction for nonviral DNA delivery has received far less attention than the development of new condensing agents. In this dissertation, we have described the development of new strategies for the compaction of short oligonucleotides into smaller condensates and shown a series of DNA condensation strategies that should more generally facilitate the design of novel delivery vectors. We have designed oligonucleotides with half-sliding complementary sequences that self-assemble to form long duplexes with flexible sites at regular intervals, in the form of single-stranded nicks and single-stranded gaps. The introduction of nicks and gaps in the nucleic acid structure is a simple way to introduce nucleation sites that favor the formation of small and uniform condensates. As controlling the size of condensed DNA particles is an important factor for *in vivo* delivery, DNA with regular nicks or gaps represents a new class of nucleic acid structure that should prove useful in conjunction with a variety of non-viral nucleic acid delivery systems. The results of this thesis support a new approach for the design of vectors for efficient delivery of oligonucleotides as well as gene-length DNA where nicked or gapped DNA could be appended at one or both ends. However, further studies involving *in vitro* and *in vivo* gene delivery experiments are necessary to address whether these improvements in DNA condensation actually translate to enhanced gene/oligonucleotide transfer to target cells.

5.2. A MODEL FOR THE CONDENSATION OF BACTERIAL NUCLEOID

Prokaryotes and eukaryotes must condense genomic DNA in a manner that confers both significant compaction and accessibility of the genome for replication, transcription and repair machinery. Bacterial chromosomes are distinguished from the eukaryotic nucleus as not being organized into nucleosome structures and not being confined within a cell nucleus. The 4.6 Mb circular chromosome of *E. coli* with a contour length of approximately 1.6 mm must fit within a cell of about 1 μm in linear dimensions. However, under optimal conditions, *E. coli* replicates, segregates and repackages the chromosomes every 20 min. Thus, the bacterial chromosome is very dynamic in nature [288], and several mechanisms operate to compact and organize the bacterial chromosome [11,12,249,286].

Biochemical and physical techniques have improved our understanding of bacterial chromosome organization and dynamics. The electron microscopic and biochemical analysis confirmed that the 4.6 Mb circular *E. coli* chromosome does not organize into a single topological unit but rather package into rosette-like structures with many individually plectonemically interwound loops that emanate from a central core [251,252,254,255,289]. Initially, the average size of these domains was estimated to be several hundreds of kb [134,252,254,290]. However, most recent studies using the transcription of more than 300 supercoiling-sensitive genes in *E. coli* and electron microscopy indicate that these domains are much smaller than previously reported, with an average length of approximately 10 kb [257]. Furthermore, domain boundaries are dynamic as well distributed in a random manner throughout the genome, rather than stably fixed at specific sites [257]. Similar conclusions about the dynamic nature of the

domain boundaries were reached regarding the domain structure in a region of the *Salmonella* chromosome using the supercoiling dependent γδ site-specific recombination assay [291]. The dynamic nature of topologically isolated domains implies that barriers separating them are transient in nature. However, the factors responsible for creating topological barriers and for determining domain sizes are not known. Barriers could be the result of binding by yet unidentified proteins and perhaps RNA [11,249,257,259].

The introduction of negative supercoiling and the resulting formation of highly branched DNA structures is recognized as an effective way by which the *E. coli* chromosome reduces the size of the topologically restricted domains [12,258,290]. While topological constraints are clearly important for maintaining DNA compaction, these constraints alone do not account for the level of DNA condensation observed in the nucleoid. Proteins associated with the chromosome can facilitate the additional compaction through the energy provided by protein-DNA interactions. In bacteria, about half of the supercoils in a domain exist as branched interwound structures and half of the negative supercoils are stabilized by the association highly conserved bacterial proteins that are referred to as nucleoid-associated proteins (NAPs) [12,292,293]. The key nucleoid proteins that are highly expressed under nutrient-rich exponential growth conditions include HU, integration host factor (IHF), histone-like, nucleoid-structuring protein (H-NS).

The crowded nature of the cytoplasm and polyamines also play a critical role in bacterial chromosome condensation, dictating the well-defined structure of the nucleoid. As the nucleoid is not confined by a nuclear membrane, the extremely crowded bacterial cytoplasm, rich in proteins and RNA (~340 mg/ml), constrains the volume occupied by

the nucleoid and favors DNA condensation [294-296]. Indeed, when the cytoplasm leaks out of the cell membrane the nucleoid has been shown to expand to the entire internal volume of the *E. coli* cell [297]. Conversely, polyethylene glycol or dextrans can stabilize isolated nucleoids [233,260,296]. Cellular polyamines, which are polycationic at physiological pH, are major components of bacterial cells and also well characterized DNA condensing agents [33,298]. In prokaryotes, the most abundant polyamines are putresciene and spermidine [299-301]. The high cellular abundance of these polyamines (5-20 mM) and the ability of spermidine to stabilize the condensed bacterial chromosome in isolated nucleoids suggest an important role of polyamine in the compaction of DNA in bacterial cells [299,302].

While DNA supercoiling, nucleoid-associated proteins and other cellular factors have all been implicated in bacterial chromosome condensation, no single factor is sufficient to achieve high-density DNA condensation. The relative contribution of each factor to DNA condensation also remains unclear. Zimmerman and coworkers have presented evidence that cellular extracts from *E. coli* can work together with HU to condense DNA [232,233]. However, the molecular mechanisms by which nucleoid-associated proteins work with each other, with polyamines, macromolecular crowding and DNA topology to control chromosome condensation have not been systematically explored. Subsequent studies by Zimmerman and coworkers have even suggested that HU and other nucleoid-associated proteins are not primarily responsible for maintaining the condensed form of DNA in the isolated nucleoids [250,260]. Thus, while nucleoid-associated proteins have been implicated in the organization of the *E. coli* chromosome in the nucleoid, their modes of action *in vivo* is still the source of an ongoing debate.

We have used an experimental system for probing the function of nucleoid-associated proteins on DNA compaction in *E. coli* cell. Based on our results we conclude that HU and IHF, bacterial proteins associated with the bacterial chromosome and DNA bending, function as architectural proteins during chromosomal condensation by directing the local packing of DNA into a linear bundle-like state. Our results regarding the functionality of two DNA bending proteins associated with bacterial chromosomes in the presence of condensing agents that mimic cellular conditions (i.e. polyamines and crowding agents) suggest a model for chromosome organization in the bacterial nucleoid. In this model the chromosome is compacted in part by isolated topological domains which are further folded by negative supercoiling. The size of the domains would be dictated by the dynamic domain barriers (Figure 5.1). In presence of polyamines and macromolecular crowding agents (RNA and protein present in cytoplasm) DNA helices in the domains approach each other to maximize the attractive interactions between them. Our condensation experiments with polyamines and crowding agents showed that in absence of DNA bending proteins HU and IHF, DNA is condensed into toroidal structure. Previous experiments showed that *E. coli* treated with chloramphenicol, an inhibitor of translation induces the nucleoid to compact into toroidal structures [303,304]. Together, these observations suggest that the binding of DNA architectural proteins HU and IHF in supercoiled domains directs the local packaging of the DNA into linear bundle-like structures (Figure 5.1). The sequence independent binding of these proteins potentially allows them to effectively function throughout the chromosome.

Our model is consistent with what is currently known about DNA condensation and architectural factor binding to DNA. Linear bundle-like or rod-like structures of

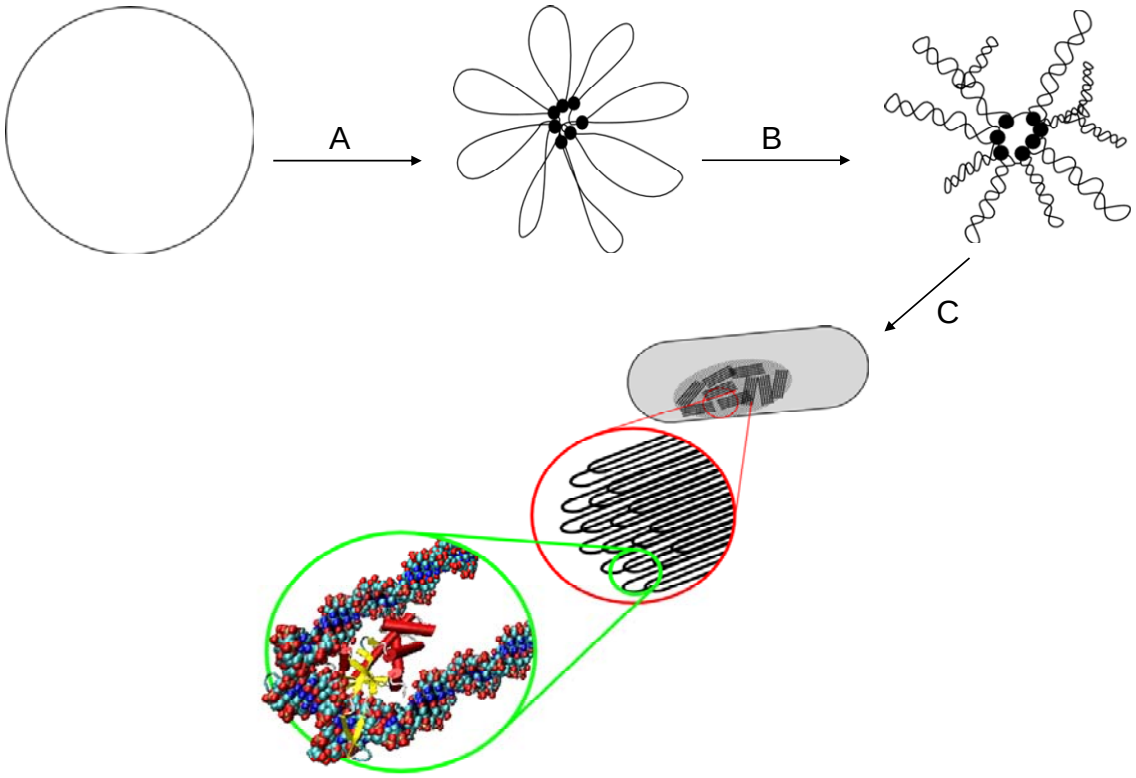

Figure 5.1. A model for the condensation of DNA in bacterial nucleoid. The different levels of organization of chromosomal DNA in bacterial cell, as described in text, are: (A) topologically isolated domain formation, (B) negatively supercoiled DNA helices within the domains and (C) local organization of DNA into linear-bundle like structures. A portion of duplex DNA is shown with bound DNA bending protein (HU/IHF) as a ribbon structure.

condensed DNA formation is facilitated and stabilized further by HU and IHF binding to DNA, which reduces the free energy required for DNA bending at ends of regions that contain DNA condensed in linear bundles. Our model suggests a generally condensed, mostly folded chromosome in which the architecture of the chromosome is partly dictated by the DNA bending proteins HU and IHF. In this model we assume that the condensation of DNA includes close interactions between the DNA helices in parallel

alignment. However, binding of some proteins could cause antagonistic effects and thereby decrease condensation (e.g., under some conditions H-NS has been reported to rigidify DNA *in vitro*) [305].

We note that cellular RNA content could also affect nucleoid condensation by modulating the availability of polyamines for DNA binding as strong competition between RNA and DNA has been reported for polyamine binding [250,306]. In the late stationary phase when most of the DNA binding proteins are degraded, the only proteins tht are present in high copy number are Dps and IHF (15,000 copies each per cell) and also HU (7,500 copies per cell) [12,264]. The bacterial chromatin reorganizes into cholesteric crystalline morphologies in which DNA filaments are arranged into local parallel bundle fashion [304,307-309]. Although the phase transition has been attributed to the DNA-Dps complex formation [307,308,310], according to our model other DNA bending proteins like IHF and HU could also facilitate reorganization of DNA into parallel bundle-like structures in the presence of polyamines (Figure 5.1). Our model is also supported by the fact that in starved *dps*$^{-}$ bacteria chromosome also organizes into cholesteric phase [307,308].

We note that the model we have developed is structurally similar to a model recently proposed by Zimmerman for DNA organization in the bacterial nucleoid during the growth phase, even though the two models are based upon completely different observations [250]. Both models suggest the formation of parallel bundles of condensed DNA, with nucleoid-associated proteins bound at the ends of the bundles. However, Zimmerman suggests that HU promotes this structure by acting as an antagonist to condensation. The results presented in this dissertation do not suggest that HU acts as an

antagonist to DNA condensation. However, additional experiments are needed to determine definitively if HU antagonizes or promotes condensation. We also note that our condensation experiments in the absence of any restricted domain barriers showed that the linear DNA condensate size is independent of DNA length and is controlled by the condensing solution conditions. The scenario could be different during bacterial chromosome compaction in the presence of cellular factors responsible for creating domain boundaries and hence dictating the size of the domains.

5.3. FUTURE WORK

5.3.1. Determining whether HU Promotes or Antagonizes DNA Condensation

The condensation studies presented here demonstrated that HU functions as an architectural protein during DNA condensation by polyamines and crowding agents. Because HU has another binding mode that could be antagonistic to DNA compaction [10,231,250,261,262] it is necessary to investigate whether such an antagonistic mode of HU binding exists during polyamine-driven or crowding-induced condition condensation. The results from such investigations will have important implications regarding previous conflicting proposals regarding the ability for HU to promote or antagonize DNA condensation.

5.3.2. Investigation of the Interplay between HU Binding and DNA Topology on Condensation

Among the different factors facilitating DNA condensation, sequence-dependent intrinsic curvature may also modulate the propensity of chromosomal DNA to compact in

a ‘programmed’ manner [311]. Indeed, phased A-tracts are found in 100 bp clusters in the *E. coli* genome [311]. Phased A-tracts promote local bending in the helix which could facilitate DNA loop formation and provide high affinity binding sites for chromosomal associated proteins, such as HU and H-NS. Similarly supercoiling are also known to provide high affinity binding sites for HU [229,237,239,244,311,312]. Accordingly, it has been proposed (but never demonstrated) that these structural features of bacterial DNA act in concert with nucleoid proteins to package chromosomal DNA.

A plasmid DNA containing fifteen phased A-tract repeats (Bluescript II SK- with the insert 5’-$ATC_2ATCGAC_2(A_6CG_3CA_6CG_2C)_7A_6GCAGTG_2A_2G$-3’) was used to investigate the activity of HU in compaction of DNA containing sequence-directed curvature. In our condensation studies of linear plasmid DNA with fifteen phased A-tract repeats, *Atract15*, we have found that HU exerts a powerful influence over the morphology of DNA particles formed upon condensation by spermidine. When *Atract15* is condensed by spermidine the population of rod-like condensates increases with HU concentration (Figure 5.2). More extensive studies are required to investigate how HU works in conjunction with DNA static curvature. *Atract15* DNA, and related plasmids with two to four identical inserts, could be used to model regions of the *E. coli* genome that contain extensive sequence-directed curvature. The circular plasmid can be linearized to separate the influence of supercoiling from sequence-directed curvature. Instead of linear DNA, similar experiments with supercoiled plasmid DNA containing phased A-tracts would enable us to determine the contribution of sequence-directed curvature and supercoiling together on DNA condensation in the presence of HU.

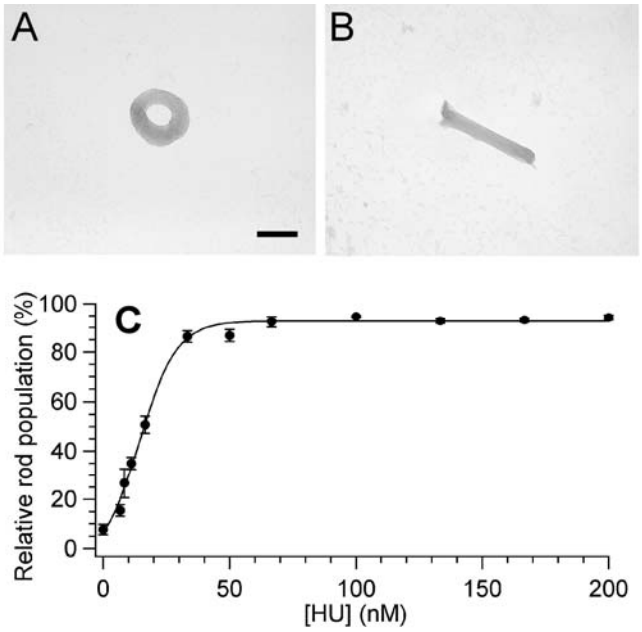

Figure 5.2. Spermidine-induced DNA condensates morphologies and morphology statistics as a function of HU concentration. (A) TEM image of a representative condensate of *Atract15* DNA condensed by spermidine (no HU present). (B) TEM image of a representative condensate produced under identical conditions as in A, except in the presence of 50 nM HU. Scale bar is 100 nm. (C) Relative rod populations versus HU concentration for *Atract15* DNA condensed by spermidine. Samples were 5 μM DNA bp, 700 μM spermidine chloride, 0.33×TE (pH 7.8), 15 mM NaCl, and indicated concentrations of HU dimer.

5.3.3. Investigation of HU Binding to Pre-Bent and Condensed DNA

A complete understanding of how HU guides DNA condensation will also require determining if HU alters the kinetics and/or the thermodynamics of condensation. This will require knowledge of the k_{on} and k_{off} rates for HU binding to linear DNA and bent DNA, and for these forms of DNA under a range of solution conditions. HU has previously been reported to exhibit greater binding affinity for circularized DNA than linear DNA [313]. Thus, we anticipate observing a stronger binding affinity of HU to the more easily bent DNA relative to unbent DNA. Our study demonstrated that the

effectiveness of HU is reduced in promoting rod formation when HU is added prior to a DNA condensing agent, as compared to coincident addition. We have hypothesized that HU added coincident with a condensing agent is more efficient in guiding condensate structure if the on-rate of binding to DNA is faster for bent DNA. In that case HU would preferentially bind at the ends of nucleated rods rather than in the linear region of a rod or along a DNA strand that has nucleated a toroid. However, it is difficult to predict how k_{on} and k_{off} rates might change during DNA condensation.

5.3.4. Determine the Mechanism by which H-NS Promotes or Antagonizes DNA Condensation

H-NS (histone-like nucleoid structuring protein) is the third protein to be identified as a major nucleoid-associated protein that was suggested to participate in the structural organization of the bacterial chromosome. H-NS is a 15.6 kDa protein with two distinct domains: an N-terminal dimerization-oligomerization domain and a C-terminal DNA binding domain, connected by a flexible linker [286]. It exists predominantly as dimer which has the ability to oligomerize into higher-order complexes via a coiled-coil domain [314]. In *E. coli* ~10 000 dimers of H-NS are present per cell [264]. H-NS binding to DNA is nonspecific, however it preferentially binds to curved DNA or A/T rich sequences [10,315,316]. Massive overexpression of H-NS in *E. coli* results in a highly condensed nucleoid with decreased global transcription and cell viability [317-319].

Microscopy studies have suggested that H-NS compacts DNA by forming bridges between distal DNA segments, but there is also evidence of H-NS coating on DNA

without inducing any significant compaction of DNA [316,320,321]. The exact role of H-NS in bacterial DNA compaction is much less understood and more contested than that of HU and IHF. Recent single molecule experiment with H-NS and λ-DNA indicate no appreciable compaction of DNA by H-NS binding, but rather the rigidification of DNA by the polymerization of H-NS [305]. If this is true, H-NS may work as an antagonist to other nucleoid proteins, including HU and IHF.

5.3.5. Determine if HU, IHF and H-NS Work Together and with Other Solution Factors to Regulate DNA Condensation

For a better understanding of how nucleoid-associated proteins function in structuring the nucleoid, it is important to investigate the possible interplay between the nucleoid-associated proteins HU, IHF and H-NS in guiding and/or promoting and/or antagonizing DNA condensation by polyamines and crowding agents. Studies of individual nucleoid proteins will not, of course, reveal how these proteins might work together (or as mutual antagonists) in DNA condensation. However, the information regarding their interplay is scarce in the literature. This deficiency originates in part from the fact that *in vivo* techniques designed to assess the biological roles of these proteins HU, IHF and H-NS in combination fail because a viable triple mutant deficient in HU, IHF and H-NS could not be constructed [322]. Thus, our experimental system can be used to gain insight into these issues. For example, the condensation of linear DNA by spermidine in the presence of HU with increasing concentrations of IHF and H-NS, respectively, IHF with H-NS, and ultimately with all three proteins together can be systematically studied. In the case of HU and H-NS, competition might be involved for

the interactions of these proteins to DNA during condensation, as both proteins exhibit preferential binding to curved DNA [229,237,323,324]. This possibility can be probed using the A-tract DNA described above. Similar studies with the supercoiled plasmid of a domain size (~10kb) can determine if the interplay between these nucleoid-associated proteins is specific to, or enhanced by, DNA supercoiling.

The intracellular abundance of HU, IHF and H-NS significantly varies with the growth phase of the bacteria. Thus, growth dependent intracellular concentrations of these proteins could have direct consequences on the architectural function of these proteins that control many cellular functions. Hence, AFM analysis could be useful for developing a better picture of the structural modulations that might occur in the nucleoid with different growth phases. Together these results could lead to a better understanding of how these proteins work together with other cellular factors in structuring the bacterial chromosome in a compact nucleoid.

REFERENCES

1. Bloomfield, V.A. (1991) *Biopolymers*, **31**, 1471-1481.

2. van Holde, K. (1989) *Chromatin*. Springer-Verlag, New York.

3. Cerritelli, M.E., Cheng, N.Q., Rosenberg, A.H., McPherson, C.E., Booy, F.P. and Steven, A.C. (1997) *Cell*, **91**, 271-280.

4. Guo, P.X., Peterson, C. and Anderson, D. (1987) *J. Mol. Biol.*, **197**, 229-236.

5. Morita, M., Tasaka, M. and Fujisawa, H. (1993) *Virology*, **193**, 748-752.

6. Petrov, A.S. and Harvey, S.C. (2007) *Structure*, **15**, 21-27.

7. Tzlil, S., Kindt, J.T., Gelbart, W.M. and Ben-Shaul, A. (2003) *Biophys. J.*, **84**, 1616-1627.

8. Ali, I., Marenduzzo, D. and Yeomans, J.M. (2004) *J. Chem. Phys.*, **121**, 8635-8641.

9. Purohit, P.K., Inamdar, M.M., Grayson, P.D., Squires, T.M., Kondev, J. and Phillips, R. (2005) *Biophys. J.*, **88**, 851-866.

10. Dame, R.T. (2005) *Mol. Microbiol.*, **56**, 858-870.

11. Travers, A. and Muskhelishvili, G. (2005) *Curr. Opin. Genet. Dev.*, **15**, 507-514.

12. Johnson, R.C., Johnson, L.M., Schmidt, J.W. and Gardner, J.F. (2005) In Higgins, N. P. (ed.), *The bacterial chromosome*. ASM Press, Washington, D.C., pp. 65-132.

13. Kornberg, R.D. and Lorch, Y.L. (1999) *Cell*, **98**, 285-294.

14. Struhl, K. (1999) *Cell*, **98**, 1-4.

15. Balhorn, R. (1989) In Adolph, K. W. (ed.), *Molecular biology of chromosome function*. 1 ed. Springer-Verlag, New York, pp. 366-395.

16. Allen, M.J., Lee, C., Lee, J.D., Pogany, G.C., Balooch, M., Siekhaus, W.J. and Balhorn, R. (1993) *Chromosoma*, **102**, 623-630.

17. Santi, S., Rubbini, S., Cinti, C., Squarzoni, S., Matteucci, A., Caramelli, E., Guidotti, L. and Maraldi, N.M. (1994) *Biol. Cell*, **81**, 47-57.

18. Richards, K.E., Williams, R.C. and Calendar, R. (1973) *J. Mol. Biol.*, **78**, 255-259.

19. Earnshaw, W. and Harrison, S. (1977) *Nature*, **268**, 598-602.

20. Earnshaw, W.C., King, J., Harrison, S.C. and Eiserling, F.A. (1978) *Cell*, **14**, 559-568.

21. Harrison, S.C. (1983) *J. Mol. Biol.*, **171**, 577-580.

22. Hud, N.V., Allen, M.J., Downing, K.H., Lee, J. and Balhorn, R. (1993) *Biochem. Biophys. Res. Commun.*, **193**, 1347-1354.

23. Gellert, M. and Davies, D.R. (1964) *J. Mol. Biol.*, **8**, 341-347.

24. North, A.C. and Rich, A. (1961) *Nature*, **191**, 1242-1245.

25. Klimenko, S., Tikchonenko, T. and Andreev, V. (1967) *J. Mol. Biol.*, **23**, 523-533.

26. Serwer, P. (1986) *J. Mol. Biol.*, **190**, 509-512.

27. Lepault, J., Dubochet, J., Baschong, W. and Kellenberger, E. (1987) *EMBO J.*, **6**, 1507-1512.

28. Hud, N. (1995) *Biophys. J.*, **69**, 1355-1362.

29. Gosule, L.C. and Schellman, J.A. (1976) *Nature*, **259**, 333-335.

30. Allen, M., Lee, J., Lee, C. and Balhorn, R. (1996) *Mol. Reprod. Devel.*, **45**, 87-92.

31. Hud, N.V., Downing, K.H. and Balhorn, R. (1995) *Proc. Natl. Acad. Sci. USA*, **92**, 3581-3585.

32. Hud, N.V. and Downing, K.H. (2001) *Proc. Natl. Acad. Sci. USA*, **98**, 14925-14930.

33. Chattoraj, D.K., Gosule, L.C. and Schellman, J.A. (1978) *J. Mol. Biol.*, **121**, 327-337.

34. Widom, J. and Baldwin, R.L. (1980) *J. Mol. Biol.*, **144**, 431-453.

35. Widom, J. and Baldwin, R.L. (1983) *Biopolymers*, **22**, 1595-1620.

36. Laemmli, U.K. (1975) *Proc. Natl. Acad. Sci. USA*, **72**, 4288-4292.

37. Hsiang, M.W. and Cole, R.D. (1977) *Proc. Natl. Acad. Sci. USA*, **74**, 4852-4856.

38. Manning, G.S. (1978) *Q. Rev. Biophys.*, **11**, 179-246.

39. Wilson, R.W. and Bloomfield, V.A. (1979) *Biochemistry*, **18**, 2192-2196.

40. Ma, C. and Bloomfield, V.A. (1994) *Biophys. J.*, **67**, 1678-1681.

41. Arscott, P.G., Ma, C.L., Wenner, J.R. and Bloomfield, V.A. (1995) *Biopolymers*, **36**, 345-364.

42. Lerman, L.S. (1971) *Proc. Natl. Acad. Sci. USA*, **68**, 1886-1890.

43. Yoshikawa, K. and Matsuzawa, Y. (1995) *Physica D*, **84**, 220-227.

44. Vasilevskaya, V.V., Khokhlov, A.R., Matsuzawa, Y. and Yoshikawa, K. (1995) *J. Chem. Phys.*, **102**, 6595-6602.

45. Maniatis, T., Venable, J.J. and Lerman, L. (1974) *J. Mol. Biol.*, **84**, 37-64.

46. Bloomfield, v.A., Crothers, D.M. and Tinoco, I. (2000) *Nucleic acids : Structures, properties and functions*. University Science Books, Sausalito, CA.

47. Bloomfield, V. (1997) *Biopolymers*, **44**, 269-282.

48. Hagerman, P.J. (1988) *Annu. Rev. Biophys. Biophys. Chem.*, **17**, 265-286.

49. Williams, L.D. (2000) *Annu. Rev. Biophys. Biomol. Struct.*, **29**, 497-521.

50. Hagerman, P.J. (1990) *Annu. Rev. Biochem.*, **59**, 755-781.

51. Schellman, J.A. and Harvey, S.C. (1995) *Biophys. Chem.*, **55**, 95-114.

52. Trifonov, E.N., Tan, R.K.Z. and Harvey, S.C. (1988) *Static persistence length of DNA*. Adenine Press, New York.

53. Vologodskaia, M. and Vologodskii, A. (2002) *J. Mol. Biol.*, **317**, 205-213.

54. Shen, M., Downing, K., Balhorn, R. and Hud, N. (2000) *J. Am. Chem. Soc.*, **122**, 4833-4834.

55. Travers, A.A., Ner, S.S. and Churchill, M.E.A. (1994) *Cell*, **77**, 167-169.

56. Riemer, S.C. and Bloomfield, V.A. (1978) *Biopolymers*, **17**, 785-794.

57. Bloomfield, V. (1996) *Curr. Opin. Struct. Biol.*, **6**, 334-341.

58. Rau, D. and Parsegian, V. (1992) *Biophys. J.*, **61**, 246-259.

59. Flock, S., Labarbe, R. and Houssier, C. (1995) *J. Biomol. Struct. Dyn.*, **13**, 87-102.

60. Buche, A., Colson, P. and Houssier, C. (1993) *J. Biomol. Struct. Dyn.*, **11**, 95-119.

61. de Frutos, M., Raspaud, E., Leforestier, A. and Livolant, F. (2001) *Biophys. J.*, **81**, 1127-1132.

62. Raspaud, E., Chaperon, I., Leforestier, A. and Livolant, F. (1999) *Biophys. J.*, **77**, 1547-1555.

63. Raspaud, E., de la Cruz, M.O., Sikorav, J.L. and Livolant, F. (1998) *Biophys. J.*, **74**, 381-393.

64. Rouzina, I. and Bloomfield, V.A. (1997) *Biophys. Chem.*, **64**, 139-155.

65. Rouzina, I. and Bloomfield, V.A. (1996) *J. Phys. Chem.*, **100**, 4292-4304.

66. Oosawa, F. (1968) *Biopolymers*, **6**, 1633-1647.

67. Oosawa, F. (1971) *Polyelectrolytes*. Mercel Dekker, New York.

68. Rouzina, I. and Bloomfield, V. (1996) *J. Phys. Chem.*, **100**, 9977-9989.

69. Ha, B.Y. and Liu, A.J. (1997) *Phys. Rev. Lett.*, **79**, 1289-1292.

70. Strey, H.H., Podgornik, R., Rau, D.C. and Parsegian, V.A. (1998) *Curr. Opin. Struct. Biol.*, **8**, 309-313.

71. Arenzon, J.J., Stilck, J.F. and Levin, Y. (1999) *Eur. Phys. J. B*, **12**, 79-82.

72. Shklovskii, B.I. (1999) *Physical Review E*, **60**, 5802-5811.

73. Shklovskii, B.I. (1999) *Phys. Rev. Lett.*, **82**, 3268-3271.

74. Gelbart, W.M., Bruinsma, R.F., Pincus, P.A. and Parsegian, V.A. (2000) *Physics Today*, **53**, 38-44.

75. GronbechJensen, N., Mashl, R.J., Bruinsma, R.F. and Gelbart, W.M. (1997) *Phys. Rev. Lett.*, **78**, 2477-2480.

76. Besteman, K., Zevenbergen, M.A.G., Heering, H.A. and Lemay, S.G. (2004) *Phys. Rev. Lett.*, **93**.

77. Rau, D. and Parsegian, V. (1992) *Biophys. J.*, **61**, 260-271.

78. Podgornik, R., Strey, H.H., Rau, D.C. and Parsegian, V.A. (1995) *Biophys. Chem.*, **57**, 111-121.

79. Leikin, S., Rau, D.C. and Parsegian, V.A. (1991) *Phys. Rev. A*, **44**, 5272-5278.

80. Rau, D., Lee, B. and Parsegian, V. (1984) *Proc. Natl. Acad. Sci. USA*, **81**, 2621-2625.

81. Hud, N.V. and Vilfan, I.D. (2005) *Annu. Rev. Biophys. Biomol. Struct.*, **34**, 295-318.

82. Park, S. and Healy, K.E. (2003) *Bioconjug. Chem.*, **14**, 311-319.

83. Arscott, P.G., Li, A.Z. and Bloomfield, V.A. (1990) *Biopolymers*, **30**, 619-630.

84. Marquet, R., Wyart, A. and Houssier, C. (1987) *Biochim. Biophys. Acta*, **909**, 165-172.

85. Vilfan, I.D., Conwell, C.C., Sarkar, T. and Hud, N.V. (2006) *Biochemistry*, **45**, 8174-8183.

86. Plum, G.E., Arscott, P.G. and Bloomfield, V.A. (1990) *Biopolymers*, **30**, 631-643.

87. Vijayanathan, V., Thomas, T., Shirahata, A. and Thomas, T.J. (2001) *Biochemistry*, **40**, 13644-13651.

88. Haynes, M., Garrett, R.A. and Gratzer, W.B. (1970) *Biochemistry*, **9**, 4410-&.

89. Deng, H. and Bloomfield, V.A. (1999) *Biophys. J.*, **77**, 1556-1561.

90. Allison, S.A., Herr, J.C. and Schurr, J.M. (1981) *Biopolymers*, **20**, 469-488.

91. Fang, Y. and Hoh, J. (1999) *FEBS Lett.*, **459**, 173-176.

92. Lin, Z., Wang, C., Feng, X., Liu, M., Li, J. and Bai, C. (1998) *Nucleic Acids Res.*, **26**, 3228-3234.

93. Yoshikawa, Y., Yoshikawa, K. and Kanbe, T. (1999) *Langmuir*, **15**, 4085-4088.

94. Conwell, C.C. and Hud, N.V. (2004) *Biochemistry*, **43**, 5380-5387.

95. Conwell, C.C., Vilfan, I.D. and Hud, N.V. (2003) *Proc. Natl. Acad. Sci. USA*, **100**, 9296-9301.

96. Park, S.Y., Harries, D. and Gelbart, W.M. (1998) *Biophys. J.*, **75**, 714-720.

97. Vasilevskaya, V.V., Khokhlov, A.R., Kidoaki, S. and Yoshikawa, K. (1997) *Biopolymers*, **41**, 51-60.

98. Yoshikawa, K. and Matsuzawa, Y. (1996) *J. Am. Chem. Soc.*, **118**, 929-930.

99. Brewer, L.R., Corzett, M. and Balhorn, R. (1999) *Science*, **286**, 120-123.

100. Noguchi, H. and Yoshikawa, K. (2000) *J. Chem. Phys.*, **113**, 854-862.

101. Sakaue, T. and Yoshikawa, K. (2002) *J. Chem. Phys.*, **117**, 6323-6330.

102. Stevens, M.J. (1999) *Phys. Rev. Lett.*, **82**, 101-104.

103. Su, T.J., Theofanidou, E., Arlt, J., Dryden, D.T.F. and Crain, J. (2004) *J. Fluoresc.*, **14**, 65-69.

104. Koo, H.S., Drak, J., Rice, J.A. and Crothers, D.M. (1990) *Biochemistry*, **29**, 4227-4234.

105. Koo, H.S., Wu, H.M. and Crothers, D.M. (1986) *Nature*, **320**, 501-506.

106. Kuznetsov, Y.A., Timoshenko, E.G. and Dawson, K.A. (1996) *J. Chem. Phys.*, **105**, 7116-7134.

107. Schellman, J.A. and Parthasarathy, N. (1984) *J. Mol. Biol.*, **175**, 313-329.

108. Marx, K. and Rubin, G. (1983) *Nucleic Acids Res.*, **11**, 1839-1854.

109. Marx, K.A. and Ruben, G.C. (1984) *J. Biomol. Struct. Dyn.*, **1**, 1109-1132.

110. Keller, D. and Bustamante, C. (1986) *J. Chem. Phys.*, **84**, 2972-2981.

111. Böttcher, C., Endisch, C., Fuhrhop, J.H., Catterall, C. and Eaton, M. (1998) *J. Am. Chem. Soc.*, **120**, 12-17.

112. Eickbush, T. and Moudrianakis, E. (1978) *Cell*, **13**, 295-306.

113. Golan, R., Pietrasanta, L.I., Hsieh, W. and Hansma, H.G. (1999) *Biochemistry*, **38**, 14069-14076.

114. Martin, A.L., Davies, M.C., Rackstraw, B.J., Roberts, C.J., Stolnik, S., Tendler, S.J.B. and Williams, P.M. (2000) *FEBS Lett.*, **480**, 106-112.

115. Schnurr, B., MacKintosh, F.C. and Williams, D.R.M. (2000) *Europhys. Lett.*, **51**, 279-285.

116. Schnurr, B., Gittes, F. and MacKintosh, F.C. (2002) *Physical Review E*, **65**.

117. Ou, Z. and Muthukumar, M. (2005) *J. Chem. Phys.*, **123**, 074905-074901-074905-074909.

118. Reich, Z., Levin-Zaidman, S., Gutman, S.B., Arad, T. and Minsky, A. (1994) *Biochemistry*, **33**, 14177-14184.

119. Boles, T.C., White, J.H. and Cozzarelli, N.R. (1990) *J. Mol. Biol.*, **213**, 931-951.

120. Grosberg, A.Y. and Zhestkov, A.V. (1985) *J. Biomol. Struct. Dyn.*, **3**, 515-520.

121. Marx, K. and Ruben, G. (1986) *J. Biomol. Struct. Dyn.*, **4**, 23-39.

122. Reich, Z., Ghirlando, R. and Minsky, A. (1992) *J. Biomol. Struct. Dyn.*, **9**, 1097-1109.

123. Ma, C., Sun, L. and Bloomfield, V.A. (1995) *Biochemistry*, **34**, 3521-3528.

124. Schnell, J.R., Berman, J. and Bloomfield, V.A. (1998) *Biophys. J.*, **74**, 1484-1491.

125. Goodman, S.D. and Nash, H.A. (1989) *Nature*, **341**, 251-254.

126. Drew, H.R. and Travers, A.A. (1985) *J. Mol. Biol.*, **186**, 773-790.

127. Crothers, D.M. (1993) *Curr. Biol.*, **3**, 675-676.

128. Crothers, D.M., Haran, T.E. and Nadeau, J.G. (1990) *J. Biol. Chem.*, **265**, 7093-7096.

129. Wu, H.M. and Crothers, D.M. (1984) *Nature*, **308**, 509-513.

130. Schultz, S.C., Shields, G.C. and Steitz, T.A. (1991) *Science*, **253**, 1001-1007.

131. Swinger, K.K., Lemberg, K.M., Zhang, Y. and Rice, P.A. (2003) *EMBO J.*, **22**, 3749-3760.

132. Rice, P.A., Yang, S.W., Mizuuchi, K. and Nash, H.A. (1996) *Cell*, **87**, 1295-1306.

133. Swinger, K.K. and Rice, P.A. (2004) *Curr. Opin. Struct. Biol.*, **14**, 28-35.

134. Drlica, K. and Rouviere-Yaniv, J. (1987) *Microbiol. Rev.*, **51**, 301-319.

135. Bianchi, M.E., Beltrame, M. and Paonessa, G. (1989) *Science*, **243**, 1056-1059.

136. Bustin, M. and Reeves, R. (1996), *Progress in nucleic acid research and molecular biology, vol 54*, Vol. 54, pp. 35-100.

137. He, Q., Ohndorf, U.M. and Lippard, S.J. (2000) *Biochemistry*, **39**, 14426-14435.

138. Paull, T.T., Haykinson, M.J. and Johnson, R.C. (1993) *Genes Dev.*, **7**, 1521-1534.

139. Paull, T.T. and Johnson, R.C. (1995) *J. Biol. Chem.*, **270**, 8744-8754.

140. Ross, E.D., Hardwidge, P.R. and Maher, L.J. (2001) *Mol. Cell. Biol.*, **21**, 6598-6605.

141. MacAlpine, D.M., Perlman, P.S. and Butow, R.A. (1998) *Proc. Natl. Acad. Sci. USA*, **95**, 6739-6743.

142. Love, J.J., Li, X.A., Case, D.A., Giese, K., Grosschedl, R. and Wright, P.E. (1995) *Nature*, **376**, 791-795.

143. Werner, M.H., Ruth, J.R., Gronenborn, A.M. and Clore, G.M. (1995) *Cell*, **81**, 705-714.

144. Ellwood, K.B., Yen, Y.M., Johnson, R.C. and Carey, M. (2000) *Mol. Cell. Biol.*, **20**, 4359-4370.

145. Travers, A.A. (2003) *EMBO Rep.*, **4**, 131-136.

146. Mills, J.B., Vacano, E. and Hagerman, P.J. (1999) *J. Mol. Biol.*, **285**, 245-257.

147. Mills, J.B., Cooper, J.P. and Hagerman, P.J. (1994) *Biochemistry*, **33**, 1797-1803.

148. Mills, J.B. and Hagerman, P.J. (2004) *Nucleic Acids Res.*, **32**, 4055-4059.

149. Furrer, P., Bednar, J., Stasiak, A.Z., Katritch, V., Michoud, D., Stasiak, A. and Dubochet, J. (1997) *J. Mol. Biol.*, **266**, 711-721.

150. Protozanova, E., Yakovchuk, P. and Frank-Kamenetskii, M.D. (2004) *J. Mol. Biol.*, **342**, 775-785.

151. Rolland, A. (1998) *Crit. Rev. Ther. Drug Carrier Syst.*, **15**, 143-198.

152. Plank, C., Tang, M.X., Wolfe, A.R. and Szoka, F.C., Jr. (1999) *Hum. Gene Ther.*, **10**, 319-332.

153. Mahato, R.I., Smith, L.C. and Rolland, A. (1999) *Adv. Genet.*, **41**, 95-156.

154. Luo, D. and Saltzman, W.M. (2000) *Nat. Biotechnol.*, **18**, 33-37.

155. Ledley, F. (1991) *Hum. Gene Ther.*, **2**, 77-83.

156. O'Malley, B.J. and Ledley, F. (1993) *Arch. Otolaryngol. Head Neck Surg.*, **119**, 1100-1107.

157. Anderson, W. (1992) *Science*, **256**, 808-813.

158. Anderson, W.F. (1998) *Nature*, **392**, 25-30.

159. Li, S.D. and Huang, L. (2006) *Gene Ther.*, **13**, 1313-1319.

160. Morgan, R. and Anderson, W. (1993) *Annu. Rev. Biochem.*, **62**, 191-217.

161. Zabner, J., Fasbender, A., Moninger, T., Poellinger, K. and Welsh, M. (1995) *J. Biol. Chem.*, **270**, 18997-19007.

162. Behr, J.P. (1994) *Bioconjug. Chem.*, **5**, 382-389.

163. Blessing, T., Remy, J.-S. and Behr, J.-P. (1998) *Proc. Natl. Acad. Sci. USA*, **95**, 1427-1431.

164. Davis, S. (1997) *Trends Biotechnol.*, **15**, 217-224.

165. Pitard, B., Aguerre, O., Airiau, M., Lachages, A.M., Boukhnikachvili, T., Byk, G., Dubertret, C., Herviou, C., Scherman, D., Mayaux, J.F. *et al.* (1997) *Proc. Natl. Acad. Sci. USA*, **94**, 14412-14417.

166. Gao, X. and Huang, L. (1996) *Biochemistry*, **35**, 1027-1036.

167. Stull, R.A. and Szoka, F.C. (1995) *Pharm. Res.*, **12**, 465-483.

168. Agrawal, S. (1996) *Trends Biotechnol.*, **14**, 376-387.

169. Pawlak, W., Zolnierek, J., Sarosiek, T. and Szczylik, C. (2000) *Cancer Treat. Rev.*, **26**, 333-350.

170. Thompson, J.D. (2002) *Drug Discov. Today*, **7**, 912-917.

171. Elbashir, S.M., Harborth, J., Lendeckel, W., Yalcin, A., Weber, K. and Tuschl, T. (2001) *Nature*, **411**, 494-498.

172. Hannon, G.J. (2002) *Nature*, **418**, 244-251.

173. Song, E.W., Lee, S.K., Wang, J., Ince, N., Ouyang, N., Min, J., Chen, J.S., Shankar, P. and Lieberman, J. (2003) *Nat. Med.*, **9**, 347-351.

174. Chakraborty, C. (2007) *Curr. Drug Targets*, **8**, 469-482.

175. Dykxhoorn, D.M. and Lieberman, J. (2006) *Annu. Rev. Biomed. Eng.*, **8**, 377-402.

176. Verreault, M., Webb, M.S., Ramsay, E.C. and Bally, M.B. (2006) *Curr. Gene Ther.*, **6**, 505-533.

177. LabatMoleur, F., Steffan, A., Brisson, C., Perron, H., Feugeas, O., Furstenberger, P., Oberling, F., Brambilla, E. and Behr, J. (1996) *Gene Ther.*, **3**, 1010-1017.

178. Capaccioli, S., Dipasquale, G., Mini, E., Mazzei, T. and Quattrone, A. (1993) *Biochem. Biophys. Res. Commun.*, **197**, 818-825.

179. Lewis, J.G., Lin, K.Y., Kothavale, A., Flanagan, W.M., Matteucci, M.D., DePrince, R.B., Mook, R.A., Hendren, R.W. and Wagner, R.W. (1996) *Proc. Natl. Acad. Sci. USA*, **93**, 3176-3181.

180. Yoo, H. and Juliano, R.L. (2000) *Nucleic Acids Res.*, **28**, 4225-4231.

181. Boussif, O., Lezoualch, F., Zanta, M.A., Mergny, M.D., Scherman, D., Demeneix, B. and Behr, J.P. (1995) *Proc. Natl. Acad. Sci. USA*, **92**, 7297-7301.

182. Godbey, W.T., Wu, K.K. and Mikos, A.G. (1999) *J. Controlled Release*, **60**, 149-160.

183. Robaczewska, M., Guerret, S., Remy, J.S., Chemin, I., Offensperger, W.B., Chevallier, M., Behr, J.P., Podhajska, A.J., Blum, H.E., Trepo, C. *et al.* (2001) *Gene Ther.*, **8**, 874-881.

184. Lochmann, D., Jauk, E. and Zimmer, A. (2004) *Eur. J. Pharm. Biopharm.*, **58**, 237-251.

185. Akasaka, T., Matsuura, K. and Kobayashi, K. (2001) *Bioconjug. Chem.*, **12**, 776-785.

186. Dauty, E. and Behr, J.P. (2003) *Polym. Int.*, **52**, 459-464.

187. Dunlap, D., Maggi, A., Soria, M. and Monaco, L. (1997) *Nucleic Acids Res.*, **25**, 3095-3101.

188. Ma, C.L. and Bloomfield, V.A. (1994) *Biophys. J.*, **67**, 1678-1681.

189. Bloomfield, V.A. (2000) *Biopolymers*, **54**, 168-172.

190. Zintchenko, A., Rother, G. and Dautzenberg, H. (2003) *Langmuir*, **19**, 2507-2513.

191. Nakanishi, M., Eguchi, A., Akuta, T., Nagoshi, E., Fujita, S., Okabe, J., Senda, T. and Hasegawa, M. (2003) *Curr. Protein Pept. Sci.*, **4**, 141-150.

192. Vives, E., Brodin, P. and Lebleu, B. (1997) *J. Biol. Chem.*, **272**, 16010-16017.

193. Ignatovich, I.A., Dizhe, E.B., Pavlotskaya, A.V., Akifiev, B.N., Burov, S.V., Orlov, S.V. and Perevozchikov, A.P. (2003) *J. Biol. Chem.*, **278**, 42625-42636.

194. Torchilin, V.P., Levchenko, T.S., Rammohan, R., Volodina, N., Papahadjopoulos-Sternberg, B. and D'Souza, G.G.M. (2003) *Proc. Natl. Acad. Sci. USA*, **100**, 1972-1977.

195. Chiu, Y.L., Ali, A., Chu, C.Y., Cao, H. and Rana, T.M. (2004) *Chem. Biol.*, **11**, 1165-1175.

196. Vitiello, L., Chonn, A., Wasserman, J.D., Duff, C. and Worton, R.G. (1996) *Gene Ther.*, **3**, 396-404.

197. Kwoh, D.Y., Coffin, C.C., Lollo, C.P., Jovenal, J., Banaszczyk, M.G., Mullen, P., Phillips, A., Amini, A., Fabrycki, J., Bartholomew, R.M. *et al.* (1999) *BBA-Gene Struct. Expr.*, **1444**, 171-190.

198. ElOuahabi, A., Thiry, M., Pector, V., Fuks, R., Ruysschaert, J.M. and Vandenbranden, M. (1997) *FEBS Lett.*, **414**, 187-192.

199. Kircheis, R., Kichler, A., Wallner, G., Kursa, M., Ogris, M., Felzmann, T., Buchberger, M. and Wagner, E. (1997) *Gene Ther.*, **4**, 409-418.

200. Wadhwa, M.S., Collard, W.T., Adami, R.C., McKenzie, D.L. and Rice, K.G. (1997) *Bioconjug. Chem.*, **8**, 81-88.

201. McKenzie, D.L., Collard, W.T. and Rice, K.G. (1999) *J. Pept. Res.*, **54**, 311-318.

202. Vijayanathan, V., Thomas, T., Antony, T., Shirahata, A. and Thomas, T.J. (2004) *Nucleic Acids Res.*, **32**, 127-134.

203. Lamer, V.K. and Dinegar, R.H. (1950) *J. Am. Chem. Soc.*, **72**, 4847-4854.

204. Roll, C., Ketterle, C., Faibis, V., Fazakerley, G.V. and Boulard, Y. (1998) *Biochemistry*, **37**, 4059-4070.

205. Lecam, E., Fack, F., Menissierdemurcia, J., Cognet, J.A.H., Barbin, A., Sarantoglou, V., Revet, B., Delain, E. and Demurcia, G. (1994) *J. Mol. Biol.*, **235**, 1062-1071.

206. Lane, M.J., Paner, T., Kashin, I., Faldasz, B.D., Li, B., Gallo, F.J. and Benight, A.S. (1997) *Nucleic Acids Res.*, **25**, 611-616.

207. Cohen, S.B. and Cech, T.R. (1998) *Rna-a Publication of the Rna Society*, **4**, 1179-1185.

208. Godbey, W.T., Ku, K.K., Hirasaki, G.J. and Mikos, A.G. (1999) *Gene Ther.*, **6**, 1380-1388.

209. Koehler, J.K. (1966) *J. Ultrastruct. Res.*, **16**, 359-375.

210. Koehler, J.K., Wurschmidt, U. and Larsen, M.P. (1983) *Gamete Res.*, **8**, 357-370.

211. Allen, M.J., Bradbury, E.M. and Balhorn, R. (1995) *J. Struct. Biol.*, **114**, 197-208.

212. Hud, N., Milanovich, F. and Balhorn, R. (1994) *Biochemistry*, **33**, 7528-7535.

213. Allen, M., Bradbury, E. and Balhorn, R. (1997) *Nucleic Acids Res.*, **25**, 2221-2226.

214. Balhorn, R., Brewer, L. and Corzett, M. (2000) *Mol. Reprod. Dev.*, **56**, 230-234.

215. Li, S. and Huang, L. (1997) *Gene Ther.*, **4**, 891-900.

216. Faneca, H., Simoes, S. and de Lima, M.C.P. (2004) *Journal Of Gene Medicine*, **6**, 681-692.

217. Maruyama, K., Iwasaki, F., Takizawa, T., Yanagie, H., Niidome, T., Yamada, E., Ito, T. and Koyama, Y. (2004) *Biomaterials*, **25**, 3267-3273.

218. Vilfan, I.D., Conwell, C.C. and Hud, N.V. (2004) *J. Biol. Chem.*, **279**, 20088-20095.

219. Huisman, O., Faelen, M., Girard, D., Jaffe, A., Toussaint, A. and Rouviere-Yaniv, J. (1989) *J. Bacteriol.*, **171**, 3704-3712.

220. Hillyard, D.R., Edlund, M., Hughes, K.T., Marsh, M. and Higgins, N.P. (1990) *J. Bacteriol.*, **172**, 5402-5407.

221. Dri, A.M., Rouviere-Yaniv, J. and Moreau, P.L. (1991) *J. Bacteriol.*, **173**, 2852-2863.

222. Goodman, S.D., Nicholson, S.C. and Nash, H.A. (1992) *Proc. Natl. Acad. Sci. USA*, **89**, 11910-11914.

223. Lavoie, B.D. and Chaconas, G. (1993) *Genes Dev.*, **7**, 2510-2519.

224. Lavoie, B.D., Shaw, G.S., Millner, A. and Chaconas, G. (1996) *Cell*, **85**, 761-771.

225. Aki, T. and Adhya, S. (1997) *EMBO J.*, **16**, 3666-3674.

226. Megraw, T.L. and Chae, C.B. (1993) *J. Biol. Chem.*, **268**, 12758-12763.

227. Bianchi, M.E. (1994) *Mol. Microbiol.*, **14**, 1-5.

228. Bewley, C.A., Gronenborn, A.M. and Clore, G.M. (1998) *Annu. Rev. Biophys. Biomol. Struct.*, **27**, 105-131.

229. Wojtuszewski, K. and Mukerji, I. (2003) *Biochemistry*, **42**, 3096-3104.

230. Sagi, D., Friedman, N., Vorgias, C., Oppenheim, A.B. and Stavans, J. (2004) *J. Mol. Biol.*, **341**, 419-428.

231. van Noort, J., Verbrugge, S., Goosen, N., Dekker, C. and Dame, R.T. (2004) *Proc. Natl. Acad. Sci. USA*, **101**, 6969-6974.

232. Murphy, L.D. and Zimmerman, S.B. (1995) *Biophys. Chem.*, **57**, 71-92.

233. Murphy, L.D. and Zimmerman, S.B. (1994) *BBA-Gene Struct. Expr.*, **1219**, 277-284.

234. Sarkar, T., Conwell, C.C., Harvey, L.C., Santai, C.T. and Hud, N.V. (2005) *Nucleic Acids Res.*, **33**, 143-151.

235. Wojtuszewski, K., Hawkins, M.E., Cole, J.L. and Mukerji, I. (2001) *Biochemistry*, **40**, 2588-2598.

236. Hansma, H.G., Golan, R., Hsieh, W., Lollo, C.P., Mullen-Ley, P. and Kwoh, D. (1998) *Nucleic Acids Res.*, **26**, 2481-2487.

237. Shindo, H., Furubayashi, A., Shimizu, M., Miyake, M. and Imamoto, F. (1992) *Nucleic Acids Res.*, **20**, 1553-1558.

238. Tanaka, H., Goshima, N., Kohno, K., Kano, Y. and Imamoto, F. (1993) *J. Biochem. (Tokyo).* **113**, 568-572.

239. Shimizu, M., Miyake, M., Kanke, F., Matsumoto, U. and Shindo, H. (1995) *Biochim. Biophys. Acta*, **1264**, 330-336.

240. Pinson, V., Takahashi, M. and Rouviere-Yaniv, J. (1999) *J. Mol. Biol.*, **287**, 485-497.

241. Lang, D. (1973) *J. Mol. Biol.*, **78**, 247-254.

242. Lang, D., Taylor, T.N., Dobyan, D.C. and Gray, D.M. (1976) *J. Mol. Biol.*, **106**, 97-107.

243. Herskovits, T. and Singer, S.J. (1961) *Arch. Biochem. Biophys.*, **94**, 99-114.

244. Broyles, S.S. and Pettijohn, D.E. (1986) *J. Mol. Biol.*, **187**, 47-60.

245. Porschke, D. (1984) *Biochemistry*, **23**, 4821-4828.

246. Tecle, M., Preuss, M. and Miller, A.D. (2003) *Biochemistry*, **42**, 10343-10347.

247. Pettijohn, D.E. (1988) *J. Biol. Chem.*, **263**, 12793-12796.

248. Schmid, M.B. (1988) *Trends Biochem. Sci.*, **13**, 131-135.

249. Stavans, J. and Oppenheim, A. (2006) *Phys. Biol.*, **3**, R1-R10.

250. Zimmerman, S.B. (2006) *J. Struct. Biol.*, **156**, 255-261.

251. Delius, H. and Worcel, A. (1974) *J. Mol. Biol.*, **82**, 107-109.

252. Kavenoff, R. and Bowen, B.C. (1976) *Chromosoma*, **59**, 89-101.

253. Kavenoff, R. and Ryder, O.A. (1976) *Chromosoma*, **55**, 13-25.

254. Sinden, R.R. and Pettijohn, D.E. (1981) *Proc. Natl. Acad. Sci. USA*, **78**, 224-228.

255. Pettijohn, D.E. (1982) *Cell*, **30**, 667-669.

256. Cunha, S., Woldringh, C.L. and Odijk, T. (2001) *J. Struct. Biol.*, **136**, 53-66.

257. Postow, L., Hardy, C.D., Arsuaga, J. and Cozzarelli, N.R. (2004) *Genes Dev.*, **18**, 1766-1779.

258. Vologodskii, A.V. and Cozzarelli, N.R. (1994) *Annu. Rev. Biophys. Biomol. Struct.*, **23**, 609-643.

259. Higgins , N.P., Deng, S., Pang, Z., Stein, R., Champion, K. and Manna, D. (2005) In Patrick Higgins, N. (ed.), *The bacterial chromosome*. ACM Press, Washington, DC, pp. 133-153.

260. Murphy, L.D. and Zimmerman, S.B. (1997) *J. Struct. Biol.*, **119**, 336-346.

261. Dame, R.T. and Goosen, N. (2002) *FEBS Lett.*, **529**, 151-156.

262. Skoko, D., Wong, B., Johnson, R.C. and Marko, J.F. (2004) *Biochemistry*, **43**, 13867-13874.

263. Zimmerman, S.B. (2006) *J. Struct. Biol.*, **153**, 160-175.

264. Azam, T.A., Iwata, A., Nishimura, A., Ueda, S. and Ishihama, A. (1999) *J. Bacteriol.*, **181**, 6361-6370.

265. Wery, M., Woldringh, C.L. and Rouviere-Yaniv, J. (2001) *Biochimie*, **83**, 193-200.

266. Rouviere-Yaniv, J., Yaniv, M. and Germond, J.E. (1979) *Cell*, **17**, 265-274.

267. Friedman, D.I. (1988) *Cell*, **55**, 545-554.

268. Freundlich, M., Ramani, N., Mathew, E., Sirko, A. and Tsui, P. (1992) *Mol. Microbiol.*, **6**, 2557-2563.

269. Goosen, N. and Vandeputte, P. (1995) *Mol. Microbiol.*, **16**, 1-7.

270. Yang, S.W. and Nash, H.A. (1995) *EMBO J.*, **14**, 6292-6300.

271. Wang, S.Q., Cosstick, R., Gardner, J.F. and Gumport, R.I. (1995) *Biochemistry*, **34**, 13082-13090.

272. Murtin, C., Engelhorn, M., Geiselmann, J. and Boccard, F. (1998) *J. Mol. Biol.*, **284**, 949-961.

273. Goodrich, J.A., Schwartz, M.L. and McClure, W.R. (1990) *Nucleic Acids Res.*, **18**, 4993-5000.

274. Hales, L.M., Gumport, R.I. and Gardner, J.F. (1996) *Nucleic Acids Res.*, **24**, 1780-1786.

275. Hales, L.M., Gumport, R.I. and Gardner, J.F. (1994) *J. Bacteriol.*, **176**, 2999-3006.

276. Tanaka, I., Appelt, K., Dijk, J., White, S.W. and Wilson, K.S. (1984) *Nature*, **310**, 376-381.

277. White, S.W., Wilson, K.S., Appelt, K. and Tanaka, I. (1999) *Acta Crystallographica Section D-Biological Crystallography*, **55**, 801-809.

278. White, S.W., Appelt, K., Wilson, K.S. and Tanaka, I. (1989) *Proteins-Structure Function and Genetics*, **5**, 281-288.

279. Lorenz, M., Hillisch, A., Payet, D., Buttinelli, M., Travers, A. and Diekmann, S. (1999) *Biochemistry*, **38**, 12150-12158.

280. Ussery, D., Larsen, T.S., Wilkes, K.T., Friis, C., Worning, P., Krogh, A. and Brunak, S. (2001) *Biochimie*, **83**, 201-212.

281. Ali, B.M.J., Amit, R., Braslavsky, I., Oppenheim, A.B., Gileadi, O. and Stavans, J. (2001) *Proc. Natl. Acad. Sci. USA*, **98**, 10658-10663.

282. Holbrook, J.A., Tsodikov, O.V., Saecker, R.M. and Record, M.T. (2001) *J. Mol. Biol.*, **310**, 379-401.

283. Sarkar, T., Vitoc, I., Mukerji, I. and Hud, N.V. (2007) *Nucleic Acids Res.*, **35**, 951-961.

284. Santai, C.T. (2006), Georgia Institute of Technology, Atlanta.

285. Holmes, V.F. and Cozzarelli, N.R. (2000) *Proc. Natl. Acad. Sci. USA*, **97**, 1322-1324.

286. Luijsterburg, M.S., Noom, M.C., Wuite, G.J.L. and Dame, R.T. (2006) *J. Struct. Biol.*, **156**, 262-272.

287. Wagner, R.W. (1994) *Nature*, **372**, 333-335.

288. Sherratt, D.J. (2003) *Science*, **301**, 780-785.

289. Worcel, A. and Burgi, E. (1972) *J. Mol. Biol.*, **71**, 127-147.

290. Trun, N.J. and Marko, J.F. (1998) *Asm News*, **64**, 276-283.

291. Higgins, N.P., Yang, X.L., Fu, Q.Q. and Roth, J.R. (1996) *J. Bacteriol.*, **178**, 2825-2835.

292. Pettijohn, D.E. and Pfenninger, O. (1980) *Proc. Natl. Acad. Sci. USA-Biol. Sci.*, **77**, 1331-1335.

293. Bliska, J.B. and Cozzarelli, N.R. (1987) *J. Mol. Biol.*, **194**, 205-218.

294. Zimmerman, S.B. and Trach, S.O. (1991) *J. Mol. Biol.*, **222**, 599-620.

295. Cayley, S., Lewis, B.A., Guttman, H.J. and Record, M.T. (1991) *J. Mol. Biol.*, **222**, 281-300.

296. Zimmerman, S.B. and Murphy, L.D. (1996) *FEBS Lett.*, **390**, 245-248.

297. Murphy, L.D. and Zimmerman, S.B. (2001) *J. Struct. Biol.*, **133**, 75-86.

298. Gosule, L.C. and Schellman, J.A. (1978) *J. Mol. Biol.*, **121**, 311-326.

299. Tabor, C.W. and Tabor, H. (1985) *Microbiol. Rev.*, **49**, 81-99.

300. Tabor, C.W. and Tabor, H. (1984) *Annu. Rev. Biochem.*, **53**, 749-790.

301. Nakabachi, A. and Ishikawa, H. (2000) *Appl. Environ. Microbiol.*, **66**, 3305-3309.

302. Kornberg, T., Lockwood, A. and Worcel, A. (1974) *Proc. Natl. Acad. Sci. USA*, **71**, 3189-3193.

303. Zimmerman, S.B. (2002) *J. Struct. Biol.*, **138**, 199-206.

304. Eltsov, M. and Zuber, B. (2006) *J. Struct. Biol.*, **156**, 246-254.

305. Amit, R., Oppenheim, A.B. and Stavans, J. (2003) *Biophys. J.*, **84**, 2467-2473.

306. Rubin, R.L. (1977) *J. Bacteriol.*, **129**, 916-925.

307. Frenkiel-Krispin, D., Levin-Zaidman, S., Shimoni, E., Wolf, S.G., Wachtel, E.J., Arad, T., Finkel, S.E., Kolter, R. and Minsky, A. (2001) *EMBO J.*, **20**, 1184-1191.

308. Minsky, A. and Kolter, R. (2005) In Higgins, N. P. (ed.), *The bacterial chromosome* ASM Press, Washington, D.C., pp. 155-176.

309. Eltsov, M. and Dubochet, J. (2006) *J. Bacteriol.*, **188**, 6053-6058.

310. Wolf, S.G., Frenkiel, D., Arad, T., Finkel, S.E., Kolter, R. and Minsky, A. (1999) *Nature*, **400**, 83-85.

311. Tolstorukov, M.Y., Virkin, K.M., Adhya, S. and Zhurkin, V.B. (2005) *Nucleic Acids Res.*, **33**, 3907-3918.

312. Kobryn, K., Lavoie, B.D. and Chaconas, G. (1999) *J. Mol. Biol.*, **289**, 777-784.

313. Benevides, J.M., Serban, D. and Thomas, G.J. (2006) *Biochemistry*, **45**, 5359-5366.

314. Smyth, C.P., Lundback, T., Renzoni, D., Siligardi, G., Beavil, R., Layton, M., Sidebotham, J.W., Hinton, J.C.D., Driscoll, P.C., Higgins, C.F. *et al.* (2000) *Mol. Microbiol.*, **36**, 962-972.

315. Rimsky, S., Zuber, F., Buckle, M. and Buc, H. (2001) *Mol. Microbiol.*, **42**, 1311-1323.

316. Dame, R.T., Wyman, C. and Goosen, N. (2001) *Biochimie*, **83**, 231-234.

317. Spurio, R., Durrenberger, M., Falconi, M., Lateana, A., Pon, C.L. and Gualerzi, C.O. (1992) *Mol. Gen. Genet.*, **231**, 201-211.

318. Dorman, C.J., Bhriain, N.N. and Higgins, C.F. (1990) *Nature*, **344**, 789-792.

319. Mojica, F.J.M. and Higgins, C.F. (1997) *J. Bacteriol.*, **179**, 3528-3533.

320. Dame, R.T., Wyman, C. and Goosen, N. (2000) *Nucleic Acids Res.*, **28**, 3504-3510.

321. Tupper, A.E., Owenhughes, T.A., Ussery, D.W., Santos, D.S., Ferguson, D.J.P., Sidebotham, J.M., Hinton, J.C.D. and Higgins, C.F. (1994) *EMBO J.*, **13**, 258-268.

322. Yasuzawa, K., Hayashi, N., Goshima, N., Kohno, K., Imamoto, F. and Kano, Y. (1992) *Gene*, **122**, 9-15.

323. Yamada, H., Yoshida, T., Tanaka, K., Sasakawa, C. and Mizuno, T. (1991) *Mol. Gen. Genet.*, **230**, 332-336.

324. Owenhughes, T.A., Pavitt, G.D., Santos, D.S., Sidebotham, J.M., Hulton, C.S.J., Hinton, J.C.D. and Higgins, C.F. (1992) *Cell*, **71**, 255-265.